SYNTHESIS OF HIGH-STRENGTH AND DURABLE METAKAOLIN-BASED GEOPOLYMER CURED AT AMBIENT TEMPERATURE

Hashimu Hamisi

A Dissertation Submitted in Partial Fulfilment of the Requirements for the Award of the Degree of Doctor of Philosophy in Materials Science and Engineering of the Nelson Mandela African Institution of Science and Technology

Arusha, Tanzania

August, 2025

ABSTRACT

This study aimed to synthesize high-strength and durable metakaolin-based geopolymers cured at ambient temperature, with a focus on enhancing the pozzolanic reactivity of metakaolin. It employed Taguchi design methods to optimize the compressive strength. The growing need for environmentally friendly building materials has sparked interest in geopolymers, which offer a viable substitute for conventional cement-based systems. Metakaolin, a pozzolanic material that results from kaolin clay, significantly enhances the mechanical properties and durability of geopolymers, making it an ideal candidate for this application. Using The Response Surface Methodology under the Box-Behnken Design, the study systematically examined the effects of several key parameters, including calcination temperature (650-850°C), heating rate (1-19°C/min), and soaking time (1-12 h), revealing that a temperature of 765°C at a rate 10°C/min and soaking time of 6.46 h yields the most reactive Metakaolin, characterized by high pozzolanic reactivity and optimized particle morphology both critical factors for effective polymerization. In achieving maximum compressive strength, the Taguchi method was applied, facilitating a structured approach to assess the influence of multiple variables: The concentration of sodium hydroxide solution (NaOH: 8-12M), the ratio of the Na_2SiO_3 to NaOH (SS/SH-1.5-2.5), and the solution to binder ratio (S/B-0, 6-1.0) on the mechanical-properties of the resultant geopolymers. The findings indicate that the optimal formulation achieved compressive strengths exceeding 70 MPa at 12M NaOH, 2.5 SS/SH, and a solution-to-binder ratio of 0.80. This significant improvement is attributed to the synergistic effects of the highly reactive Metakaolin and the strategic optimization of mixing ingredients. The strategic incorporation of RHA enhances compressive strength and improves durability, as evidenced by the geopolymers' strong resistance to rapid chloride permeability and acidic environments. Experimental results demonstrated minimal degradation in aggressive environments, underscoring the materials' suitability for diverse construction applications. A dense, homogenous matrix necessary for the geopolymers' mechanical integrity was proven by microstructural investigation using methods including X-ray Diffraction (XRD) and Scanning Electron Microscopy (SEM). The development of extra binding phases through pozzolanic interactions between Rice Husk Ash and Metakaolin enhanced the composite material's overall performance.

DECLARATION

I, Hashimu Hamisi do hereby declare to the Senate of Nelson Mandela African institution of Science and technology that this dissertation is my original work and that it has neither been submitted nor being concurrently submitted for the degree award in other institution.

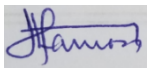

10th August 2025

Hashimu Hamisi — Date

The above declaration is confirmed by:

10th August 2025

Prof. Askwar Hilonga — Date

10th August 2025

Prof. Yusufu Abeid Jande Chande — Date

10th August 2025

Prof. Youssef Tamraoui — Date

COPYRIGHT

CERTIFICATION

The undersigned certify that they have read and hereby recommend for acceptance by the Senate of the Nelson Mandela African Institution of Science and Technology a dissertation entitled "*Synthesis of High-Strength and Durable Metakaolin-Based Geopolymer Cured at Ambient Temperature*" in Fulfilment of the Requirements for the Degree of Doctor of Philosophy in Materials Science and Engineering at Nelson Mandela African Institution of Science and Technology, Arusha Tanzania.

10th August 2025

Prof. Askwar Hilonga — Date

10th August 2025

Prof. Yusufu Abeid Jande Chande — Date

10th August 2025

Prof. Youssef Tamraoui — Date

ACKNOWLEDGMENTS

I thank Allah, the Most Merciful, for his constant protection, guidance, endurance, and spiritual healing since my PhD Programme began. I want to thank The Partnership for Skills in Applied Sciences, Engineering, and Technology (PASET) under the Regional Scholarship and Innovation Fund (RSIF) for supporting my PhD studies financially. I am grateful to my employer, the Nelson Mandela African Institution of Science and Technology (NM AIST), for granting me study leave to pursue PhD studies. I want to express my gratitude to my supervisors, Prof. Askwar Hilonga and Prof Yusufu Abeid Chande Jande, for their substantial contributions in the form of passionate support, motivation, constructive critiques, invaluable counsel, and continuous supervision. Special thanks should go to Prof. Yossef Tamraoui for his generosity and acceptance of my internship at the Mohamed VI Polytechnic University (UM6P) - Department of Materials Science and Nano Engineering (MSN), as well as his substantial assistance in reviewing drafts of my papers and thesis. I would like to thank Dr. Said Mansouri, Dr. Wafaa Borja, and Dr. Hicham Majdoubi for their technical support during my internship at UM6P. I would also like to thank my fellow students, Dr. Ishaq Kariim, Dr. Tusekile Alfred, Ms. Collette Abimana, and Mr. Safiel T. Chambua for their courage and moral support. I also appreciate the lab technicians, Ms. Irene Tesha and Mr. Idd Hussein, for their technical support during my laboratory work at NM-AIST Laboratories. It is an honor to express my heartfelt gratitude to my lovely wives, Ms. Asia Shbani Idd and Ms. Hadija Abdallah Sengasu, for their patience, support, and lavish care, which has enabled me to pursue my PhD studies with unwavering support.

DEDICATION

This work is dedicated to my father, Hamisi Ally Mzava; my mother, Saadia Hemed Mngujini; and my lovely wives, Asia Shaban Idd and Hadija Abdallah Sengasu.

TABLE OF CONTENTS

LIST OF TABLES

LIST OF FIGURES

LIST OF ABBREVIATIONS AND SYMBOLS

3D	Three-Dimensional
a.u	Arbitrary Unit
ANOVA	Analysis of Variance
AS/B	Alkaline Solution-to-Binder ratio
ASTM	American Society for Testing and Materials
BET	Brunauer–Emmett–Teller
CH	Calcium Hydrate
CO2	Carbon dioxide
COD ID	Crystallography Open Database Identifier
C-S-H	Calcium Silicate Hydrate
CV	Coefficient of Variance
EDX/EDS	Energy-Dispersive X-ray
FA	Fly Ash
FT-IR	Fourier transform infrared spectroscopy
GBFS	Ground Blast Furnace Slag
GPC	Geopolymer Concrete
H2SO4	Sulfuric Acid
HCl	Hydrochloric Acid
IEA	International Energy Agency
K2SiO3	Pottasium Silicate
KOH	Pottasium Hydroxide
LOK	Low Order Kaolinite
Ma	Mass (g) after immersion
Mb	Mass(g) before immersion
Min	Minutes
MK	Metakaolin
Na2SiO3	Sodium Silicate
NaCl	Sodium Chloride
NaOH	Sodium Hydroxide
NMK	Nano-Metakaolin
OPC	Ordinary Portland Cement
POFA	Palm Oil fuel Ash

RCP	Recycled Concrete Powder
RCPT	Rapid Chloride Permeability Test
RHA	Rice Husk Ash
RPP	Recycled Paste Powder
RSM	Response Surface Method
SCM	Supplementary Cementitious Material
SEM	Scanning Electron Microscope
SS/SH	Sodium Silicate-to-Sodium Hydroxide ratio
TGA	Thermalgravimetric Analysis
Wa	Mass (g) after exposure
Wa	Water Absorption (%)
Wb	Mass(g) before exposure
Wl	Weight loss (%)
XRD	X-Ray Diffraction
XRF	X-ray fluorescence

CHAPTER ONE

INTRODUCTION

1.1 Background of the Problem

Concrete remains the world's most versatile building and maintenance material due to its numerous mechanical properties, increased durability, ease of adaptation and affordability (Jindal, 2019; Lämmlein *et al*., 2019). It is one of the materials used extensively worldwide, with over thirty (30) billion tonnes consumed yearly (Amran *et al*., 2021a; Chen *et al*., 2021a; Monteiro *et al*., 2017). Figure 1 illustrates the continuous increase in global demand for concrete. It is projected that between 2017 and 2050, the yearly production of Ordinary Portland Cement (OPC) will escalate by almost 12%. The increase is due to the fact that, in developing nations, people invest heavily in building new infrastructure. In contrast, in developed countries, the existing infrastructure needs to be upgraded and occasionally replaced (Monteiro *et al*., 2017).

One of the constituents required to make concrete is cement, whose production involves significant energy consumption and the use of bulk resources (Chen *et al*., 2021a; Lämmlein *et al*., 2019; Xie *et al*., 2019). The cement industry is the third most energy-intensive sector, accounting for a 2% to 3% share of global energy demand (Miller *et al*., 2020; Ofosu-Adarkwa *et al*., 2020). However, between 8% and 9% of carbon dioxide (CO_2) emissions are linked to the manufacturing of cement (Amran *et al*., 2021a; Chen *et al*., 2021a; Ofosu-Adarkwa *et al*., 2020; Turkey *et al*., 2021). It is also claimed that the direct cause of environmental harm and global warming is the manufacture of cement (Benhelal *et al*., 2021; El-Sayed *et al*., 2021; Imtiaz *et al*., 2020). When cement is produced, at least one ton of carbon dioxide is released for each ton of cement (Amran *et al*., 2021a). By 2050, the world's cement production is anticipated to increase by 12% to 23% due to population growth and urbanization (Ofosu-Adarkwa *et al*., 2020). The International Energy Agency (IEA) 2050 roadmap projects that the direct CO_2 emission rate will increase to 4% by 2050 from the current estimate of 3% (Imtiaz *et al*., 2020; Ofosu-Adarkwa *et al*., 2020).

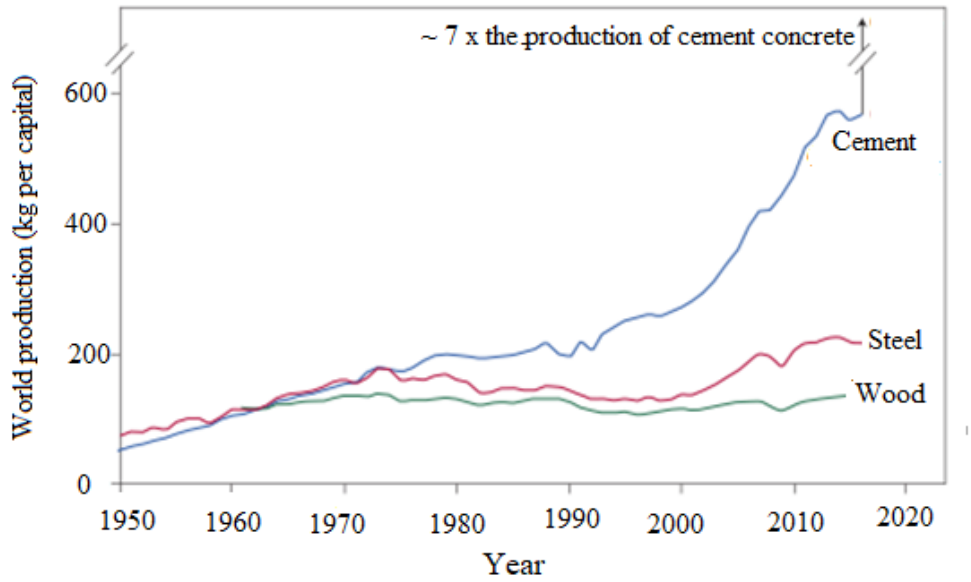

Figure 1: Historical growth in infrastructure material demand is exemplified through per capita cement, steel and wood production (Monteiro *et al.*, 2017)

Given the consequences of cement manufacture, there is a growing demand for green concrete alternatives that are more environmentally friendly. Several initiatives have been employed to mitigate the impact, including the use of industrial waste materials, bio-waste, marine debris and agricultural waste to supplement green concrete (Vishwakarma *et al*., 2018). Studies are underway to fully replace OPC with an environmentally cementitious binder, including geopolymer concrete, for environmental sustainability (Amran *et al*., 2021a; Khan *et al*., 2016). Geopolymer has drawn a lot of attention and is anticipated to displace OPC due to its ability to reduce CO_2 emissions and energy consumption (Abbas *et al*., 2020; Amran *et al*., 2021a; Bajpai *et al*., 2020; Chen *et al*., 2021a; Juenger *et al*., 2011). Reports indicate that geopolymer solids can reduce CO_2 emissions and energy consumption by 73% and 43%, respectively, with the potential to decrease global warming by 61% (Abbas *et al*., 2020; Chen *et al*., 2021a). Geopolymer concrete offers long-term cost advantages, even if its initial cost may be slightly higher than that of conventional concrete. Its durability and resistance to deterioration can result in reduced maintenance and repair costs over the lifespan of a structure (Abiodun *et al*., 2022; Almutairi *et al*., 2021; Devarajan *et al*., 2023; Unis Ahmed *et al*., 2022).

Ideal geopolymer precursors for the polymerization process are pozzolan materials containing fine alumina and silica, as they dissolve quickly in an alkaline solution. Several sources of aluminosilicate precursors include blast slag, metakaolin, fly ash, silica fume and rice husk ashes (Amran *et al*., 2021a; John *et al*., 2021). Aluminosilicate-rich materials, like metakaolin, are the primary source of geopolymer mortar and concrete. Other aluminosilicate sources

include mine tailings, metallurgical slag, fly ash, blast furnace slag, incinerator bottom ash, ladle slag, ceramic waste, high magnesium nickel slag and debris from construction and demolition (Ayeni *et al*., 2021). Geopolymer is considered a low calcium scheme (e.g., alkaline-activated fly ash, metakaolin, etc.) when mainly NASH gel is a highly cross-linked or high calcium scheme (including alkaline-activated Class C fly ash, steel slag) when CSH gel with tobermorite–like is present (Chen *et al*., 2021a). The standard of the materials utilized heavily influences how well GPC performs. Because the physical and chemical characteristics of precursors vary, standardizing geopolymer batches becomes challenging.

Industrial and agricultural waste precursors (e.g., steel slag, fly ash, and rice husk ash) have varying particle sizes and chemical compositions. As a result, getting the same performance will require a different preparation routine with the mixture design (Chen *et al*., 2021a). Metakaolin's natural silica and alumina have led to its use as a mineral ingredient in Portland cement concrete, enhancing its durability and mechanical properties (Assi *et al*., 2020; Kakali *et al*., 2001). The characteristics of the ingredients will significantly influence the final properties of the end product. In that instance, producing the most effective metakaolin is crucial because it will generate the best metakaolin-based geopolymer. Kaolinite has little or no cementitious value but can be modified to become reactive.

Consideration of multiple parameters during metakaolin conversion yields the optimal processing conditions. Kaolin deposits have different properties, which makes it vital to establish optimum conditions for a distinctive kaolin deposit. The Response Surface Methodology under the Box-Behnken Design has been adopted in the current study to optimize the processing conditions for kaolin-to-metakaolin conversion for improved reactivity. Taguchi was applied in optimizing the mixing ingriedient to ensure enhancement of the mechanical properties of the metakaolin geopolymer. To imrpove durability of the optimized metakaolin geopolymer, the influence of rice husk ash addition was explored.

1.2 Statement of the Problem

The main geopolymer mortar and the concrete source are aluminosilicate-rich sources, and metakaolin is among them. Other aluminosilicate sources include mine tailings, metallurgical slag, fly ash, blast furnace slag, incinerator bottom ash, ladle slag, ceramic waste, high magnesium nickel slag, and debris from construction and demolition (Ayeni *et al*., 2021). Metakaolin has been used as a mineral admixture in Portland Cement Concrete to boost mechanical properties and durability due to its inherent silica and alumina (Assi *et al*., 2020;

Kakali *et al*., 2001). Intensive studies on fly ash in geopolymer concrete have been conducted, with reports indicating that it struggles to achieve outstanding performance under ambient curing conditions due to its low reactivity (Khan *et al*., 2016). Heat curing has been applied to improve its mechanical and durability properties (Atiş *et al*., 2015), but this limits its applicability to precast construction. In addition, metakaolin appears to be a viable precursor for geopolymer application, as it is widely accessible and highly reactive, depending on its processing, and has a more consistent mineral composition than fly ash and slag (Huseien *et al*., 2018).

However, metakaolin has been underutilized as the primary precursor for geopolymer applications due to inadequate information on the optimal processing conditions of the raw materials and mix design for enhancing mechanical and durability properties at ambient curing. For construction materials, the use requires a thorough understanding of their mechanical and durability features when exposed to an adverse environment. Therefore, this study aims to synthesize a high-strength and durable metakaolin-based geopolymer that is cured at ambient temperature, ensuring in-situ application with enhanced mechanical and durability properties. The study will employ the RSM method to optimize metakaolin conversion's processing condition for enhanced pozzolanic reactivity and the Taguchi for mechanical properties opmtimization of the mix parameters. The impact of rice husk ash on the metakaolin geopolymer's mechanical and durability properties was also evaluated.

1.3 The Rationale of the Study

Alternative materials that can potentially replace cement have been identified as necessary due to the increasing demand for concrete worldwide for the construction of substantial new infrastructure, the improvement or replacement of aging infrastructure, and concerns about reducing carbon dioxide emissions associated with cement manufacturing. Geopolymer is found to be an environmentally friendly material that could be an alternative to ordinary Portland cement. However, geopolymers are typically synthesized from aluminosilicate-rich materials, such as fly ash, metakaolin and rice husk ash, which have varying particle sizes and chemical compositions. In that incident, the resulting geopolymer batches became challenging to standardize. Therefore, optimizing the materials preparation and batching process is necessary to enhance the mechanical and durability properties.

1.4 Research Objective

1.4.1 General Objective

Synthesize high-strength and durable metakaolin-based geopolymer cured at ambient temperature.

1.4.2 Specific Objectives

(i) To optimize the processing conditions of the potential aluminosilicate sources for metakaolin-based geopolymer mortar.

(ii) To optimize the alkaline activator and solution-to-binder ratio for improving the compressive strength of metakaolin-based geopolymer mortar.

(iii) To investigate the influence of rice husk ash on the mechanical and durability properties of metakaolin-based geopolymer mortar.

1.5 Research Questions

(i) What are the optimal processing conditions for potential aluminosilicate sources used in metakaolin-based geopolymer mortars?

(ii) What are the optimal alkaline activator and solution-to-binder ratio for improving the compressive strength of metakaolin-based geopolymer mortar?

(iii) How does rice husk ash affect the mechanical and durability properties of metakaolin-based geopolymer mortar?

1.6 Significance of the Study

Geopolymer, an eco-friendly alternative to cement, is gaining attention for its potential to reduce CO_2 emissions and energy intensity in cement manufacturing. Fly ash, being the most studied precursor for geopolymer application, has struggled to achieve outstanding properties at normal temperatures, which limits its application to pre-cast construction. Metakaolin, a calcined clay, exhibits high pozzolanic activity, enabling it to react with alkaline solutions to form a durable and strong binding matrix that cures at ambient temperatures.

Additionally, metakaolin-based geopolymers exhibit enhanced mechanical properties, thermal stability, and resistance to chemical attacks, making them suitable for various applications in construction, infrastructure and environmental remediation. As the demand for eco-friendly building materials increases, understanding and optimizing metakaolin-based geopolymers can significantly advance sustainable construction practices. Therefore, synthesizing high-strength and durable metakaolin-based geopolymer cured at ambient temperature will broaden the choice of geopolymer precursors for optimal in-situ applications.

1.7 Delineation of the Study

The study assesses the potential of kaolinite in synthesizing the ambient cured metakaolin-based geopolymer with enhanced mechanical and durability properties. This dissertation is organized into five chapters. Chapter One comprises the background information, problem statement, study rationale, research objective, research questions, and significance. Chapter two offers a detailed literature review ranging from the influencing factors for kaolinite to metakaolin conversion, geopolymer mortar preparation and characterization and durability studies. Chapter three, labeled 'Materials and Methods,' describes the sources of kaolinite materials, rice husk ash, nano silica and other chemicals used in the study. It also describes the optimization protocol for the kaolinite-to-metakaolin conversion and characterization techniques, as well as procedures for synthesizing and assessing the geopolymer. The fourth chapter is dedicated to results and discussion. The effect of different processing parameters for producing highly reactive metakaolin is discussed. The parameters that influence the improvement of mechanical and durability properties are also discussed. The fifth chapter, titled "Conclusion and Recommendations," presents a summary of the observations in this study.

CHAPTER TWO

LITERATURE REVIEW

2.1 Introduction

Concerns about climate change have prompted a shift towards low-carbon substitutes, such as geopolymer concrete, which addresses the pressing demand for environmentally friendly building materials. Several sources of aluminosilicate precursors for geopolymer synthesis exist, including blast slag, metakaolin, fly ash, silica fume and rice husk ashes (Amran *et al*., 2021a; John *et al*., 2021). Metakaolin, a calcined clay known for its exceptional pozzolanic activity, reacts with alkaline activators to form a robust binding matrix that exhibits superior mechanical properties and durability (Jindal *et al*., 2022). The ability to cure metakaolin-based geopolymers at room temperature, eliminating the need for energy-intensive heat treatment, significantly enhances their environmental and economic appeal. This feature not only reduces energy consumption and associated carbon emissions but also simplifies the manufacturing process, making these materials more accessible for practical applications in green construction and infrastructure. As a result, metakaolin-based geopolymers present a viable solution for achieving sustainable building practices while meeting the increasing demand for high-performance materials in the construction industry (Jindal *et al*., 2022; Samuel *et al*., 2020).

This literature review examines the advancements in formulation and processing techniques that enable the practical synthesis of geopolymers, particularly under ambient curing conditions. By analyzing various factors, including processing conditions of aluminosilicate sources, the influence of mixing ratios, activator concentrations and the incorporation of additives, this review aims to highlight the critical parameters that contribute to optimizing the performance of metakaolin-based geopolymers.

2.2 Conversion of Kaolinite to Metakaolin

2.2.1 Calcination of Kaolinite

A high level of amorphousness, a strong pozzolanic reactivity, and a specific surface area define the ideal metakaolin for geopolymer concrete (Shvarzman *et al*., 2003; Shvarzman *et al*., 2002). The preparation of metakaolin involves the calcination of kaolin, resulting in a highly reactive metakaolin. Generally, calcination involves two independent processes leading to structural modifications: firstly, the persistent dehydration of physisorbed water as per the

reaction H_2O (l, free) → H_2O (g) at approximately 100°C; and secondly, intermittent dehydroxylation of structural hydroxyls from the kaolin as per the reaction $Al_2Si_2O_5(OH)_4$ (Kaolin)→ $Al_2Si_2O_7$ (Metakaolin) + $2H_2O$ happening in 500 to 900°C temperature range. Amorphous aluminosilicate ($Al_2Si_2O_7$) is left behind after removing structurally bound water in kaolinite ($Al_2Si_2O_5(OH)_4$) through calcination (Eldin *et al*., 2022; Ilic *et al*., 2010; Rashad, 2013).

The calcination temperature for producing reactive metakaolin varies from 500 to 900°C, depending on the kaolinite source (Ramezanianpour, 2014; Tironi *et al*., 2012b). Overheating leads to recrystallization, which reduces the pozzolanic reactivity of metakaolin (Fabbri *et al*., 2013; Rashad, 2013; Usman *et al*., 2013). The final properties of the calcined kaolin depend on the processing conditions, including calcination temperature, rate and holding time (Kenne Diffo *et al*., 2018; Shafiq *et al*., 2015; Shvarzman *et al*., 2003).

It is testified that the effect of heating rate on the metakaolin employed in geopolymer concrete production was from 1–20°C/min at a constant temperature of 700°C and duration of 30 minutes (Kenne-Diffo *et al*., 2018), and it was found that the best properties were obtained at a low heating rate. Additionally, Elimbi *et al*. (2011) investigated the effect of calcination temperature at a rate of 5°C/min and a holding time of 10 h, spanning a temperature range of 500–800°C in 50°C increments. They found that 700°C yielded the best metakaolin properties. A study on the influence of the degree of de-hydroxylation on the pozzolanic reactivity of metakaolin at a temperature array of 500–850°C at a time interval of 30 minutes to 15 hours concluded that prolonged heating above 5 hours resulted in a reduction of the pozzolanic reactivity of the produced metakaolin (Bich *et al*., 2009).

In a different investigation, calcined kaolin from Malaysia's Perak state was found to be converted to highly reactive metakaolin at a temperature of 800°C for three hours (Shafiq *et al*., 2015). Also, a study on four kaolin deposits in the western region of Turkey concluded that the optimal calcination condition was at 850°C for 3 hours (Güneyisi *et al*., 2012). Several previous studies have also reported a 2-hour calcination time as the optimum soaking time to transfigure kaolin to extremely reactive metakaolin at a temperature above 600°C (Ilic *et al*., 2010; Salahudeen, 2018). This conclusion contradicts the study by Mehsas *et al*. (2021), who concluded that a soaking period of two hours was inadequate to transform the kaolin to the reactive phase after analyzing two metakaolin samples from Algeria. Table 1 summarizes the metakaolin processing conditions from the previous studies.

Table 1: Various Kaolin to metakaolin conversion parameters

Reference	Temperature (°C)	Rate (°C/min)	Soaking time (h)	Comment
Kenne-Diffo *et al.* (2018)	700 Constantly	1, 2.5, 5, 10, 15, and 20	0.5	A low heating rate was found to be ideal.
Elimbi *et al.* (2011)	450–800 constant at a 50 increment	5 constant	10	A temperature of 700°C resulted in the best properties.
Bich *et al.* (2009)	500-850	Not stated	0.5 – 15	A calcination duration of 5 h or less at a temperature above 650°C yielded the best properties.
Shafiq *et al.* (2015)	600–800 at a 100 increment	Not stated	1-5	800°C for a time of 3 h was found to be the optimum
Güneyisi *et al.* (2012)	550–850 at a 50 increment	Not stated	3	A temperature of 750°C was found to be the optimum

It is well observed that kaolin from different sources exhibits varying properties, and the optimum processing conditions may also differ. Therefore, it is crucial to determine the optimal processing conditions for a specific source of kaolin. The best way to achieve the critical optimum parameter is to use multi-parameter effect consideration rather than one factor at a time, which has been used for most reported works (Badogiannis *et al*., 2005; Elimbi *et al*., 2011; Ilic *et al*., 2010; Kenne-Diffo *et al*., 2018; Król *et al*., 2019; Usman *et al*., 2013).

One of the most used experimental techniques for optimization is the Response Surface Method (RSM). The RSM optimization technique assesses the impact of various factors and their interactions with one or more response variables by integrating statistical and mathematical methods for model fitting, regression analysis, and experimental design (Li *et al*., 2021).

2.2.2 Pozzolanic Reactivity of Metakaolin

Metakaolin is a valuable material in construction because of its pozzolanic reactivity. Its capacity to improve durability and strength while lessening its environmental impact makes it an essential part of sustainable building materials. Due to its pozzolanic properties, it is a desirable supplemental cementitious material (SCM) for concrete and other construction applications. While higher temperatures tend to increase the reactivity of materials, excessive heat can cause over-crystallization, which reduces the material's reactivity. Their large surface area increases the reactivity of finer particles. The performance of metakaolin in cementitious

systems can be significantly enhanced by grinding it to finer sizes. The quality of kaolin influences MK's final composition; higher silica and alumina concentrations are associated with higher reactivity (Mathur, 2014; Weise *et al*., 2023).

Various analytical methods are frequently employed to investigate the pozzolanic reactivity of metakaolin. The used approaches provide valuable insights into how the material responds to different stimuli, allowing for a detailed examination of its intrinsic properties and performance characteristics. Consequently, these insights enhance our understanding of the material's overall behavior in various applications. The techniques include:

(i) Frattini Test

This technique measures the amount of calcium hydroxide (CH) consumed in a solution after mixing Portland cement and metakaolin to assess the pozzolanic activity of the mixture. The variation in Ca^{2+} and OH^- ion concentrations is traced to determine pozzolanic reactivity (EN, 2011).

(ii) Thermogravimetric Analysis (TGA)

When metakaolin samples are hydrated over time, TGA evaluates their mass loss and thermal stability. It assists in measuring the quantity of CH used in the pozzolanic reaction (Weise *et al*., 2021).

(iii) Modified Chapelle Test

By measuring the fixed calcium hydroxide content following hydration, this test makes it possible to quantify pozzolanic activity by calculating how much the interaction with metakaolin consumes CH (NFP18-513, 2010).

The modified Chapelle method and the Frattini test are well-established methods for assessing the pozzolanic reactivity of metakaolin. Although they both aim to determine how well a pozzolan reacts with calcium hydroxide (CH), their methods, time commitments, and the precise reactivity they measure vary. The comparison between the two methods is summarized in Table 2.

Table 2: The Frattini test and the modified Chapelle method Comparison

Feature	Modified Chapelle method	Frattini test
Measurement focus	Direct consumption of $Ca(OH)_2$	Saturation of Portlandite
Time required	Less than 1 day	8 to 15 days
Output Format	mg $Ca(OH)_2$ fixed/g sample	Concentrations of ions
Reproducibility	Improved repeatability	interlaboratory variation
Sophistication	Simple and faster	More complex due to longer duration

The X-ray diffraction (XRD) serves as a vital indirect technique for evaluating the pozzolanic reactivity of materials such as metakaolin by analyzing their mineralogical composition. This method provides critical insights into the reactive phases present and allows for the detection of crystalline phase transformations that occur during the hydration process. To complement the mineralogical analysis, scanning electron microscopy (SEM) combined with Energy-Dispersive X-ray Spectroscopy (EDX) is frequently employed to investigate the microstructural evolution of metakaolin at a microscopic level. This combined approach facilitates a detailed examination of the morphological changes and chemical interactions between metakaolin and cementitious matrices, thereby enhancing the understanding of its role and performance within composite materials.

The specific surface area of metakaolin is determined via Brunauer–Emmett–Teller (BET) Surface Area Analysis, which is crucial for understanding its reactivity. Because more surface area is available for reaction, higher surface area usually translates into higher pozzolanic activity. While indirect techniques, such as XRD and SEM, offer qualitative insights into structural changes and interactions within cementitious systems, direct methods, like the Frattini and modified Chapelle tests, provide quantitative assessments.

2.3 Geo-polymerization Reaction of Metakaolin-based Geopolymer

The geopolymerization process is a chemical reaction that transforms aluminosilicate materials into a hardened, durable polymeric material known as geopolymer. This process is highly interested in sustainable construction due to its lower carbon footprint than traditional Portland cement. The process involves mainly three steps:

2.3.1 Dissolution

When metakaolin ($Al_2O_3 \cdot 2SiO_2$) is combined with the alkaline activator, the first step is the dissolution of metakaolin, as shown in Equation (1):

$$Al_2O_3 \cdot 2SiO_2 + 2NaOH + 2H_2O \rightarrow 2Na_2SiO_3 + 2NaAl(OH)_4 \quad (1)$$

Where Metakaolin decomposes in the presence of sodium hydroxide and water, releasing soluble silicate (sodium silicate, Na_2SiO_3) and soluble aluminate (sodium aluminate, $NaAl(OH)_4$). The hydroxide ions (OH^-) from NaOH disrupt the bonds in the metakaolin, allowing the silica and alumina to enter the solution. After dissolution, the soluble silicate and aluminate ions become available as the reactive ions for the polymerization reaction. The Sodium silicate dissociates in the solution to form SiO_3^{2-}, and the Sodium aluminate dissociates to form $Al(OH)_4^-$.

2.3.2 Polymerization

The released silicate and aluminate ions undergo polymerization following the dissolution to form a geo-polymeric gel. This step is crucial for creating the geopolymer structure, as Equation (2) indicates:

$$nNa_2SiO_3 + mNaAl(OH)_4 \rightarrow \text{Geopolymer Gel} \quad (2)$$

The silicate ions (SiO_4^{4-}) and aluminate ions ($Al(OH)_4^-$) condense to form a 3-dimensional network through the creation of siloxane (Si-O-Si) and aluminate (Si-O-Al) bonds. The specific values of n and m depend on the reactant ratios.

2.3.3 Curing

As the geopolymer undergoes continuous chemical reactions and hardening, the initially formed gel progressively develops into a solid, cohesive structure. This maturation process involves ongoing reactions within the geopolymer gel that facilitate densification and promote crystallization, resulting in a material characterized by enhanced mechanical strength and durability. The evolution of the geopolymer's microstructure and its final performance properties are significantly influenced by curing conditions, such as temperature and humidity, which govern the rate and extent of these reactions. Therefore, optimizing these environmental factors is crucial for achieving the desired structural integrity and functional characteristics of the geopolymer.

.

2.4 Geopolymer Mortar Preparation and Properties Optimization

This section reviews various information available on the preparation and optimization of geopolymer mortars. The review process enables a comprehensive understanding of the material's performance characteristics, facilitating the development of high-strength, durable alternatives to traditional cement.

2.4.1 Alkali Activator

The Alkali Activator Solution is the first and most crucial stage in the fabrication of geopolymer mortar and concrete. Sodium hydroxide (NaOH), potassium hydroxide (KOH), sodium silicate (Na_2SiO_3) and potassium silicate (K_2SiO_3) are all components of the alkali activator (Amran *et al*., 2021a; Zhang *et al*., 2020b). The most often utilized alkali activator solutions are sodium hydroxide (NaOH) and sodium silicate (Na_2SiO_3). They are preferred more due to their high capability to increase the reactivity of aluminosilicate precursors, which is necessary to form durable and long-lasting binders (Esparham *et al*., 2021). Sodium hydroxide solution is prepared by dissolving the supplied pellets in distilled water and stirring the mixture continuously. The sodium hydroxide solution is gradually added to the silicate solution to prevent an exothermic reaction. After achieving a uniform mixture through stirring, the liquid is left to stabilize for efficient activation.

2.4.2 Compressive Strength Optimization Process

As with any construction material, proper design, testing and quality control are crucial to ensure their successful implementation in various applications. Numerous factors, including the desired properties and the specific application, influence the design of geopolymer mortar mixes. However, the overall performance of metakaolin-based geopolymer concrete and mortar is determined by several key mix design parameters that have been extensively studied. Central to these is the alkaline solution-to-binder ratio (S/B), which plays a vital role in controlling workability, setting time and mechanical properties by regulating the availability of reactive species essential for geopolymerization.

Equally important is the ratio of sodium silicate to sodium hydroxide (SS/SH) within the alkaline activator, as it influences the polymerization process, affecting the development of the geopolymer gel and the microstructure of the material. The concentration of sodium hydroxide (NaOH) itself critically affects the dissolution rate of aluminosilicate precursors and the

kinetics of geopolymerization, thereby impacting compressive strength and durability. Moreover, the addition of various supplementary materials or additives in specific proportions can alter the physical and chemical interactions within the geopolymer matrix, potentially enhancing or reducing mechanical performance and resistance to environmental factors. These parameters interact in complex ways, making their careful optimization essential for customizing metakaolin-based geopolymer composites to fulfill targeted engineering specifications and service conditions (Kantarcı *et al*., 2019; Naghizadeh *et al*., 2019).

Studies have shown that increasing the NaOH concentration and the sodium silicate-to-sodium hydroxide (SS/SH) ratio increases compressive strength, morphological changes, and geopolymer gel distribution (Azzahran-Abdullah *et al*., 2018; Mhanna *et al*., 2023; Tuyan *et al*., 2018). It is noted that a higher sodium silicate-to-sodium hydroxide ratio leads to more silicate species reacting with aluminate ions to form a strong geopolymer, and a high sodium hydroxide concentration speeds up the dissolution of aluminosilicate and geopolymer gel formation (Jan *et al*., 2021). In a study that optimized the production parameters of geopolymer mortar and concrete (Kantarcı *et al*., 2019), volcanic tuff was utilized as the aluminosilicate source. In this study, the alkaline concentration, curing temperature, solution-binder ratio and curing time were found to affect the compressive strength. When the alkaline solution-to-binder ratio reached 0.6, the compressive strength increased with both increasing sodium hydroxide concentration and curing temperature up to 120°C.

Additionally, another study revealed that the compressive strength increased as the sodium hydroxide concentration was elevated from 8 M to 14 M. The sodium silicate-to-sodium hydroxide ratio was adjusted to 2.5 while investigating the effects of these variables on the strength and water absorption of a geopolymer cured at 60°C with fly ash and ground granulated blast furnace slag (Oleiwi *et al*., 2018). A study on the compressive optimization of metakaolin-based geopolymer cured at 70°C was conducted using a central composite design and revealed SH (14), SS/SH (2.5), and B/AS (1.5) as the optimal parameters (Aouan *et al*., 2021). Other studies have shown that SH molar concentrations above 12 M dramatically reduce compressive strength (Jan *et al*., 2021). Optimization of locally modified metakaolin-based geopolymer concrete using the Taguchi method revealed that the maximum compressive strength was achieved under specific mix design conditions. These optimal parameters included an alkaline solution-to-binder ratio of 0.65, a sodium hydroxide concentration of 13 M, and a sodium silicate-to-sodium hydroxide ratio of 2.5.

Additionally, the binder content was set at 372 kg/m³ of modified metakaolin, which incorporated binary replacements consisting of 5% silica fume (SF) and 5% calcium oxide (CaO) by weight. This combination of factors was found to synergistically enhance the geopolymerization process and microstructural development, resulting in a geopolymer concrete with superior mechanical performance. The findings underscore the critical influence of precise mix design optimization in tailoring the properties of metakaolin-based geopolymers for improved structural applications (Al-Obeidy *et al*., 2024). However, the optimum combination for most factors would also depend on the aluminosilicate source (Oleiwi *et al*., 2018).

Metakaolin geopolymer mortar is a complex material with various constituents and parameters that influence its final properties; optimizing these parameters is vital. An optimization model helps determine the optimal ingredients and proportions for achieving favorable mechanical, durability and rheological properties (Kantarcı *et al*., 2019). It also enables the identification of the optimal mix design that meets performance requirements while minimizing material costs. In large-scale applications, the cost of raw materials can significantly impact the overall project budget (Ma *et al*., 2023). Without an optimization model, the mix design process for metakaolin geopolymer mortar may require numerous experimental trials, which can be time-consuming and costly (Aouan *et al*., 2021; Ferone *et al*., 2013; Oakes *et al*., 2018). Taguchi's experimental design can be used to efficiently determine the most influential factors and their ideal levels to maximize compressive strength. The technique minimizes the number of experimental runs and can manage various variables while producing statistically sound results and minimizing uncontrollable parameters (Siyal *et al*., 2016).

Taguchi developed the concept of signal-to-noise (S/N) ratios as a robustness metric for evaluating product or process performance variability (Hamzaçebi *et al*., 2020). The method utilizes orthogonal arrays to conduct efficient experiments with multiple factors, thereby reducing the number of experimental runs. It also incorporates a signal-to-noise ratio to assess performance by maximizing signal output and minimizing noise variation (Davis *et al*., 2018). Taguchi uses a structured approach that simplifies the experimental process, enhances reliability and is applicable across various industries, including manufacturing and service sectors, by identifying problems, selecting relevant factors, and conducting experiments (Karna *et al*., 2012).

The S/N ratio helps determine the factor levels that optimize the intended result (signal) while minimizing undesirable variation (noise). Noise is a factor that results from unintended or variable departure from the target, whereas signal is the desired performance characteristic. One can create a process or product that operates reliably well, even in the presence of uncontrollable variables or outside disruptions, by optimizing the S/N ratio. Three common types of S/N ratios are used, depending on the nature of the objective, as explained in Equations (3) to (5).

(i) The Smaller is Better

This approach is adopted when the objective is to minimize a response variable. The formula used for this is as shown in Equation (3):

$$\frac{S}{N} = -10\log\{\frac{1}{n}\sum_{i=1}^{n} {y_i}^2\} \tag{3}$$

Whereby, y_i represents individual measurements, and n is the number of observations.

(ii) The Lagger is Better

Applied when maximizing a response variable. The formula used for this is Equation (4):

$$\frac{S}{N} = -10\log\{\frac{1}{n}\sum_{i=1}^{n} \frac{1}{{y_i}^2}\} \tag{4}$$

(iii) Nominal is Best

This approach targets a specific value for the response variable, balancing the mean and variance. The formula used for this is as shown in Equation (5):

$$\frac{S}{N} = 10\log\{\frac{\bar{y}^2}{s^2}\} \tag{5}$$

Whereby, $\bar{y}$ is the mean, and s is the standard deviation of the measurements.

2.5 Durability of the Geopolymer

Geopolymer concrete has a comprehensive range of applications, and exposure to harsh conditions, such as high temperatures, regions where chloride can infiltrate and acidic environments, is unavoidable. Thus, the longer the life span of such concrete depends on its high resistance to hostile environmental exposure. It is, therefore, favorable to consider the resistance of the produced geopolymer to harsh environments for durability purposes.

2.5.1 Heat Resistance Assessment

The heat resistance of geopolymer concrete is a significant advantage over traditional cement-based materials. Additional research and development can optimize GPC for various applications requiring increased fire safety and durability. The building industry's use of geopolymers is expected to increase as awareness of sustainable building materials grows. Studies have shown that the geopolymer concrete retains its structural integrity even when imperiled to high temperatures. Research on Fire-Exposed Fly-Ash-Based Geopolymer Concrete has shown that when exposed to temperatures of 500°C and 1200°C, there was only slight cracking and little mass loss, as opposed to the considerable spalling and strength loss seen in OPC concrete under comparable circumstances. The exposure at 1200°C resulted in a 50% loss in strength, whereas the OPC demonstrated a more dramatic loss (Alzeebaree *et al*., 2021; Razak *et al*., 2022).

Geopolymers' resilience to heat is a result of their inorganic structure. The geopolymer concrete microstructure, comprising a dense network of Al-O and Si-O bonds, is durable at high temperatures and resists the breakdown processes that damage OPC concrete (Klima *et al*., 2022; Lingyu *et al*., 2021). Geopolymers' resilience is attributed to their chemical composition, which lacks water, which reduces the likelihood of explosive spalling: A common failure mode in ordinary concrete when heated that contributes to this stability (Alzeebaree *et al*., 2021).

The type of precursor material used has a significant impact on the heat resistance of geopolymer concrete. For instance, introducing materials Such as Metakaolin or granulated blast furnace slag at high temperatures can enhance strength retention and thermal stability. Likewise, incorporating fiber reinforcement such as steel or carbon fibers has enhanced heat resistance by reducing spalling during heat exposure (Aziz *et al*., 2016; Wong, 2022). Also, because of the superior heat resistance of geopolymers, there is more exploration of their usage in high-risk settings where fire safety is crucial, such as tunnels, buildings and industrial

facilities. Although research on their performance in actual fire situations is ongoing, initial results have validated that they could significantly improve safety in construction applications (Wong, 2022).

Although GPC is more heat-resistant than conventional concrete, its potential for enhanced water absorption at high temperatures must be considered to guarantee long-term performance and durability in structural applications. Prolonged exposure would result in microstructural degradation, contributing to loss of mechanical properties and increased water absorption (Zhang *et al*., 2020a). Further research is needed to optimize formulations that mitigate these effects while upholding the advantageous properties of geopolymer concrete.

2.5.2 Rapid Chloride Permeability Analysis

Chloride intrusion-induced corrosion of reinforcing steel is one of the most common environmental hazards that impair the integrity of concrete construction. Chloride ions are the major contributors to steel reinforcement corrosion, particularly in structures exposed to marine or de-icing salt conditions (Alcántara *et al*., 2017; Silva *et al*., 2019). Corrosion-related damage to manufacturing facilities, parking garages, marine structures, and bridge deck overlays incurs millions of dollars in repair costs annually (Yang *et al*., 2024).

Researchers have placed a lot of emphasis on the durability issues caused by chloride ingress, primarily because of how common they are and how expensive the repair is. Even uncracked concrete can be penetrated by chloride ions by several methods, including diffusion, capillary absorption, hydrostatic pressure and evaporative transport. The main channel of these processes is known to be diffusion, which happens when the concentration of chlorides at the surface of the concrete is higher than within, causing the chlorides to flow into the substance (Joshi *et al*., 2002; Sanchez *et al*., 2022). Chloride ions migrate through the concrete matrix to the reinforcement. When this occurs alongside alternating wetting and drying cycles in an oxygen-rich environment, it creates conditions favorable for rebar corrosion. Significantly, the rate of chloride ion penetration is determined by the internal pore structure of the concrete (Wee *et al*., 2000). Consequently, the pore structure influences construction techniques, hydration level, curing conditions, mix design and other properties of cementitious materials. Therefore, the chloride permeability of the concrete should be evaluated wherever there is a risk of chloride-induced deterioration.

Concrete's resistance to chloride ion intrusion is commonly evaluated using the rapid chloride permeability test (RCPT), which rates the material's capacity to withstand chloride ion penetration. A key component of concrete structure durability against corrosion is the material's resistance to chloride ion intrusion, which is measured by this test by measuring the electrical current that flows through a cylindrical specimen when exposed to a voltage. An electrical current passing through a sample 100 mm in diameter and 50 mm in thickness is monitored for six hours to perform the RCPT; see schematic in Fig. 2. Usually, this sample is sliced as a cylinder or core slice.

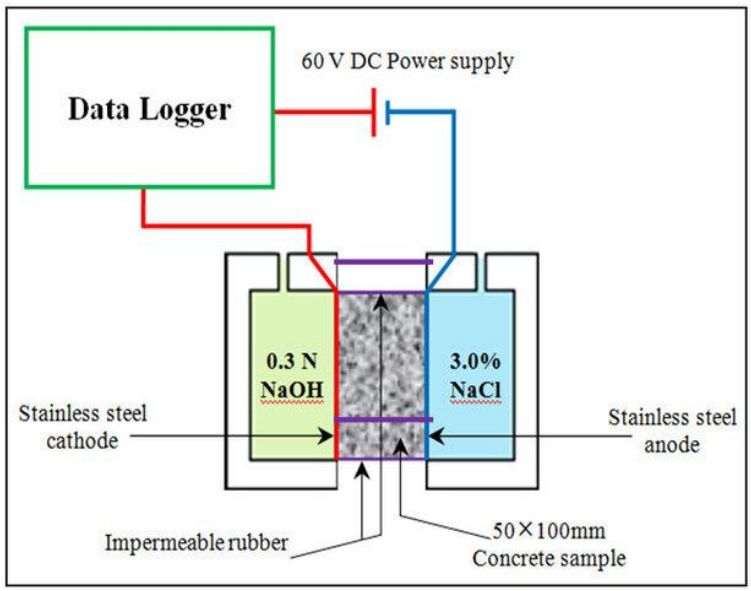

Figure 2: Rapid chloride penetration test RCPT (ASTM, C1202)

Throughout the test, a 60 V DC voltage is maintained across the sample's ends. Two leads are submerged: A 3.0% salt (NaCl) solution and a 0.3 M sodium hydroxide (NaOH) solution. Results from the traditional 90-day salt ponding test show a strong correlation with RCPT (Thomas *et al*., 2018). The concrete's chloride permeability rating, based on the RCPT, is shown in Table 3.

Table 3: Rating of chloride permeability of concrete according to the RCPT

Chloride Permeability	Charge Passing, Coulombs	Typical Concrete type
High	>4000	High w/c ratio (> 0.6) conventional PC concrete
Moderate	2000 to 4000	Moderate w-c ratio (0.40 to 0.50), conventional PC concrete
Low	1000 to 2000	Low w/c ratio (< 0.40) conventional PC concrete
Very Low	100 to 1000	Latex-modified concrete, internally sealed concrete
Negligible	<100	Polymer-impregnated concrete, polymer concrete

ASTMC (1202)

According to research, OPC has higher permeability than geopolymer concrete. Higher slag concentration significantly reduced chloride ingress, improving permeability and making the concrete more corrosion-resistant than OPC, according to a study on steel corrosion and chloride ingress in slag and fly ash blended geopolymer concrete (Singh *et al*., 2024; Tennakoon *et al*., 2017). Another study shows that reactive Metakaolin in geopolymer reduces permeable pores, with the optimal mix being essential (Sadrmomtazi *et al*., 2021; Wong, 2022). In other studies, using large portions and finer Metakaolin has led to a denser microstructure that reduces pore connectivity and enhances chloride ion ingress. Additionally, blending Metakaolin with other cementitious materials rich in silicate, such as rice husk ash, bottom ash, and nano silica, has improved mechanical properties and permeability resistance (Lingyu *et al*., 2021; Wong, 2022).

2.5.3 Acidic Resistance of Geopolymer

Construction practices are shifting towards more sustainable materials, and as a result, understanding the performance of geopolymers in acidic environments is crucial for advancing green building solutions (Madirisha *et al*., 2024). Investigating their resistance to acids advances the more general objective of sustainable development in the construction sector. The acidic resistance of geopolymer refers to its ability to withstand deterioration in acidic environments without experiencing a significant loss of its mechanical, chemical or physical properties. Geopolymers are frequently used in acidic environments, such as sewage systems, industrial effluents and chemical processing plants (De Oliveira *et al*., 2022). It is, therefore, essential to comprehend how geopolymers resist acid attacks to guarantee their long-term functionality and structural soundness in these applications. Compared to conventional Portland cement, the unique composition of geopolymers provides them with greater resilience to chemical attacks, such as acidic environments (Singh *et al*., 2020).

Compared to traditional Ordinary Portland Cement (OPC) pastes, geopolymer materials have a notably higher resistance to acid assaults. According to research, geopolymers particularly those derived from fly ash or metakaolin retain their structural integrity and degrade less readily in acidic solutions, such as acetic and sulfuric acids. According to research, geopolymer specimens exhibit significantly less mass loss and strength degradation under comparable conditions compared to OPC specimens, which deteriorate severely due to their higher calcium content and larger pore size (Aiken *et al*., 2020; Lezzerini *et al*., 2024).

Fibers and other additives can enhance the performance of geopolymer mortars in acidic environments. Including fibers can help reduce porosity and improve mechanical qualities, increasing resistance to chemical attacks (Koushkbaghi *et al*., 2019; Lezzerini *et al*., 2024). The RHA's amorphous silica combines with calcium hydroxide ($Ca(OH)_2$), which is released when cement hydrates, to form more silicate compounds that enhance the concrete's overall strength and durability. The reaction effectively decreases the quantity of free lime, which is the primary agent responsible for concrete deterioration when exposed to acidic environments. Furthermore, the incorporation of rice husk ash (RHA) into geopolymer concrete contributes to the development of a denser microstructure characterized by a reduction in the size and number of large pores. This refinement in pore architecture significantly lowers the material's permeability, thereby limiting the ingress of aggressive acidic ions. As a result, the decreased permeability impedes the penetration of harmful substances, substantially enhancing the concrete's resistance to acid attack and improving its durability in harsh chemical conditions (Kim *et al*., 2014).

2.6 The Effect of Rice-Husk-Ash on Geopolymer Performance

An environmentally friendly method of managing agricultural waste is to utilize rice husk ash, a byproduct of rice milling, in geopolymer concrete. This practice aligns with the principles of a circular economy by transforming agrarian residues into high-performance construction materials, thereby mitigating the environmental challenges associated with RHA disposal and repurposing it as a valuable resource within the building industry (Endale *et al*., 2022; Ro *et al*., 2024). The high content of amorphous silica in RHA significantly enhances its pozzolanic reactivity, which contributes to the formation of additional calcium silicate hydrate (C-S-H) gel during the geopolymerization process. This gel forms through the reaction of RHA with calcium hydroxide ($Ca(OH)_2$) produced in the matrix, ultimately improving the microstructural integrity and mechanical properties of the geopolymer concrete (Amran *et al*., 2021b; Somna *et al*., 2022).

The presence of Rice Husk Ash contributes to a refined pore structure within the geopolymer matrix by void filling and microstructure improvement. The incorporation of rice husk ash (RHA) into concrete significantly enhances its overall strength and durability. However, the extent of improvement in mechanical properties is highly dependent on the proportion of RHA used. Empirical studies indicate that an optimal replacement range, generally between 10% and 20%, achieves a balance that maximizes strength gains while mitigating potential negative

effects such as increased porosity or reduced workability. This optimal dosage ensures that the beneficial pozzolanic reactions of RHA are fully leveraged without compromising the concrete's structural integrity or ease of handling (Hossain *et al*., 2021). According to some studies, for example, the compressive strength of geopolymer concrete with a 15% replacement level was higher than that of plain geopolymer concrete; however, it began to decrease at 20% due to the additional silica content (Hossain *et al*., 2021; Ro *et al*., 2024).

CHAPTER THREE

MATERIALS AND METHODS

3.1 Materials

The kaolinite used in this work was sampled from a natural deposit along Pugu Hills, Tanzania (6°55'18" S; 39°2'54"E and 215 m altitude). The raw material was sun-dried for a day and ground. The raw material was then oven-dried at 110 ± 5°C overnight. It was then sieved using a sieve shaker and a 63 μm sieve before calcination. Rice husk was sourced from a rice milling facility in Usa-River, Tanzania. Sodium hydroxide (98% pure) in pellet form from Sigma Aldrich Chemicals Pvt Ltd and sodium silicate solutions from SCIM CHIMIQUE Moroccan Chemical and Industrial Society, which had a chemical composition comprising 15.1% Na_2O, 34.9% SiO_2 and 50% H_2O, were used to make an alkaline activator solution.

3.2 Conversion of Kaolinite to Metakaolin

3.2.1 Calcination of Kaolinite

The Lindberg/Blue M (BF51731BC-1) box furnace was used for calcination. The kaolinite materials were placed in a crucible and put inside the box furnace. This kaolinite material was calcined to a 650–850°C temperature array at a 1–19°C/min rate for 1-12 h, and the experimental coding is shown in Table 4. The calcination temperature was set, and the time to reach the designed temperature was calculated depending on the selected rate. Then, when the calcination temperature was reached, the samples were held isothermally for the scheduled soaking time before being quenched and prepared for the necessary examination.

Table 4: Box-Behnken Experimental Design Coding

Factor code	Factor	Units	Coded minimum	Coded maximum
A	Temperature	(°C)	-1 ↔ 650.00	+1 ↔ 850.00
B	Rate	(°C/min)	-1 ↔ 1.00	+1 ↔ 19.00
C	Soaking time	h	-1 ↔ 1.00	+1 ↔ 12.00

Table 5: Independent variables and response

Run Order	Process Variables			Response (Pozzolanic Reactivity (mg $Ca(OH)_2/g$))		
	Temperature (°C)	Heating Rate (°C/min)	Soaking time (h)	Actual Value	Predicted Value	Residual
1	650	19	6.5	120.32	114.43	5.89
2	750	19	12	43.12	41.11	2.01
3	750	1.0	1.0	264.21	266.22	-2.01
4	750	19	1.0	332.62	321.31	11.31
5	750	1.0	12	392.36	403.66	-11.30
6	750	10	6.5	1359.82	1375.19	-15.37
7	650	10	12	382.10	390.01	-7.91
8	850	1.0	6.5	411.30	417.19	-5.89
9	750	10	6.5	1397.06	1375.19	21.87
10	750	10	6.5	1359.82	1375.19	-15.37
11	850	10	1.0	618.34	610.43	7.91
12	850	19	6.5	791.84	811.05	-19.21
13	750	10	6.5	1399.42	1375.19	24.23
14	650	10	1.0	784.32	801.52	-17.20
15	650	1.0	6.5	834.97	815.75	19.22
16	750	10	6.5	1359.82	1375.19	-15.37
17	850	10	12	896.37	879.17	17.20

3.2.2 Optimization by Response Surface Methodology

The response surface methodology (RSM), a mathematical and statistical technique, is used in modeling and analyzing a process to optimize a desired response impacted by several input variables (Li *et al*., 2021; Myers *et al*., 2009; Oyebisi *et al*., 2021). The RSM, under Box-Behnken design, aided by Design-Expert 13 software version 5, was used to design the experiment for studying the effect of calcination temperature, soaking time, and heating rate on maximizing Metakaolin's pozzolanic reactivity. Hence, seventeen (17) experimental works with five replicates of the center point run were designed and, at the same time, randomized to ensure no unexplained results occurred due to the variance of unrelated variables. The independent variables and related responses from the seventeen designed experiments were recorded, as shown in Table 5. The table also indicates the residual values of experimental values and the predicted values of Metakaolin's pozzolanic reactivity.

3.2.3 Pozzolanic Reactivity of Metakaolin

Metakaolin's pozzolanic reactivity was assessed using the modified Chappelle test protocol (NFP18-513, 2010). The arrangement of the experiment is indicated in Fig. 3. One gram of

metakaolin sample and two grams of calcium oxide were added to a clean, dry Erlenmeyer flask. A Teflon stirrer bar and 250 mL of carbon dioxide-free water were introduced to the flask to homogenize its contents. The flask was attached to the reflux apparatus, set on a heating mantle at 90 °C for 16 hours, and continuously stirred. After continuous stirring under heat, the flask was cooled to room temperature, and then 250 mL of 0.7 M sucrose was added. The flask was stirred for 30 minutes, then about 200 mL was filtered. Then, a 25 mL aliquot of the sample was collected and titrated with 0.1 M HCl using an auto-titrator, with phenolphthalein used as the indicator. After titration, the fixed mg $Ca(OH)_2$ was calculated using Equation 6.

Calculations:

$$\text{mg Ca(OH)2} = 2\frac{\text{V1} - \text{V2}}{\text{V1}}\text{x}\frac{74}{56}\text{x1000} \quad (6)$$

Wherby, V1 is the volume of 0.1N HCl in ml necessary for the complete titration of the blank sample, and V2 is the volume of 0.1N HCl in ml required for the complete titration of Metakaolin.

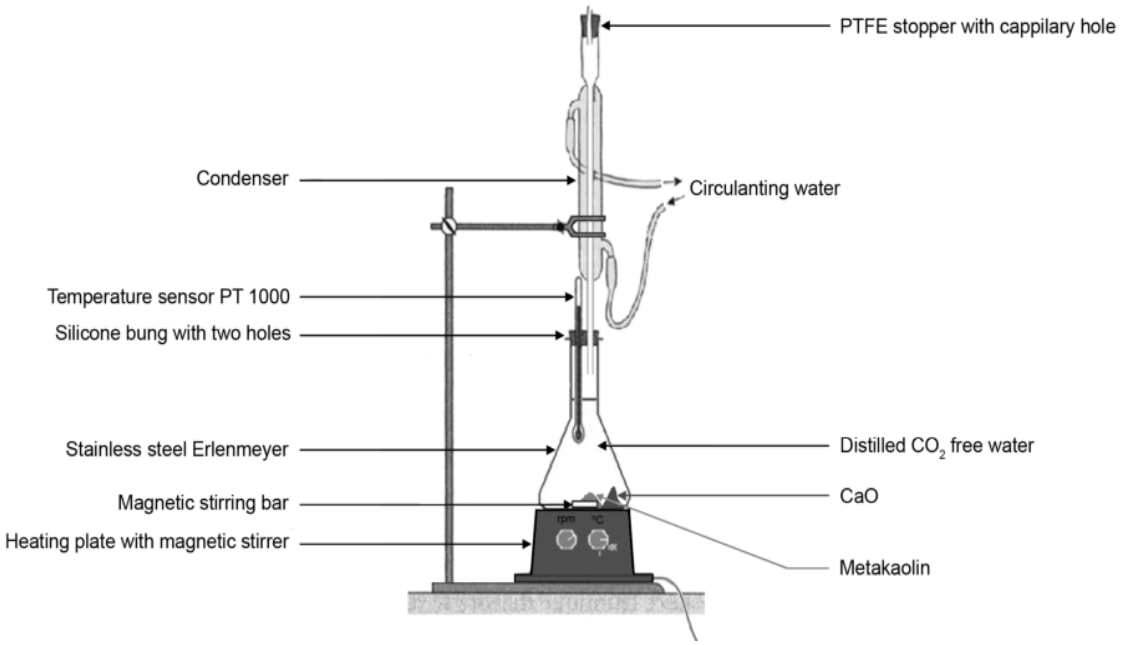

Figure 3: Chapelle Test setup

3.3 Geopolymer Mortar Optimization Process, Preparation and its Properties

3.3.1 Compressive Strength Optimization Process

A Taguchi design was employed to ensure an optimal design with fewer experiments and reduced resource utilization. Three parameters at three levels (Table 6), resulting in nine (L9)

formulations, were used to maximize compressive strength. In this study, the signal-to-noise (S/N) ratio corresponding to the larger-is-better criterion was utilized to optimize the experimental parameters. Three key factors were investigated: The concentration of sodium hydroxide solution (NaOH), the ratio of sodium silicate to sodium hydroxide (SS/SH), and the solution-to-binder ratio (S/B). The selection of factor levels was informed by preliminary trials as well as insights drawn from relevant literature to ensure appropriate ranges for effective analysis. Specifically, the concentration levels of NaOH were adopted based on values reported in previous studies, thereby grounding the experimental design in established research and enhancing the reliability of the optimization process (Adewumi *et al*., 2021; Görhan *et al*., 2014).

Additionally, trials were conducted using varying concentrations, while keeping other factors constant, to assess their influence on compressive strength gain. Trials were also conducted on the effect of the solution-to-binder ratio, considering the workability of the mortar. The too-low value of the solution-to-binder ratio led to a stiff mortar, and the high ratio led to very high workability. Also, based on some commonly used levels (S/B; 0.35-1.2), as testified in some studies (Aouan *et al*., 2021; Kantarcı *et al*., 2019), were considered. Previous studies found the typical range for SS/SH ratios was 1.0-3.0 (Değirmenci, 2017; Morsy *et al*., 2014).

Table 6: Factors and Levels of Mortar Mix Design

Levels	Factors		
	NaOH (M)	SS/SH	S/B
1	8	1.5	0.6
2	10	2.0	0.8
3	12	2.5	1.0

3.3.2 Geopolymer Mortar Preparation

The activator solution was prepared using sodium hydroxide and sodium silicate prior to mixing the mortar. The sodium silicate solutions comprised 15.1% Na_2O, 34.9% SiO_2 and 50% H_2O, whilst the sodium hydroxide was 98% pure and provided in pellet form. The NaOH pellets were dissolved in distilled water to create sodium hydroxide solutions with concentrations of 8 M, 10 M and 12 M. Subsequently, sodium silicate solution was blended with sodium hydroxide to prepare an activator solution featuring varying hydroxide concentrations and silicate-to-hydroxide ratios of 1.5, 2.0 and 2.5.

Given that the dissolution of sodium hydroxide is an exothermic process, the resulting activator solution was allowed to rest for 24 hours prior to use to ensure stabilization. Dry mixing of

sand and metakaolin was performed before the gradual addition of the activator solution, which was continuously stirred until a homogeneous mixture was achieved. The prepared mixture was then cast into designated molds. After 24 hours, the specimens were demolded and subsequently wrapped in plastic film to maintain consistent moisture levels throughout the ambient curing period at 25 ± 2°C, which was sustained until the day of testing. The Schematic proceedings are shown in Fig. 4.

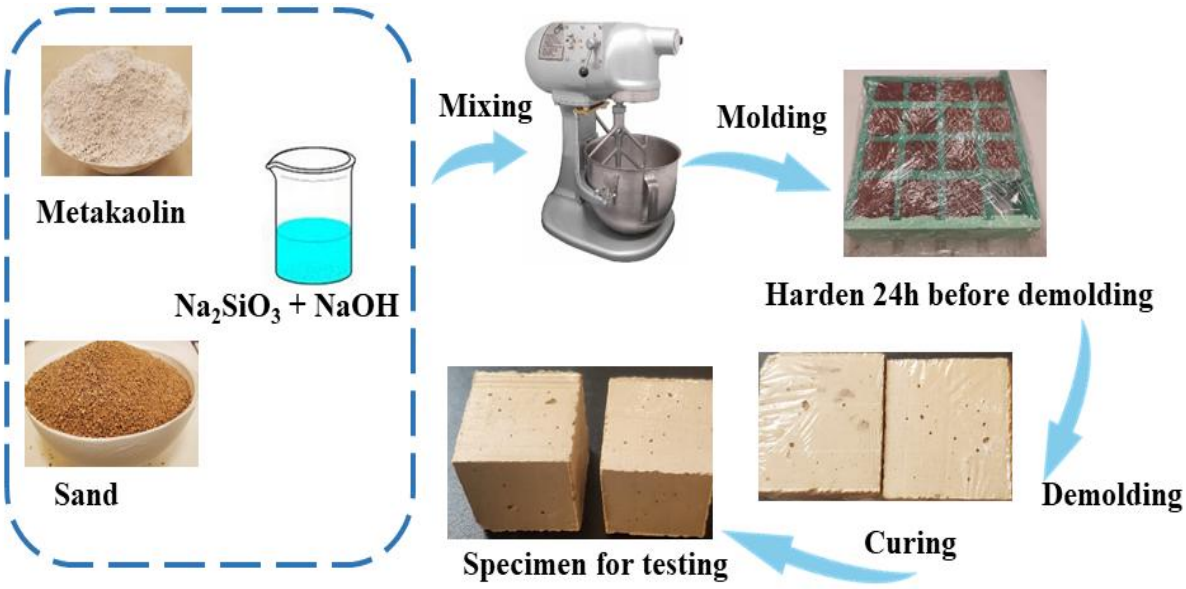

Figure 4: Schematic diagram for geopolymer mortar preparation

Nine (9) formulations, as presented in Table 7, were prepared as designed by the Taguchi method.

Table 7: Geopolymer Mortar Design Formulations by Taguchi (L9)

Designation	Factors		
	NaOH (M)	SS/SH	S/B
GP1	8	1.5	0.6
GP2	8	2.0	0.8
GP3	8	2.5	1.0
GP4	10	1.5	0.8
GP5	10	2.0	1.0
GP6	10	2.5	0.6
GP7	12	1.5	1.0
GP8	12	2.0	0.6
GP9	12	2.5	0.8

Where GP denotes geopolymer and IDs 1-9 denote the formulation number 1 to formulation number 9

3.4 Durability of the Geopolymer

The performance of the geopolymer under various adverse scenarios is evaluated using multiple techniques to test its durability. Rapid chloride permeability, acidic resistance, and heat resistance tests are among the durability tests used in this investigation.

3.4.1 Heat Resistance Assessment

The effects of elevated temperatures were assessed for the combinations under ideal mixing conditions. The specimens were gradually heated from room temperature to the target temperatures of 200°C, 400°C, 600°C, 800°C, and 1000°C over a period of two hours to achieve uniform temperature distribution, followed by spontaneous cooling to ambient temperature. The heating cycle is presented in Fig. 5. The ambient and elevated temperature specimens were tested against compressive strength, weight loss, and water absorption. Three specimens for water absorption were immersed in water for 24 hours, and the weight difference before and after immersion was used to calculate the percentage of water absorption using Equation (7).

$$\mathrm{Wa} = \frac{\mathrm{Ma} - \mathrm{Mb}}{\mathrm{Mb}} \mathrm{x}\, 100 \tag{7}$$

Whereby,

Wa is the water absorption(%), Ma is the mass (g) after immersion, and Mb is the mass(g) before immersion. The specimen's weight was recorded before and after exposure to high temperatures for weight loss computation. The weight loss percentage was computed using Equation 8:

$$\mathrm{Wl} = \frac{\mathrm{Wb} - \mathrm{Wa}}{\mathrm{Wb}} \mathrm{x}\, 100 \tag{8}$$

Where Wl is the weight loss (%), Wa is the mass (g) after exposure, and Wb is the mass(g) before exposure.

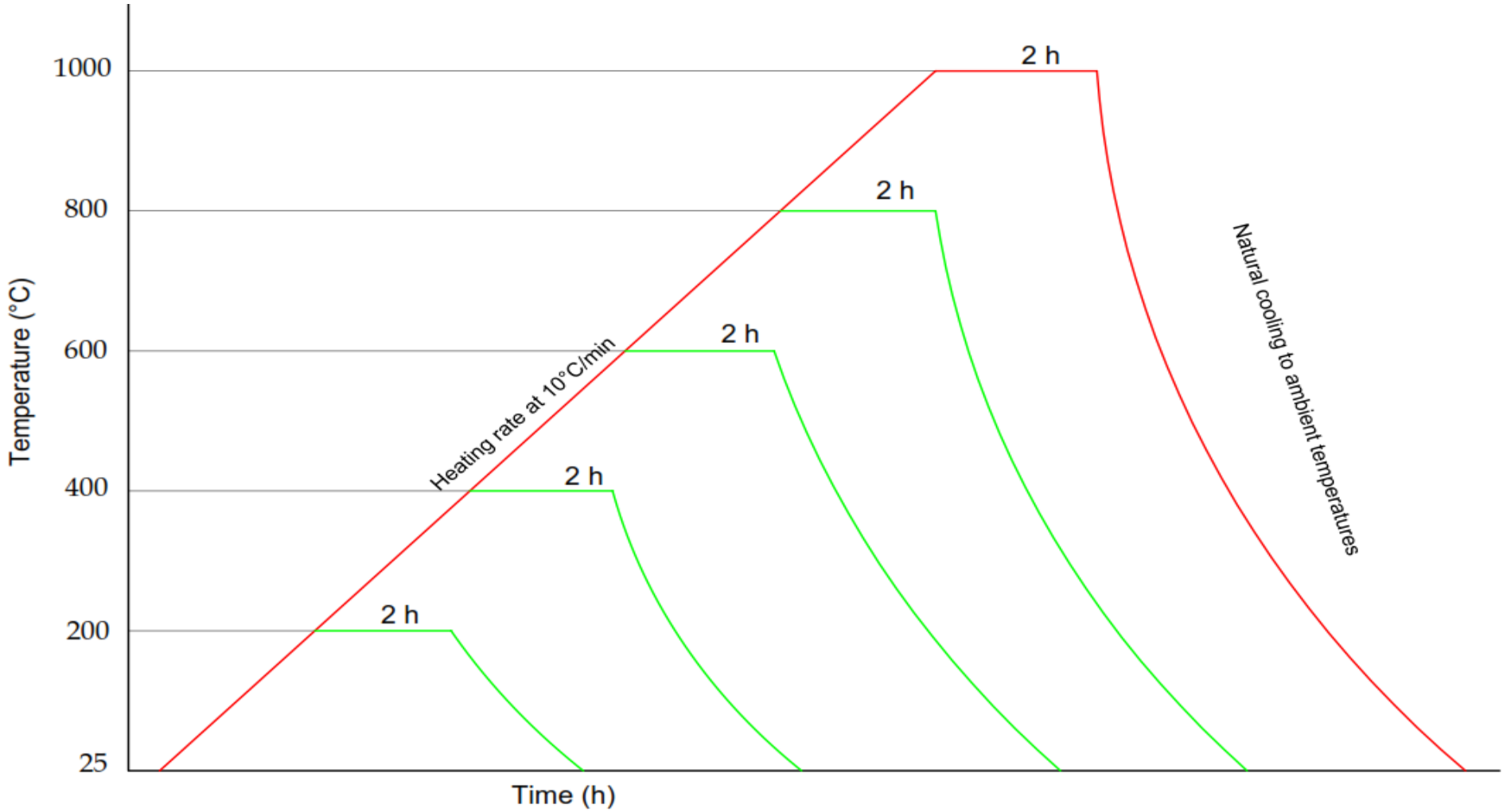

Figure 5: The heating cycle

3.4.2 Acidic Resistance Evaluation

The resilience of the geopolymer to chemical degradation was investigated using sulphuric acid. The chemical durability of the geopolymer material was assessed by exposing cube specimens measuring 30 × 30 × 30 mm to sulfuric acid, evaluating its resistance to chemical degradation. The specimens were cast and cured for 28 days at ambient temperature, covered with polyethylene film to maintain consistent curing conditions and prevent moisture loss. After this initial curing, the weight and compressive strength of three representative specimens were recorded to establish baseline mechanical properties before chemical exposure.

Subsequently, additional specimens were immersed in a 5% sulfuric acid solution to simulate aggressive acidic environments and evaluate the geopolymer's long-term durability. This immersion aimed to replicate the chemical attack mechanisms that can compromise material integrity in practical applications. Periodic monitoring of the specimens' physical and mechanical properties during and after acid exposure provided insights into the extent of degradation and the geopolymer's capacity to withstand chemical deterioration (Fig. 6) for 56 days. To ensure the consistency of the acidic environment, the sulfuric acid solution was replenished on a weekly basis to maintain a stable concentration. The specimens were evaluated after 28 and 56 days of exposure, with measurements taken for both compressive strength and percentage weight loss to quantify the extent of degradation. This assessment was performed in accordance with standardized protocols commonly employed for determining the chemical resistance of polymer concretes, mortars, grouts and monolithic surfacings, thereby ensuring the reliability and comparability of the results (C0207, 2020) and other studies (Mohamed *et al*., 2022; Sata *et al*., 2012).

Figure 6: Sulphuric acid immersion of geopolymer mortar specimens

3.4.3 Rapid Chloride Permeability Analysis

Rapid chloride permeability measurement followed the standard procedures described in ASTM C1202 (C1202, 2012). A 50 mm-thick disc specimen was placed in each of the two cells with the setup indicated in Fig. 7. One end of the cells was filled with a 0.3 N NaOH solution, while the opposite end contained a 3.0% analytical NaCl solution. A 60 V electrical potential was applied across the cells for six hours. The total charge transferred, measured in coulombs and recorded by a computer, quantified the extent of chloride ion penetration.

Figure 7: Rapid Chloride Permeability Test Setup

3.5 Effect of Rice Husk Ash on the Performance of Geopolymer

Various formulations of geopolymer mortar were prepared to investigate how rice husk affected the performance of the geopolymer. The GPRs for metakaolin/rice husk ash blends were used as the notation to identify the blends. Rice husk ash was substituted for metakaolin in both formulations. Presented in Table 8 are the mix compositions. Compressive strength and rapid chloride permeability were used to assess how rice husk ash affected the performance of the geopolymer mortar.

Table 8: Metakaolin – Rice Husk Ash Geopolymer Mortar Design Formulations

Designation	Factors	
	Metakaolin (%)	Rice Husk Ash(%)
GPR1	100	0
GPR2	95	5
GPR3	90	10
GPR4	85	15
GPR5	80	20
GPR6	75	25
GPR7	70	30

3.6 Characterization Technique

The quality of the raw materials and synthesised metakaolin geopolymer mortars was assessed using a variety of characterization techniques. These techniques shed light on the mechanical, chemical, and structural traits that affect durability and performance.

3.6.1 Characterization Technique for the Kaolinite and Metakaolin

The helium gas technique, using a Micromeritics Accupyc II 1340 Pycnometer, was employed to determine the actual density of the material, as density was required as an input during chemical composition analysis. The chemical composition of the materials used in this research was determined using X-ray fluorescence (XRF) with the EPSILON 4 energy-dispersive model. The functional group identification was conducted using Fourier transform infrared spectroscopy (FT-IR) with a Shimadzu IRSpirit series, covering the 400–4000 cm^{-1} wavenumber range. The X-ray diffraction (XRD) analysis was performed on a D8 PHASER diffractometer to confirm the kaolinite-to-metakaolin conversion. The kaolinite-to-metakaolin conversion was also confirmed by examining the morphological changes, particle size and distribution using a Zeiss EVO 10 scanning electron microscope (SEM). The physical properties of both kalonite and metakaolin, in terms of Blaine specific surface area and

fineness, were determined using an FBT-9 Automatic Blaine fineness (air permeability) apparatus adopting the protocol in ASTM C204.

3.6.2 Characterization Technique for the Synthesized Geopolymer Specimens

The compressive strength was determined using a CONTROLAB compression testing machine with a 500 kN maximum loading cell, and a displacement velocity of 1.2 kN/s was maintained. An average compressive strength value was calculated for each test from the three specimens. After the compressive strength test, the remains were taken for further analysis. Grinding was performed to obtain a powdered sample for X-ray diffraction (XRD) analysis, which was conducted using a D8 PHASER diffractometer. Some powder was used for Fourier transform infrared spectroscopy (FT-IR) analysis, utilizing the Shimadzu IRSpirit series within the 400–4000 cm-1 wavenumber range. At the same time, small pieces were taken for a density test of the hardened geopolymer specimen. The microstructural development, textural properties, and morphological shifts of the geopolymer phases were investigated using an Olympus BX63 optical microscope and a Zeiss EVO 10 scanning electron microscope (SEM). To enhance conductivity, the samples were coated with gold.

CHAPTER FOUR

RESULTS AND DISCUSSION

4.1 The Optimization Process of Pozzolanic Reactivity of Metakaolin

The optimization process of pozzolanic reactivity in metakaolin is a critical step in enhancing the performance of metakaolin-based binders at ambient temperature. This process involves adjusting various factors such as calcination temperature, rate and soaking time to maximize the reactivity of metakaolin. Examining surface response plots helps to understand how different factors interact and impact kaolinite-to-metakolin conversion efficiency. The ANOVA findings highlight essential variables that affect pozzolanic reactivity and statistically validate these interactions. Furthermore, optimization ramps can help determine the optimal parameter settings, ensuring that the conversion process maximizes the pozzolanic reactivity.

4.1.1 Response Surface Analysis

A design expert software-generated quadratic regression model was developed using the experimental results obtained from the kaolin-to-metakaolin conversion. From the model, Equation (9) was established to describe the relationship between the independent variables under study (temperature, rate and soaking time) and the pozzolanic reactivity, which is considered the response variable in this study.

$$\begin{aligned} R = 1375.19 &+ 74.5175 * A + -76.8675 * B + -35.6925 * C \\ &+ 273.797 * AB + \ \ 170.063 * AC + -104.412 * BC \\ &+ -211.688 * A^2 + -623.893 * B^2 + -493.218C^2 \end{aligned} \quad (9)$$

Whereby, R is pozzolanic reactivity (mg $Ca(OH)_2$/g), A is Temperature (°C), B is the rate (°C/min) and C is the soaking time (h).

4.1.2 The ANOVA Analysis and Model Fitting

The ANOVA statistically evaluated and validated the derived model fit by assessing the significance of the regression model, individual model coefficients, lack of fit, and pure error. The higher F-values and the smaller probability values ($p < 0.05$) indicate more significance for the corresponding coefficients. From Table 9 and Equation 1, the obtained F-value of 804.67 had a very small p-value ($p < 0.0001$), indicating that the model is highly significant and that there is only a 0.01% possibility that an F-value this large could occur due to random

noise. The terms A, B, C, AB, AC, BC, A^2, B^2 and C^2 are significant coefficients for the pozzolanic reactivity model in kaolin to metakaolin conversion. The F-value for the lack of fit, which is 1.34, indicates that the lack of fit is not notably significant compared to the pure error. An enormous lack of fit in the F-value has a 37.86% chance of being caused by noise. A non-significant lack of fit is advantageous because we want the model to fit (Noordin *et al*., 2004). The model fit statistics showed that the estimated R-squared is nearly equal to one, which suggests the accuracy of stimulated data (Akintunde *et al*., 2015).

Table 9: Variance Analysis for the Response Surface Reduced to a Quadratic Model

Source	Sum of Squares	Df	Mean Square	F-value	p-value	
Model	3.686E+06	9	4.095E+05	804.67	< 0.0001	significant
A-Temperature	44422.86	1	44 422.86	87.29	< 0.0001	
B-Rate	47 268.90	1	47 268.90	92.88	< 0.0001	
C-Soaking time	10191.64	1	10191.64	20.03	0.0029	
AB	2.999E+05	1	2.999E+05	589.19	< 0.0001	
AC	1.157E+05	1	1.157E+05	227.31	< 0.0001	
BC	43607.88	1	43607.88	85.68	< 0.0001	
A^2	1.887E+05	1	1.887E+05	370.73	< 0.0001	
B^2	1.639E+06	1	1.639E+06	3220.25	< 0.0001	
C^2	1.024E+06	1	1.024E+06	2012.55	< 0.0001	
Residual	3562.58	7	508.94			
Lack of Fit	1788.48	3	596.16	1.34	0.3786	not significant
Pure Error	1774.10	4	443.53			
Cor Total	3.689E+06	16				

Model fit statistics

R^2	Adjusted R^2	Predicted R^2	Adeq. Precision	Std. Dev.	Mean	CV%
0.9990	**0.9978**	**0.9915**	**77.1035**	**22.56**	**749.87**	**3.01**

Additionally, the difference between the projected R-squared and the adjusted R-squared was less than 0.2, indicating that the regression model is well-suited to the generated data and will accurately forecast future observations. The adequacy of precision was used to assess the signal-to-noise ratio, which was found to be greater than four and considered desirable (Silva, 2018). The results imply that using the derived regression model, one can navigate the design space.

In objective optimization, the final purpose is to maximize desirability. As shown in Fig. 8, the optimization constraints for temperature, rate and soaking time were employed to maximize the pozzolanic reactivity of the produced metakaolin. It was found that a temperature of 765°C,

a rate of 10°C/min, and a soaking time of 6.46 h resulted in the production of metakaolin with a pozzolanic reactivity of 1382.15 mg $Ca(OH)_2$/g and a desirability of 0.987. A desirability value close to one assures that the experimental design is sound and that the outcomes are trustworthy for practical uses in the kaolinite-to-metakaolin conversion process (Turkane *et al*., 2022). The higher the desirability, the greater the reliability of the obtained solution (Aydın, 2013). The optimized parameters are plotted in optimization ramps, as shown in Fig. 8.

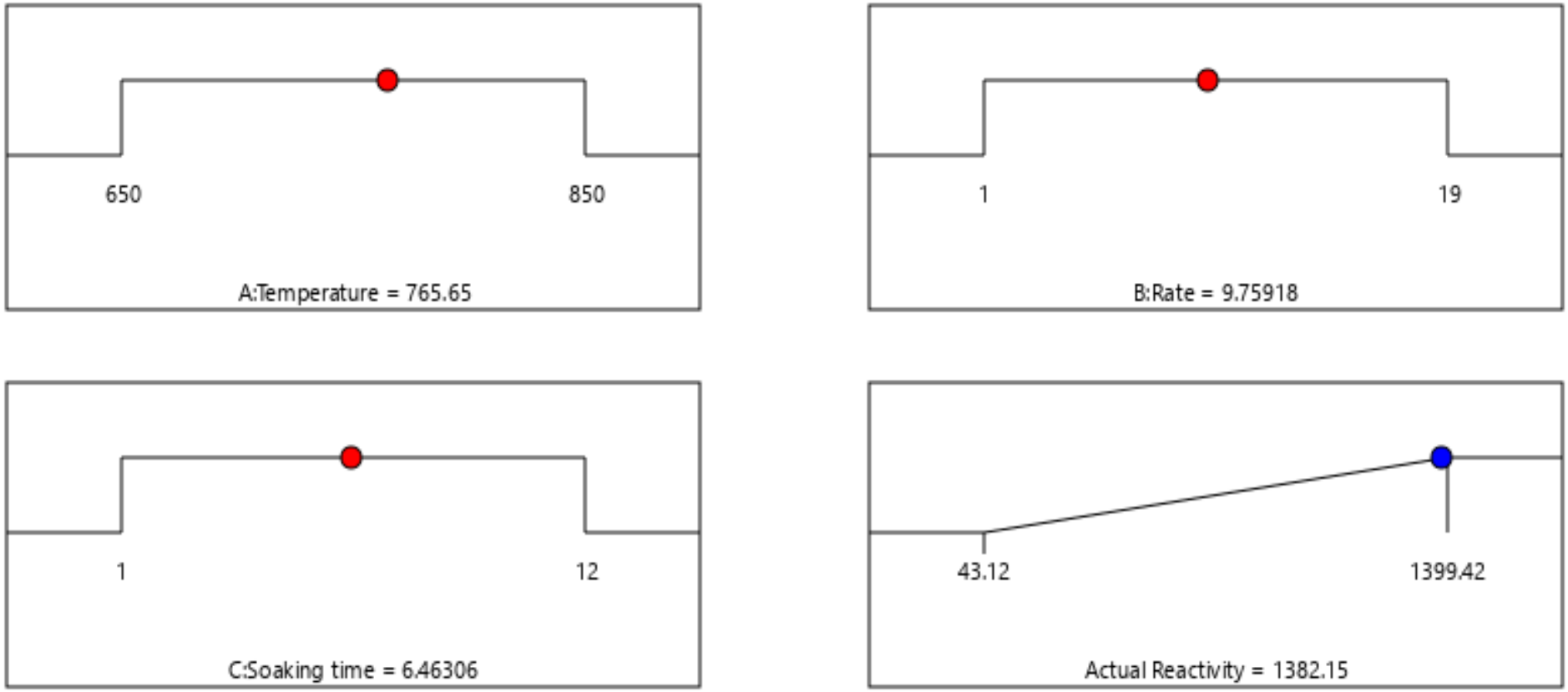

Figure 8: Optimization ramps Desirability = 0.987

To confirm the model, a confirmation location point was chosen with parameters (temperature of 765°C, rate of 10°C/min, and soaking time of 6.46 h), which gave the predicted mean value for the pozzolanic reactivity of 1381.65 mg $Ca(OH)_2$/g. The recorded pozzolanic reactivity at the prediction point parameter was 1351.05 mg $Ca(OH)_2$/g. As seen from Table 7, the prediction error is less than ten percent, which suggests the high accuracy of the model (Srinivasa *et al*., 2023). The value of pozzolanic reactivity is above 700 mg $Ca(OH)_2$/g, which indicates that the produced metakaolin is highly reactive (NFP18-513, 2010).

The interaction effect of the independent factors was analyzed using the contour and three-dimensional plots in Fig. 9. The 3D response surface plots make it easy to understand how two combined variables impact the measured response. As response surface curvature increases, the significance of the factor relationship becomes more apparent (Li *et al*., 2021). It is observed that the pozzolanic reactivity increased with an increase in temperature from 650°C to 765.61°C and declined beyond that temperature. Considering the soaking time, it is observed that the holding time beyond 6.46 h reduced the pozzolanic reactivity of the metakaolin. The decrease in pozzolanic reactivity at a higher temperature may be due to the crystallization of metakaolin (Rashad, 2013).

Figure 10 shows a normal probability plot of the residual for the pozzolanic reactivity: The predicted value versus the experimental value of pozzolanic reactivity. The almost perfectly straight distribution of the points for all dependent variables shows that the data for all residual responses has a normal distribution. A plot of actual against anticipated data is another visual tool used to assess a model's fitness. Every point in the plot is shown to be relatively near a straight line. The real versus predicted values tend to follow existing models fairly well and match the data nicely, as demonstrated by the points' smooth fitting along a straight line (Mohammed *et al*., 2018).

Table 10: Model verification for pozzolanic reactivity maximization

Temperature (°C)	Rate (°C/min)	Soaking time (h)	Experimental value (mg $Ca(OH)_2$/g)	Std Dev	Predicted value (mg $Ca(OH)_2$/g)	Error (%)
765	10	6.46	1351.05	22.5597	1381.65	2.22

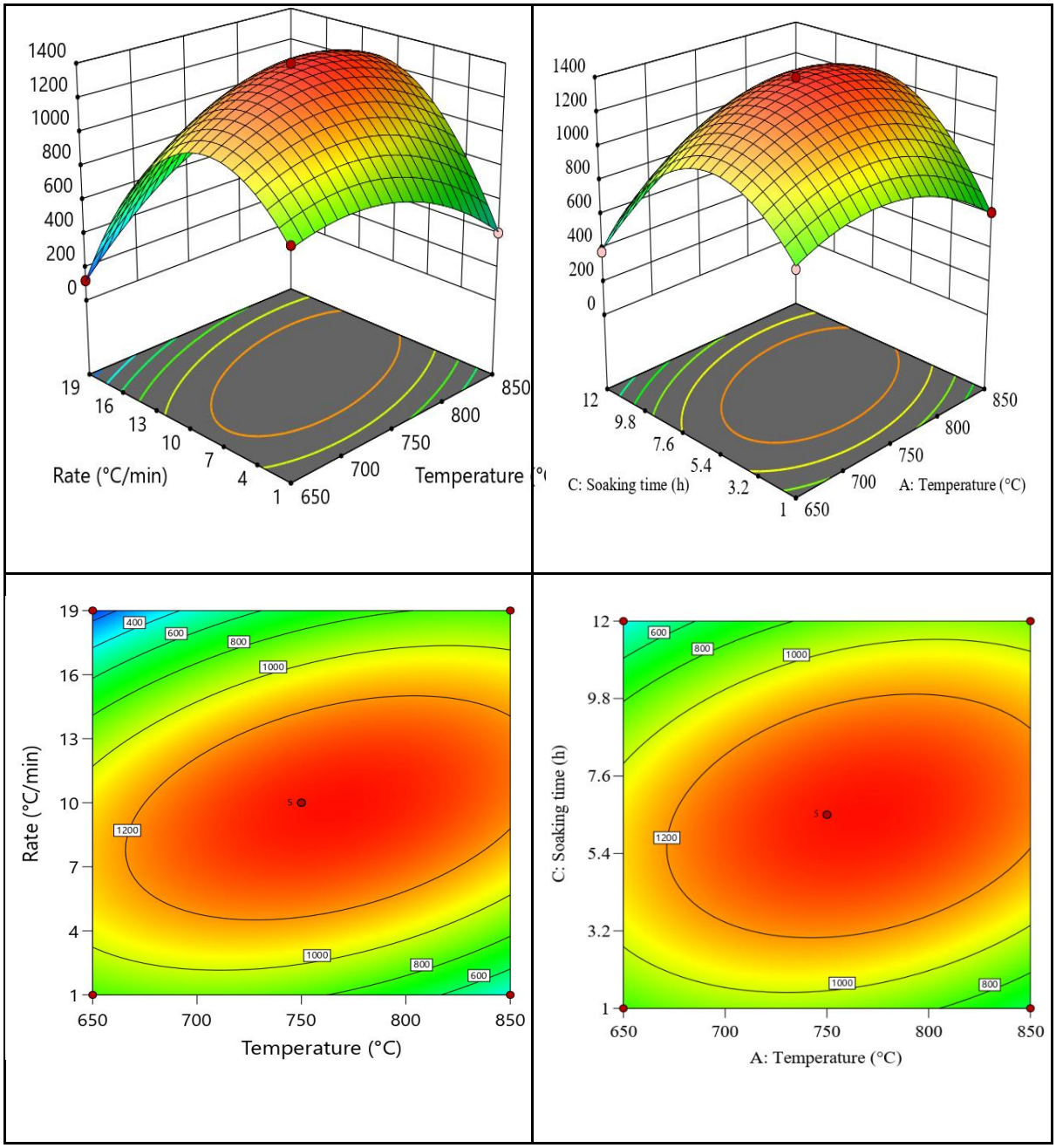

Figure 9: **Contour and 3D of the combined effect of temperature and rate, temperature, and soaking time on the pozzolanic reactivity of metakaolin**

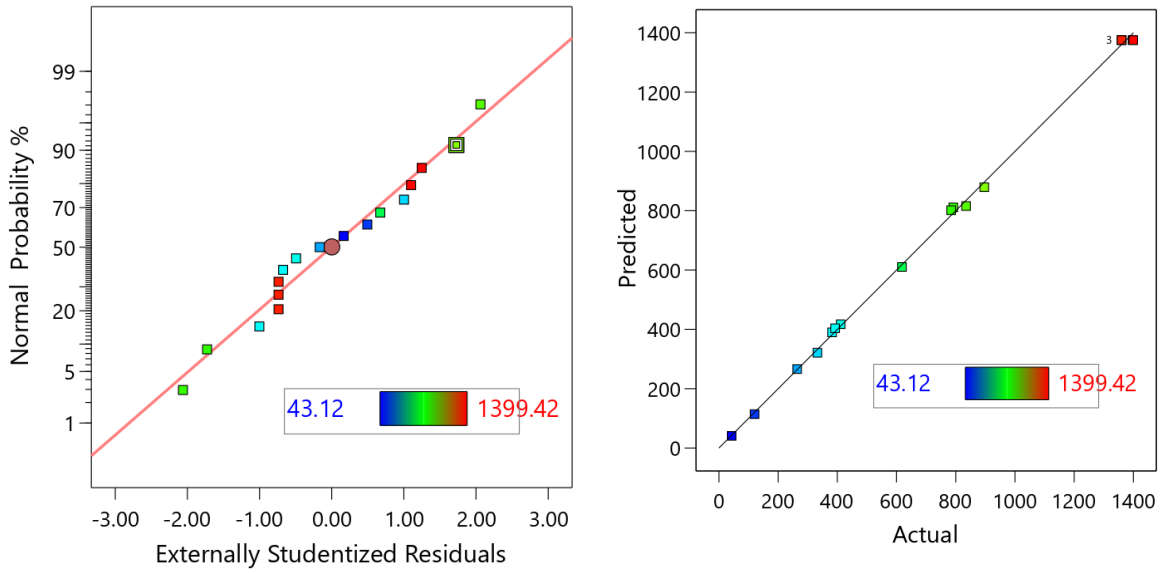

Figure 10: **Normal probability plot residual for the pozzolanic reactivity; predicted value versus the experimental value of pozzolanic reactivity**

4.1.3 Kaolinite and Metakaolin Characterization

The chemical composition of the kaolin used in this study was more reflected and characterized by silica, alumina, and iron oxide, as shown in Table 12. Other oxides were also found to be present at a deficient percentage. It is noted that silicon dioxide, aluminum oxide, and iron oxide account for more than 70% of the material's composition, indicating that it can be engaged as a cementitious starting raw material (ASTM-C618). Density is an essential property that can affect the behavior and performance of metakaolin in various applications. The higher density recorded in metakaolin (2.747 g/cm^3) may be due to the thermal treatment process of kaolin. Dehydroxylation drives the chemically bound water off, decreasing volume and contributing to a density increase. The increase in density may result in better particle packing, improving densification, and reduced porosity in the microstructure of metakaolin-based materials.

Table 11: **Physical Properties of kaolin and metakaolin**

	Density (g/cm^3)	Blaine Specific Surface area (cm^2/g)	R45 micron (%)
Kaolin	2.632	7208	8.0
Metakaolin	2.747	8909	4.4

The R45 microns of the produced metakaolin were found to be 4.4%. The results imply that 95.6% of particles were below 45 microns, and only 4.4% were retained. Generally, a lower R45 microns fraction may indicate a finer particle size distribution, which is desirable for geopolymer mortar application (Komnitsas *et al*., 2015).

The XRD patterns for kaolinite and metakaolin are shown in Fig. 11. The pattern confirms the presence of kaolinite, quartz and muscovite in the kaolinite material. After calcination, the metakaolin formation is characterized by the disappearance of kaolinite peaks. The metakaolin was found to be dominated by quartz and the formation of new phases like Annite and Ecryptite.

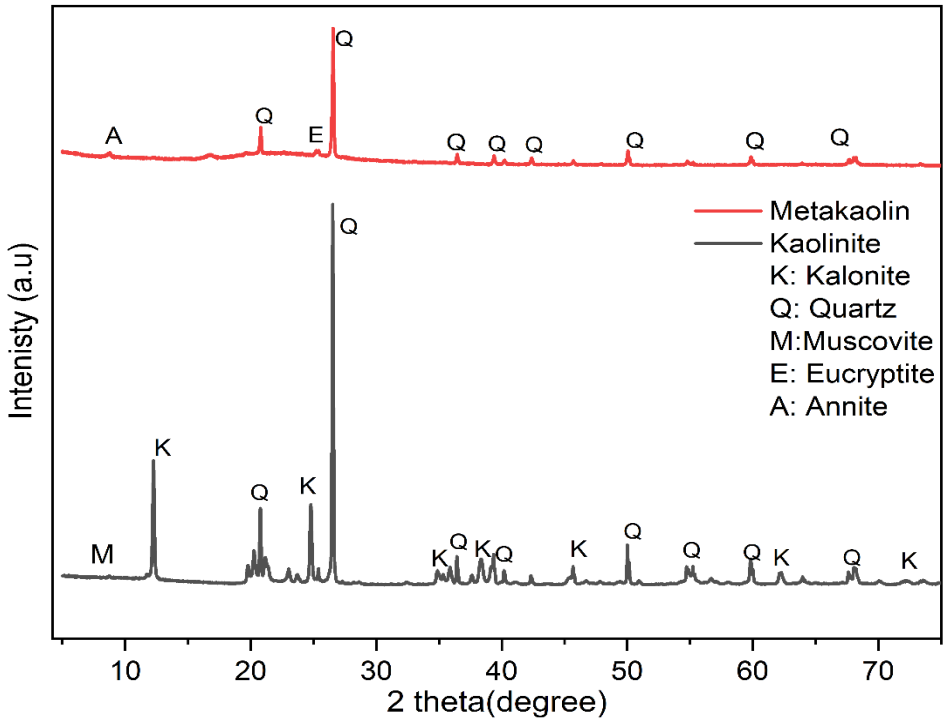

Figure 11: The XRD pattern for kaolinite and metakaolin

Table 12: Chemical composition of Kaolinite and Metakaolin

Component	SiO_2	Al_2O_3	CaO	Fe_2O_3	K_2O	Na_2O	P_2O_5	MgO	TiO_2
K	61.5	33.7	0.2	3.1	0.27	0.08	0.07	0.4	0.44
MK (%)	55.05	42.3	0.13	1.27	0.3	0.02	0.15	0.20	0.58

The Rietveld refinement method was employed to quantitatively analyze the phase composition of each sample utilizing high-quality X-ray powder diffraction (XRPD) data. A thorough understanding of the mineralogical and crystallographic characteristics of the raw kaolinite and metakaolin under study was fundamental to developing an accurate Rietveld XRPD quantification approach. The reliability of this method is evidenced by the excellent agreement between the observed and calculated diffraction patterns, as indicated by the goodness-of-fit values for both kaolinite and metakaolin, which are illustrated in Fig. 12 and 13, respectively. This strong correlation confirms the precision of the phase quantification and the robustness of the applied analytical technique.

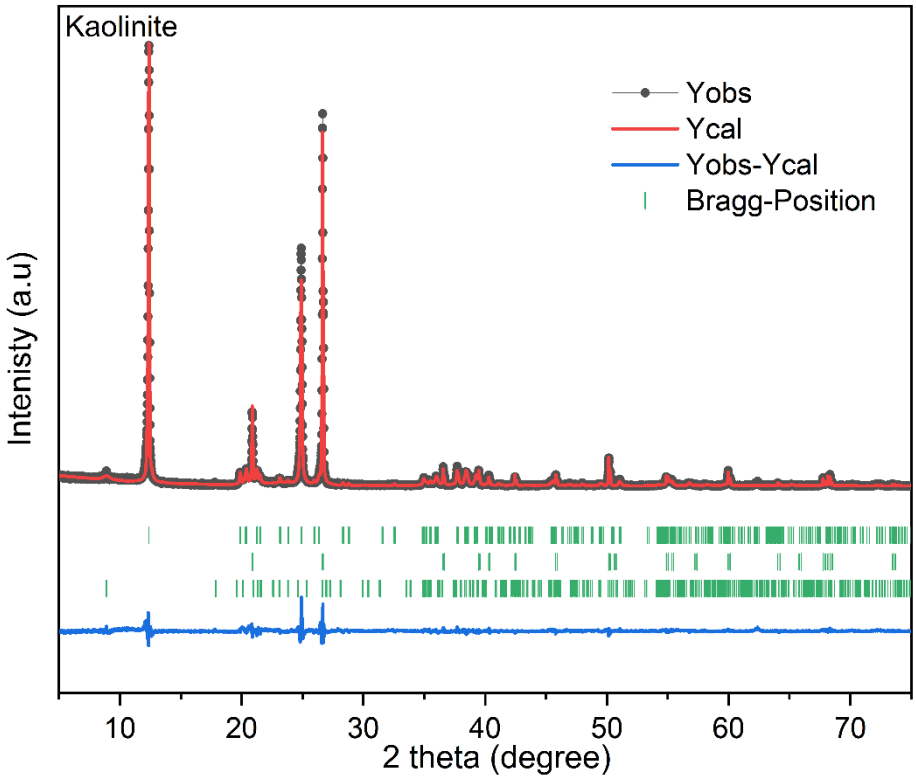

Figure 12: Rietveld refinement fitting curve for kaolinite

Dots give the observed and calculated data by a solid red line. Vertical upper and lower green lines indicate the Bragg position of kaolinite, quartz and muscovite. The blue line under the plot is the profile of the difference between the observed and calculated data

The kaolinite phase (58.02%) was predominant in the raw kaolin sample. The other phases were the quartz (29.18%) and muscovite (12.8%). The mineralogical name and weight fraction of the quantified phases by Rietveld refinement are indicated in Table 13. On the other hand, Quartz, Eucryptite and Annite were the crystalline phases in the metakaolin with 89%, 3% and 8% weight fractions, respectively. The quantitative analysis employing the Rietveld method reveals that the amorphous fraction is 60% and the crystalline fraction is 40%, as illustrated in Table 14.

Table 13: Phases Quantification in the raw kaolinite, corresponding chemical formulas and weight fraction

Mineral name	Chemical formula	Weight fractions%	COD ID	Reference
Kaolinite	$Al_2Si_2O_5(OH)_4$	58.02%	9009234	Bish (1993)
Quartz	SiO_2	29.18%	1011097	Wei (1935)
Muscovite	$K_{3.52}Na_{0.44}Al_{11.36}Fe_{0.24}Mg_{0.08}Si_{12.32}O_{48}H_8$	12.80%	9005014	Catti *et al*. (1989)

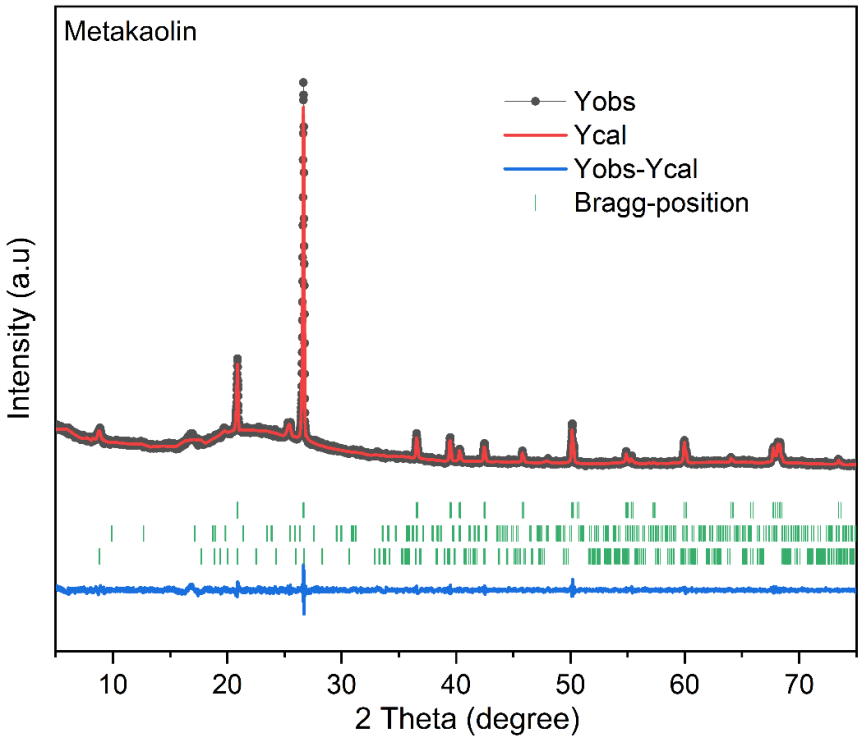

Figure 13: Rietveld refinement fitting curve for metakaolin

Dots give the observed and calculated data by a solid red line. Vertical upper and lower green lines indicate the Bragg position of Quartz, Eucryptite, and Aannite. The blue line under the plot is the profile of the difference between the observed and calculated data

The morphology of the kaolinite and metakaolin was evaluated by SEM, as shown in Fig. 14. The kaolin sample is distinguished by its greater particle size and layered, plate-like structure, which disappears with calcination. Calcination of kaolinite results in smaller, fragmented particles due to dehydroxylation, which breaks down the layered structure and leads to a non-layered morphology in the metakaolin.

Table 14: Phases Quantification in the metakaolin, corresponding chemical formulas and weight fraction

Mineral name	Chemical formula	Weight fractions%	COD ID	Reference
Quartz	Si_6O_6	89%	9010145	Ikuta *et al*. (2007)
Eucryptite	$Si_{12}Al_{12}Li_{12}O_{48}$	3%	9000368	Pillars *et al*. (1973)
Annite	$Si_{5.10}Al_{6.90}Fe_6K_{1.98}Na_{0.02}O_{24}$	8%	9002315	Redhammer *et al*. (2000)
	Amorphous	Crystalline Fraction (Quartz, Eucryptite, Annite)		
Weight%	60%			40%
Weight% of the crystalline fraction without Amorphous fraction		Quartz	Eucryptite	Annite
		89	3	8
Weight% of crystalline and amorphous	60%	35.6	1.2	3.2

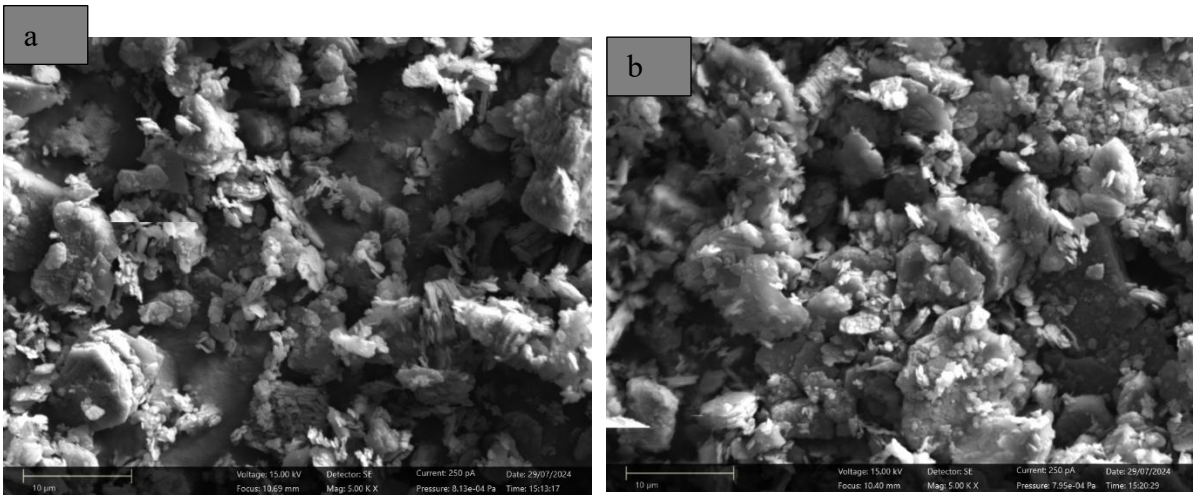

a) Kaolinite **b) Metakaolin**

Figure 14: The SEM images of Kaolinite and Metakaolin samples

The Fourier-transform infrared (FT-IR) spectra presented in Fig. 15 were employed to verify the transformation of kaolin into metakaolin, with the corresponding band assignments detailed in Table 15. Notably, the absorption bands detected at 3692 cm^{-1} and 3650 cm^{-1} correspond to the interlayer hydroxyl groups, while the band at 3620 cm^{-1} is attributed to the inner hydroxyl (OH) stretching vibrations, as documented in previous studie (Erasmus, 2016; Irfan-Khan *et al*., 2017; Tironi *et al*., 2012a). The presence of these three characteristic bands, associated with hydroxyl stretching modes, confirms the existence of kaolinite in the raw kaolin sample, corroborating findings as reported by other researchers (Bich *et al*., 2009; Souri *et al*., 2015;

Tironi *et al*., 2012a). This spectral evidence thus substantiates the successful identification of kaolinite before its thermal conversion to metakaolin. The observed three peaks define the kaolinite material under study as low-order kaolinite (LOK) (Liu *et al*., 2021; Souri *et al*., 2015).

The bands observed at 1115, 1030 and 1006 cm^{-1} correspond to Si–O stretching vibrations, while the band at 534 cm^{-1} indicates the presence of Al–Si–O bonds characteristic of the kaolinite structure under investigation. Additionally, the peak at 912 cm^{-1} is attributed to Al–OH bending vibrations (Erasmus, 2016; Souri *et al*., 2015). Other significant peaks at 798 and 677 cm^{-1} are associated with Si–O–Si stretching modes within the kaolinite material (Erasmus, 2016). Following calcination, the characteristic hydroxyl bands at 3692, 3650 and 3620 cm^{-1} disappear and are replaced by a broad absorption band in this region, confirming the formation of reactive amorphous metakaolin (Ilic *et al*., 2010; Souri *et al*., 2015). Furthermore, the calcination process transforms the distinct peaks at 1115, 1030 and 1006 cm^{-1} into broad doublet peaks at 1084 and 1047 cm^{-1}, signifying the successful conversion of kaolinite into metakaolin (Deju *et al*., 2020; Tironi *et al*., 2012a).

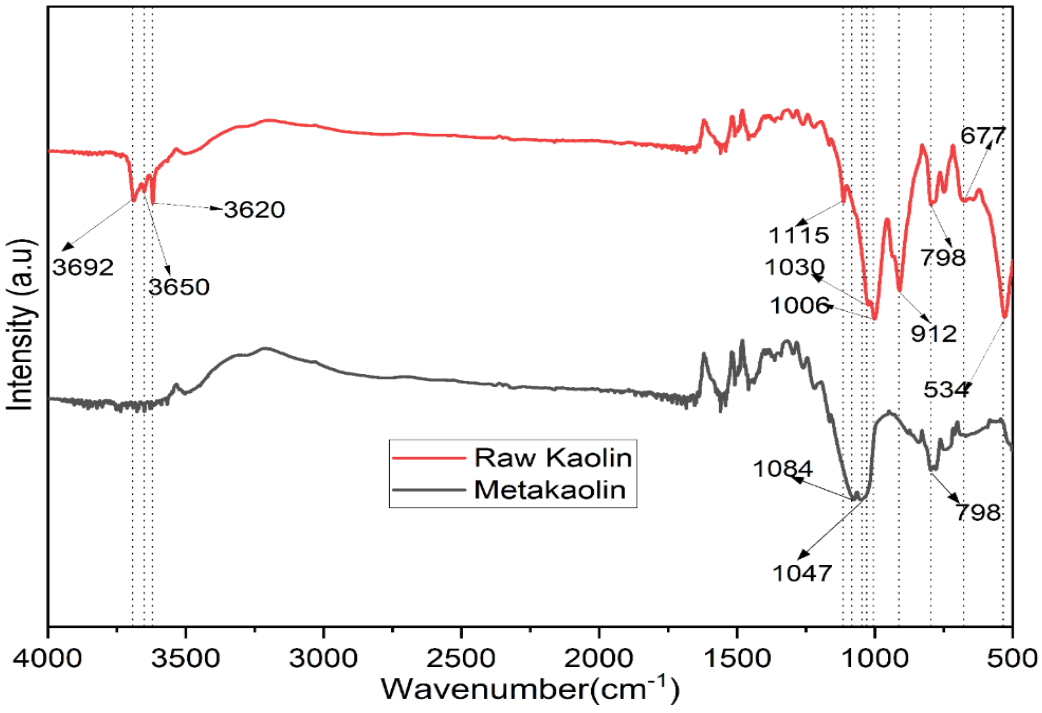

Figure 15: The FT-IR spectra for Raw Kaolin and Metakaolin

Table 15: The FT-IR Assignments of Kaolinite and Metakaolin

FTIR wavenumber (cm^{-1})	Assignment
3692, 3650 and 3620	OH stretching vibration (interlayer and inner layer)
1115, 1030 and 1006	Si-O stretching vibrations
912	Al-OH bending vibration
534	Si-O-Al bending vibration

4.2 Geopolymer Mortar Characterization and Compressive Strength Optimization

This section examines the characterization and optimization of compressive strength in geopolymer mortar. A range of characterization techniques, including compressive strength evaluation, microstructural examination, and durability testing, offer critical insights into the intrinsic behavior and long-term performance of geopolymer materials. These methods collectively facilitate a comprehensive understanding of the material's mechanical properties, structural integrity, and resistance to environmental degradation, thereby informing the development of more resilient geopolymer systems.

Concurrently, the optimization process focused on systematically investigating the influence of key mix design parameters—namely, the activator concentration, the sodium hydroxide to sodium silicate ratio, and the solution-to-binder ratio. By analyzing the effects of these variables, the study successfully tailored the composition of geopolymer mortars to maximize compressive strength under ambient curing conditions. This targeted approach underscores the importance of precise mix design control in enhancing the mechanical performance and practical applicability of geopolymer-based construction materials.

4.2.1 Mortar Density and Compressive Strength

The compressive strength and density of the mortar after 28 days of ambient curing exhibited considerable variation, ranging from 36.47 MPa to 74.17 MPa and from 2.3114 g/cm³ to 2.4501 g/cm³, respectively, as illustrated in Fig. 16. Figure 16. Among the tested formulations, GP8 demonstrated the highest compressive strength, while GP3 recorded the lowest. These results highlight the influence of mix composition on the mechanical and physical properties of the geopolymer mortar.

A strong linear correlation between density and compressive strength was identified, with a correlation coefficient (R^2) of 0.89, as depicted in Fig. 17. This relationship can be explained by the development of robust interparticle bonds within the matrix, which effectively reduce porosity. As the pore volume diminishes, the material's density increases, thereby enhancing

its load-bearing capacity and resulting in improved compressive strength. This finding underscores the critical role of microstructural densification in optimizing the mechanical performance of geopolymer mortars.

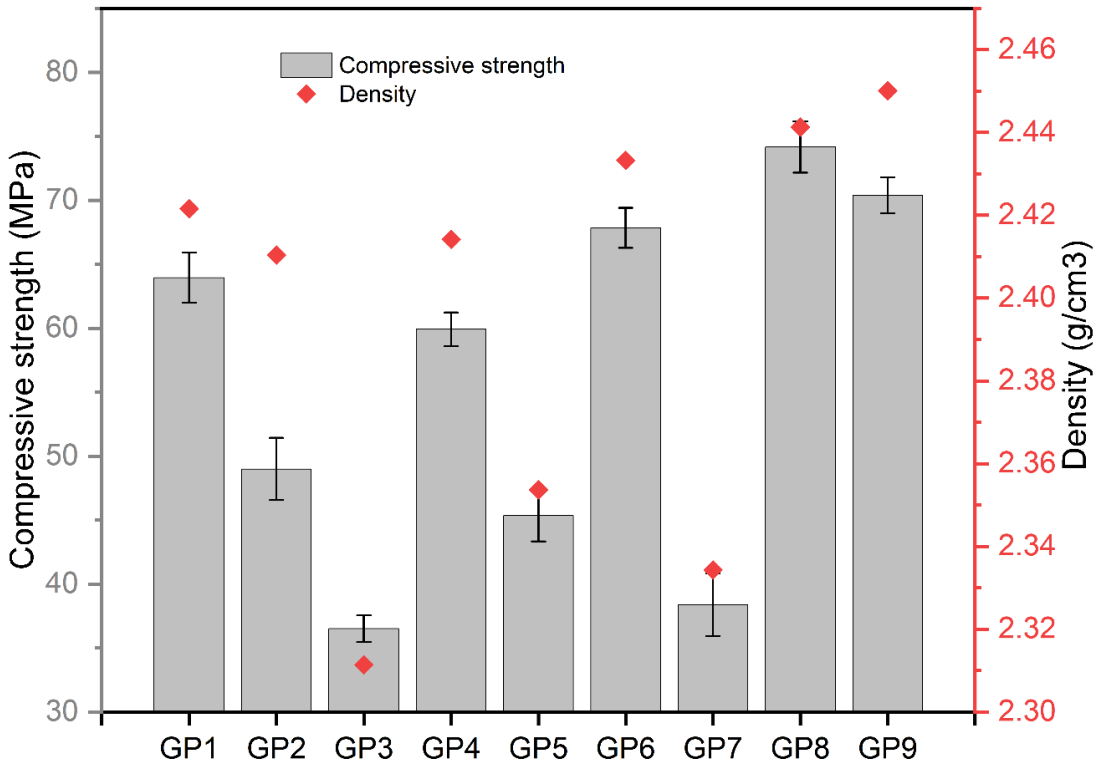

Figure 16: Mortar Compressive strength and density curve at 28 days

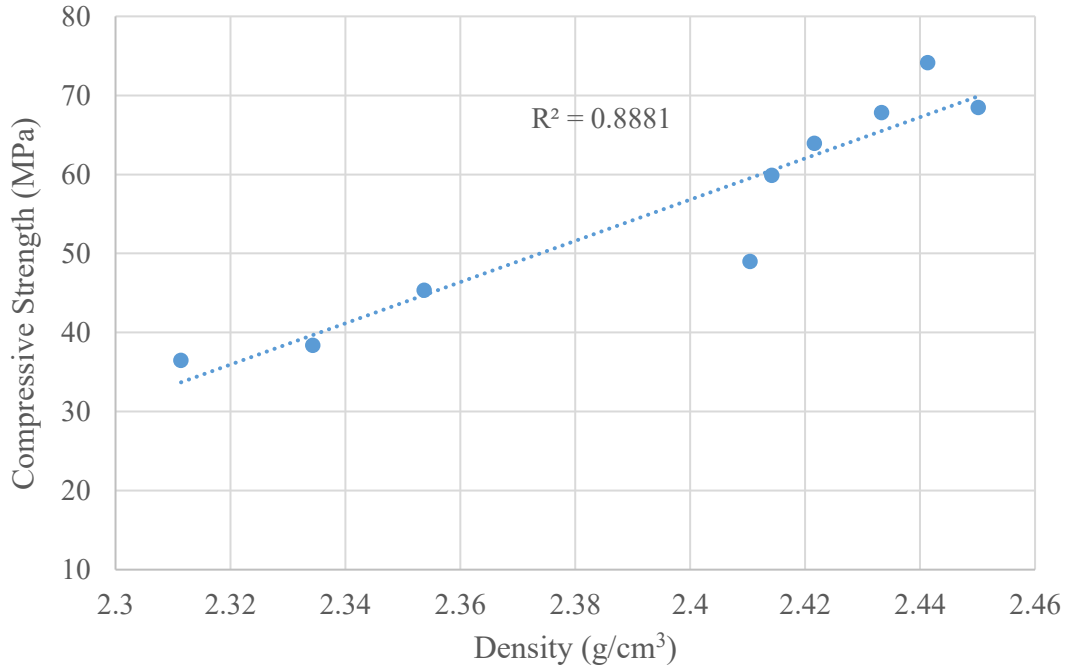

Figure 17: Density and compressive strength relationship curve

4.2.2 Selection of the Optimum Parameters

The selection of the optimal mix design parameters was guided by the objective of maximizing the compressive strength of the geopolymer mixture. This optimization was achieved by selecting the parameter set that corresponded to the highest mean signal-to-noise (S/N) ratio value, which serves as a robust indicator of performance consistency and strength enhancement. The influence of each mix design variable on compressive strength was systematically evaluated through analysis of the S/N ratio plots, as illustrated in Fig. 18 and Table 16.

From Fig. 18 and Table 16, it is evident that the combination of a sodium hydroxide concentration of 12 M, a sodium silicate-to-sodium hydroxide ratio of 2.5, and a solution-to-binder ratio of 0.6 produced the highest compressive strength values. Despite this favorable strength outcome, the mixture with a 0.6 solution-to-binder ratio exhibited considerable stiffness, resulting in poor workability. To address this practical limitation, the solution-to-binder ratio was adjusted to 0.8 while maintaining the other parameters at their optimized levels, thereby achieving a balance between mechanical performance and ease of handling.

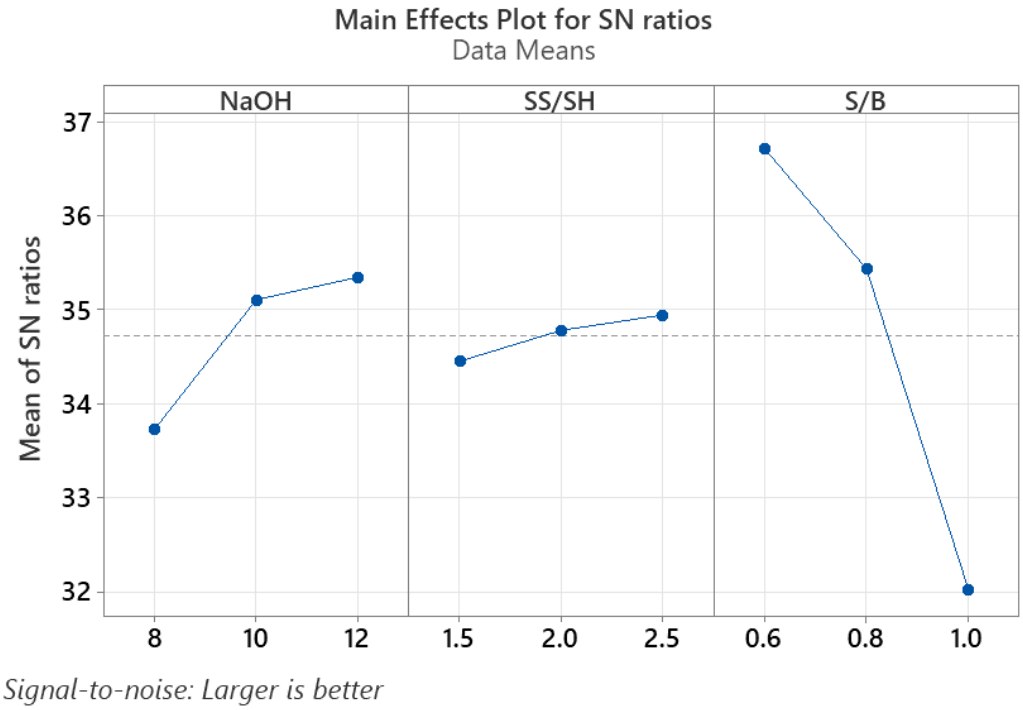

Figure 18: Mean of SN ratios of compressive strength

Table 16: Response table for S/N for compressive strength (Larger is better)

Levels	Factors		
	NaOH	SS/SH	S/B
1	33.72	34.45	36.72
2	35.10	34.78	35.43
3	35.35	34.94	32.02
Rank	**3**	**3**	**1**

4.2.3 Variance Analysis

An analysis of variance (ANOVA) was performed to evaluate the effect of each mix design parameter on the compressive strength of the geopolymer concrete. This statistical analysis was carried out using Minitab software, which enabled a rigorous assessment of the relative contributions of the variables within a 95% confidence interval. The detailed findings of this evaluation are summarized in Table 17, providing quantitative insights into the significance of each factor.

The results indicate that among the parameters studied, the solution-to-binder (S/B) ratio exerted the most pronounced impact on compressive strength enhancement. Specifically, the S/B ratio accounted for 85.15% of the total variation in strength, underscoring its critical role in optimizing the mechanical performance of the geopolymer mixture. This substantial contribution highlights the necessity of carefully controlling the S/B ratio during mix design to achieve superior compressive strength outcomes. The concentration of sodium hydroxide solution had the most considerable influence, at 13.12%, while the sodium silicate to sodium hydroxide ratio had the least impact, at 1.73%.

Table 17: Analysis of Variance for compressive strength

Source	Degree of freedom	Sum of squares	Mean squares	Percentage contribution (%)
NaOH	2	197.51	98.76	13.12
SS/SH	2	25.99	13	1.73
S/B	2	1282.33	641.16	85.15
Total	**6**	**1505.83**		**100**

4.2.4 Structure and Microstructure Investigation

The relationship between structure, microstructure, and the geopolymer mortar's performances were investigated using SEM and XRD, as presented in Fig. 19, 20, 21, 22 and 23. The formulations with lower and higher compressive strengths were used to study the relationship between microstructure and the compressive strength performance of the geopolymer specimens. The SEM images in Fig. 19 (a) indicate a loose microstructure for the formulation

with lower compressive strength (GP3). The micrographs also show partially reacted metakaolin and less gel formation, indicating incomplete geo-polymerization. The lack of a well-linked geopolymer network, as observed, may have led to lower strength due to insufficient particle bonding (Dai *et al*., 2022; Slaný *et al*., 2023). In contrast, formulations with high compressive strength (GP8 and GP9) showed denser and more homogenous matrices with significant interconnected gel formation (Fig. 19 (b) and (c)), which may have contributed to the high compressive strength (Dai *et al*., 2022; Ibrahim *et al*., 2023).

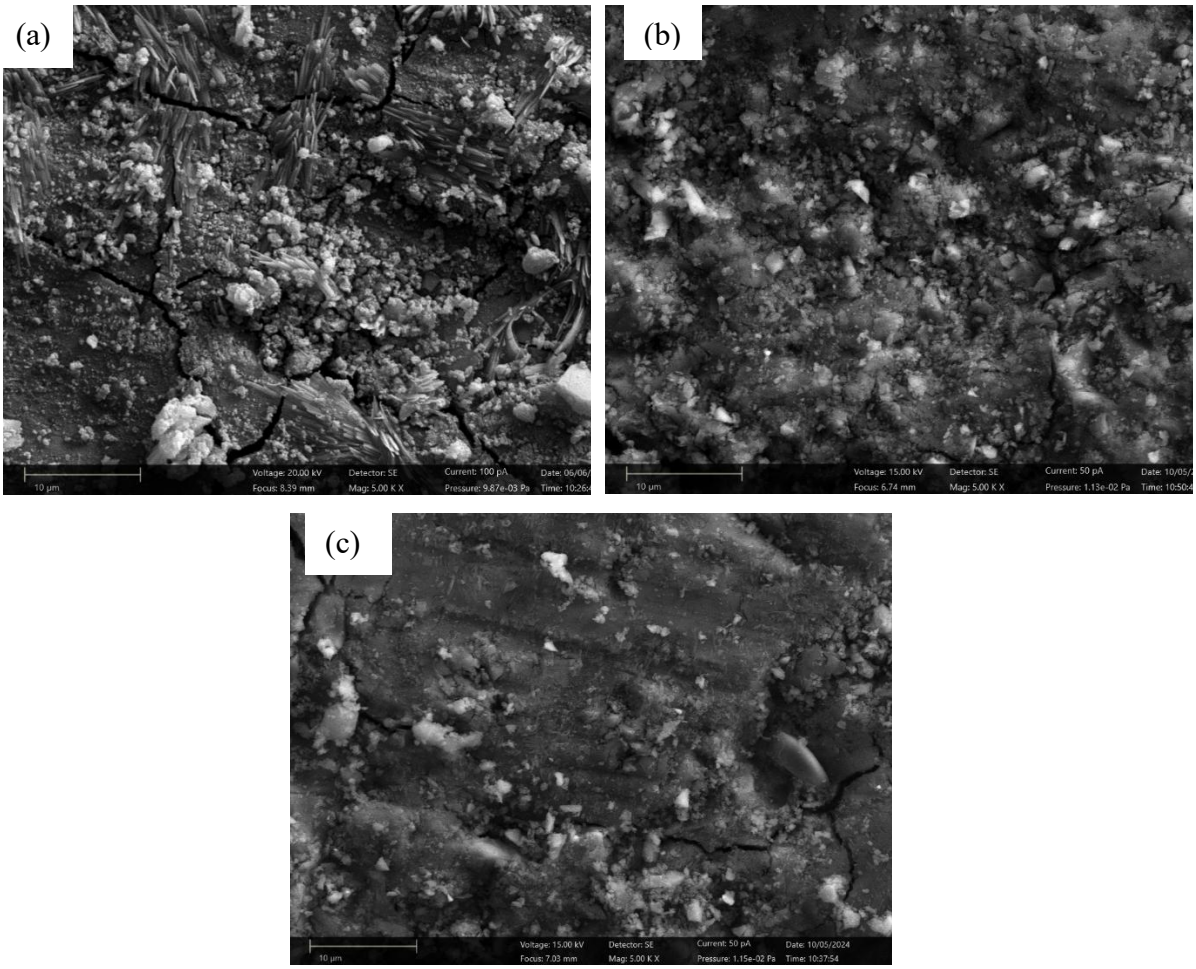

Figure 19: The SEM for (a) GP3 formulation, (b) GP8 formulation, and (c) GP9 formulation

The same formulations with lower and higher compressive strength (GP3, GP8 and GP9) were used in XRD phase analysis relating to the compressive strength performance of the geopolymer specimens. Both formulations showed the existence of quartz, albite, orthoclase and muscovite, as indicated in Fig. 20. The Rietveld refinement fitting curve of GP3, shown in Fig. 21, revealed a high amount of quartz (COD database code: 9009666) and a lower amount of albite (COD database code: 9009663) and orthoclase (COD database code: 9000311), as indicated in the quantification results in Table 18. In contrast, the Rietveld refinement fitting

curve for GP8 and GP9, as shown in Fig. 22 and 23, revealed a reduction in the amount of quartz and an increase in the amounts of albite and orthoclase, as presented in Tables 19 and 20. The increased albite and orthoclase may have provided additional reactive silica and alumina that would have enhanced the geopolymerization of metakaolin geopolymer at ambient temperature, leading to a compact aluminosilicate network (Rihan *et al*., 2024).

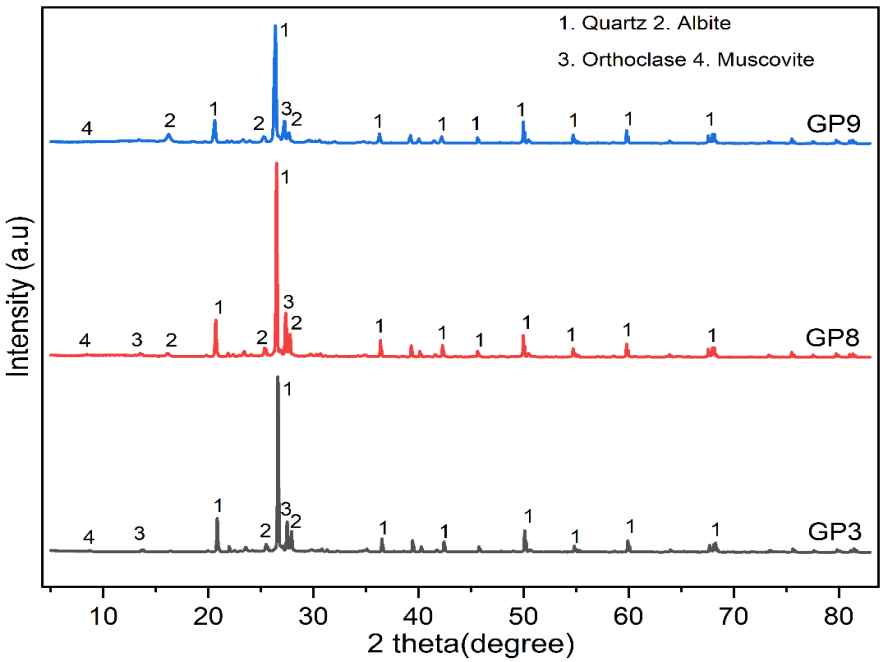

Figure 20: The XRD for the GP3, GP8 and GP9 formulations

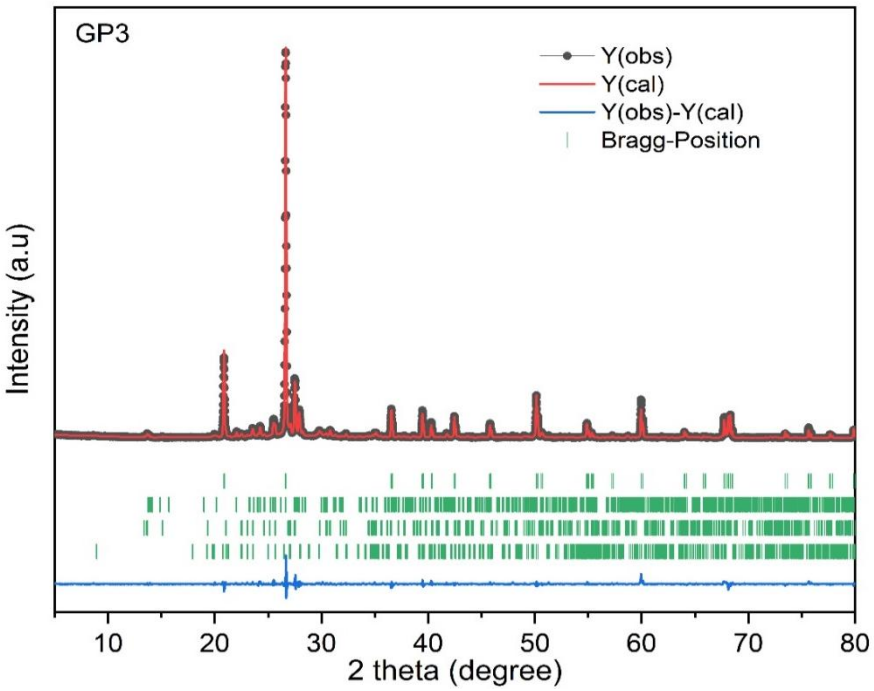

Figure 21: Rietveld refinement fitting curve for GP3 formulation

Table 18: Identifying phases in the GP3 formulation, corresponding chemical formulas and weight fractions

Mineral name	Chemical formula	Weight fractions%	COD ID	Reference
Quartz	SiO_2	38.1%	9009666	Gualtieri (2000)
Albite	$Na_{1.96}Ca_{0.04}Si_{5.96}Al_{2.04}O_{16}$	39.8%	9009663	Fabbri *et al*. (2013)
Orthoclase	$Si_{12}Al_4K_4O_{32}$	12.2%	9000311	Prince *et al*. (1973)
Muscovite	$K_4Al_{11.63}Si_{12.37}O_{40}$	9.9%	9001058	Guggenheim *et al*. (1987)

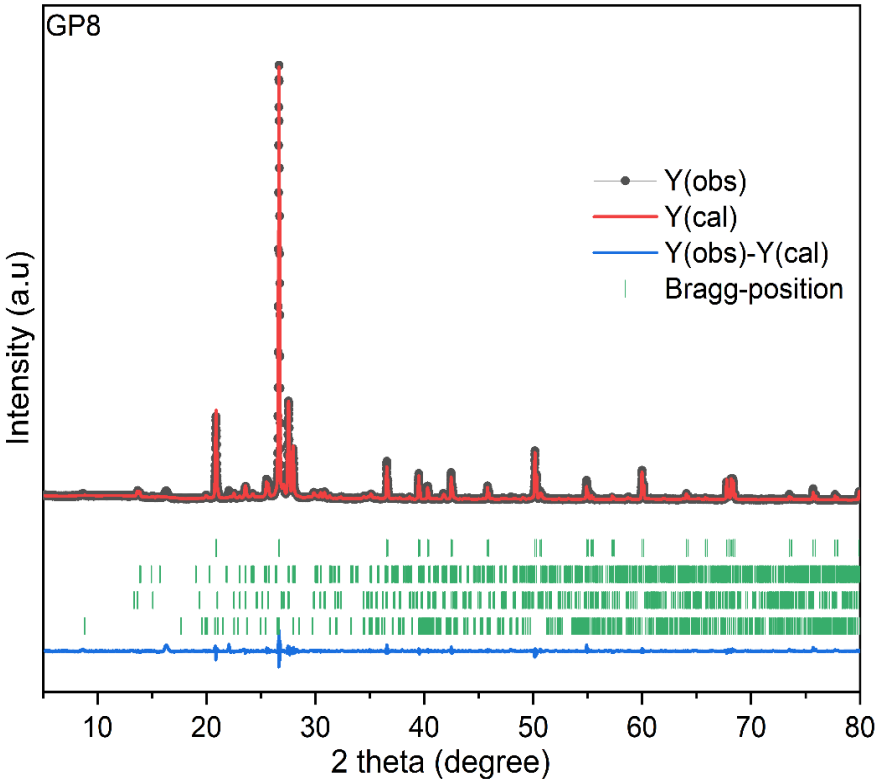

Figure 22: Rietveld refinement fitting curve for GP8 formulation

Table 19: Identifying phases in the GP8 formulation, corresponding chemical formulas, and weight fractions

Mineral name	Chemical formula	Weight fractions%	COD ID	Reference
Quartz	Si_6O_6	7.8%	9005019	Kihara (1990)
Albite	$Na_{1.96}Ca_{0.04}Si_{5.96}Al_{2.04}O_{16}$	54.1%	9009663	Gualtieri (2000)
Orthoclase	$K_4Si_{12}Al_4O_{32}$	38.0%	1011205	Chao *et al*. (1940)
Muscovite	$K_4Al_{11.63}Si_{12.37}O_{40}$	0.1%	9001058	Guggenheim *et al*. (1987)

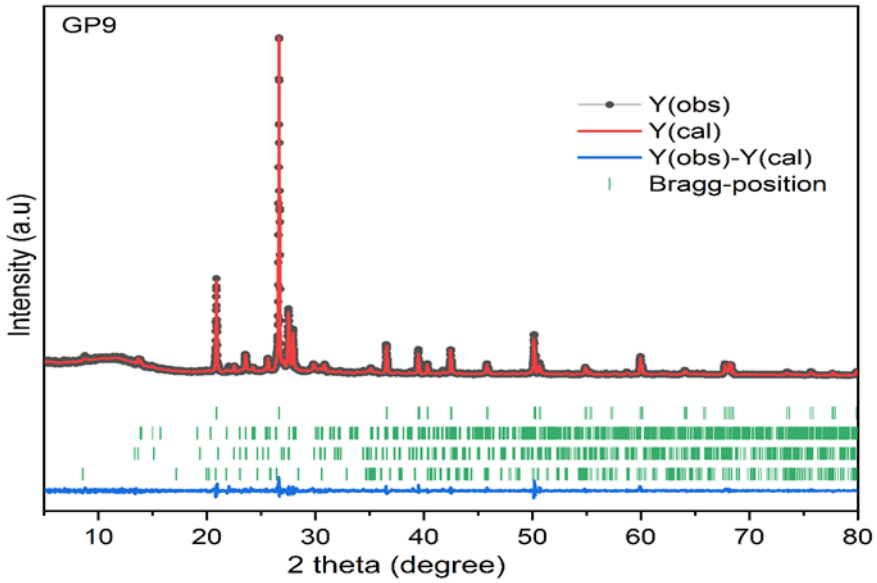

Figure 23: Rietveld refinement fitting curve for GP9 formulation

Table 20: Identifying phases in the GP9 formulation, corresponding chemical formulas and weight fractions

Mineral name	Chemical formula	Weight fractions%	COD ID	Reference
Quartz	SiO_2	13.3%	9012600	Hazen *et al*. (1989)
Albite	$Na_{1.96}Ca_{0.04}Si_{5.96}Al_{2.04}O_{16}$	51.4%	9009663	Gualtieri (2000)
Orthoclase	$Si_{12}Al_4K_4O_{32}$	33.3%	9000311	Prince *et al*. (1973)
Muscovite	$K_3Al_9Si_9O_{36}$	2.0%	9014604	GÜVEN *et al*. (1967)

4.3 Heat Resistance Assessment

Figure 24 shows images of geopolymer specimens exposed at different temperatures, as indicated in each image. A continuous color change is observed in all specimens with some minor cracks, where the concentration of the cracks increases with an increase in exposure temperature and is much more visible at exposure of more than 600°C. From visual inspection, it can be noted that the OPC specimens were dramatically affected by elevated temperatures as more micro-cracks were formed, as shown in Fig. 25.

Figure 24: Images of geopolymer specimens after exposure to elevated temperatures

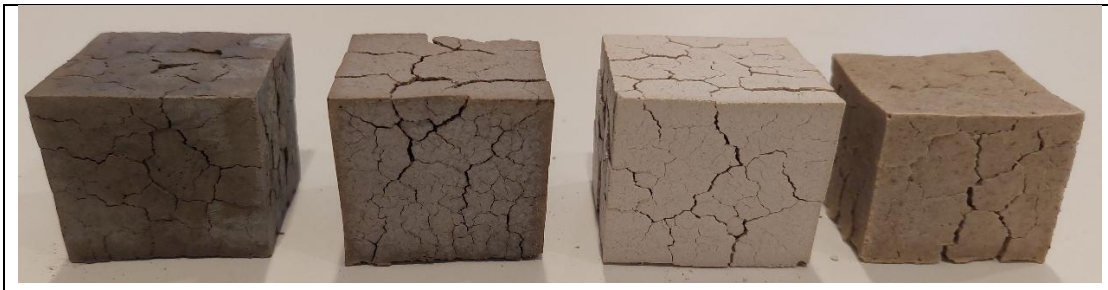

Figure 25: Images of OPC specimens after exposure to elevated temperatures

The compressive strength of the geopolymer cured at 200°C reached 79.14 MPa, representing a 15.57% improvement compared to the ambient-cured counterpart. This enhancement in mechanical performance following exposure to elevated temperature is likely due to the accelerated polymerization reactions facilitated by the heat, which may not fully occur under ambient conditions. Such temperature-induced activation of the geopolymerization process has been similarly observed and documented in previous studies, highlighting the critical influence of curing temperature on the development of the material's structural integrity (Cai *et al*., 2022; Khan *et al*., 2020; Lahalle *et al*., 2021; Ouda *et al*., 2021; Tahwia *et al*., 2023).

The reduction in compressive strength observed at intermediate temperatures of 400°C and 600°C was measured at 31.52% and 33.89%, respectively, indicating a relatively moderate decline compared to the more pronounced strength losses occurring at temperatures exceeding 600°C. At elevated temperatures of 800°C and 1000°C, the compressive strength diminished

drastically by 64.81% and 83.71%, respectively. This significant deterioration is primarily attributed to the increased formation of micro-cracks within the material's matrix, as evidenced by microstructural observations illustrated in Fig. 24, which compromise the integrity and load-bearing capacity of the geopolymer.

Moreover, the pronounced strength loss at higher temperatures correlates with notable weight reduction (depicted in Fig. 26) and thermal deformation caused by the evaporation of structural water during heat exposure. The degradation process is further compounded by phase transformations, including the emergence of sanidine, chrysotile, and nepheline, as confirmed through X-ray diffraction analysis presented in Fig. 28. These mineralogical changes contribute to the weakening of the geopolymer's microstructure, thereby exacerbating the decline in mechanical performance under extreme thermal conditions.

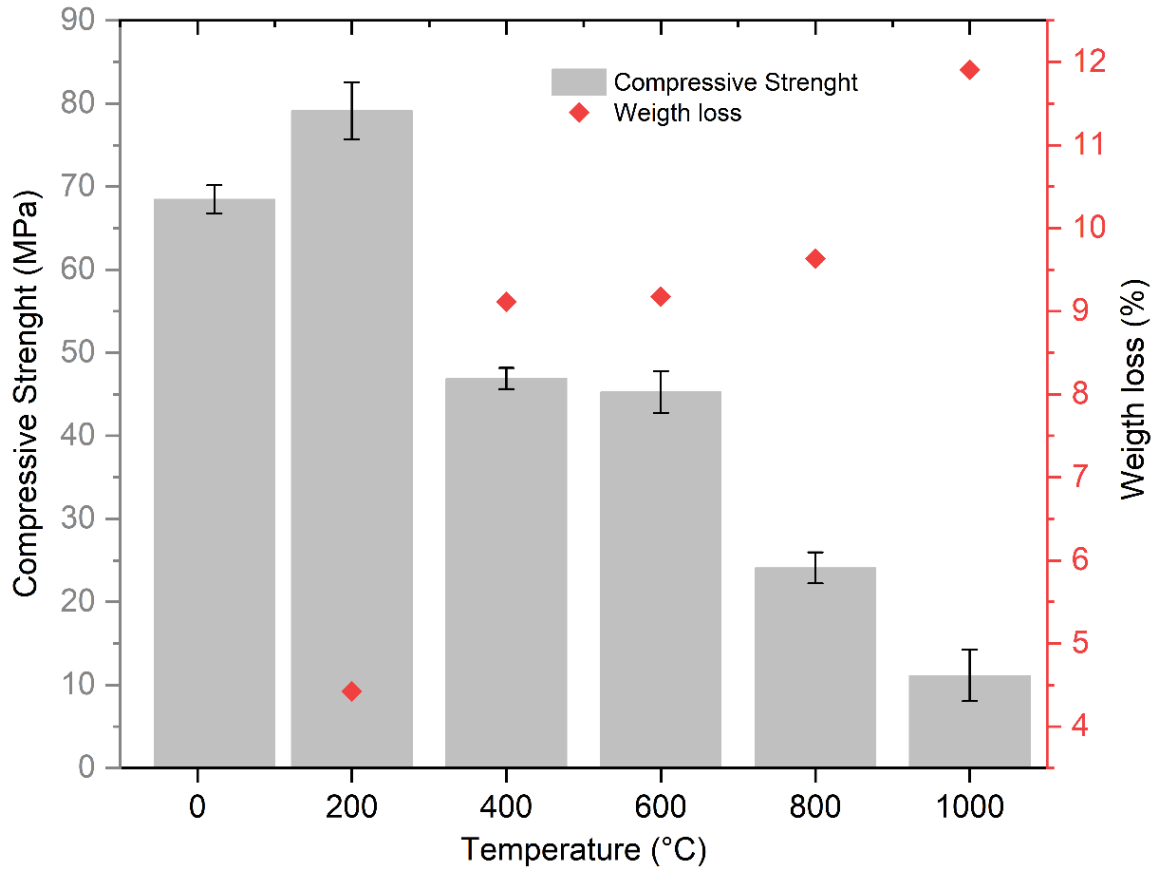

Figure 26: Effect of firing temperature on compressive strength and weight loss

Figure 27 illustrates the water absorption of geopolymer specimens exposed to varying temperatures. It is observed that water absorption was lower (4.62%) for specimens exposed to a temperature of 200°C than for those tested at ambient temperature (5.45%). This effect may be due to the improved polymerization reaction, which results in a denser structure, thereby reducing pores. The increase in water absorption for the geopolymers exposed to temperatures

exceeding 200°C may be due to the filling of pores produced by the heating effect in the specimens. The observed behavior is correlated with the compressive strength behavior, as shown in Fig. 26.

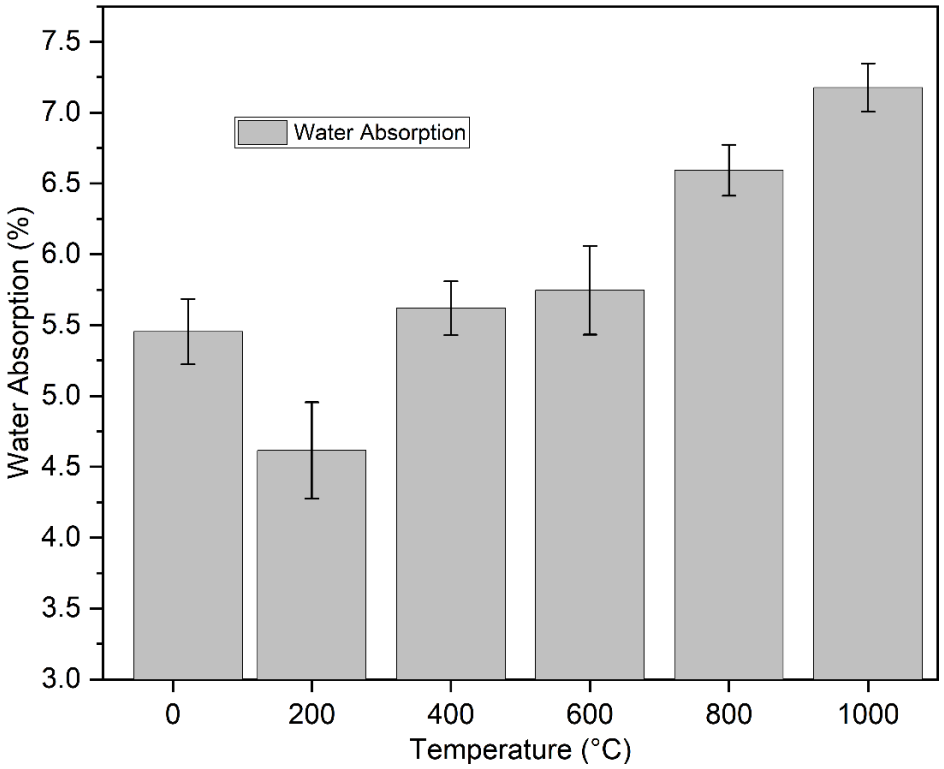

Figure 27: Water absorption at different temperature exposures

Figure 28 shows the XRD pattern for the unexposed and heat-exposed geopolymer at different temperatures. The predominant phases in the specimens at ambient temperature are quartz (COD database code: 9013321), albite, and orthoclase. The same phases were found in the specimens exposed to 200°C, but a reduction in the percentage of quartz as quantified by the FullProf method was reduced, and an increase in the amount of albite (COD database code: 9009663) and orthoclase (COD database code: 9000161) was realized. After the exposure above 200°C, other crystalline phases like sanidine (COD database code: 9004245), chrysotile (COD database code: 1010960), and nepheline (COD database code: 9004995) were formed. Chrysotile fibers act as stress concentrators, creating weak planes that compromise structural stability, especially under thermal stress (Lee *et al*., 2021). The nepheline phase formed may have remained unreacted and acted as the weak filler, reducing the mortar's strength. The formation of these phases was also observed in other studies when geopolymers were subjected to high temperatures (Kim *et al*., 2021; Kljajevic *et al*., 2022; Liu *et al*., 2020).

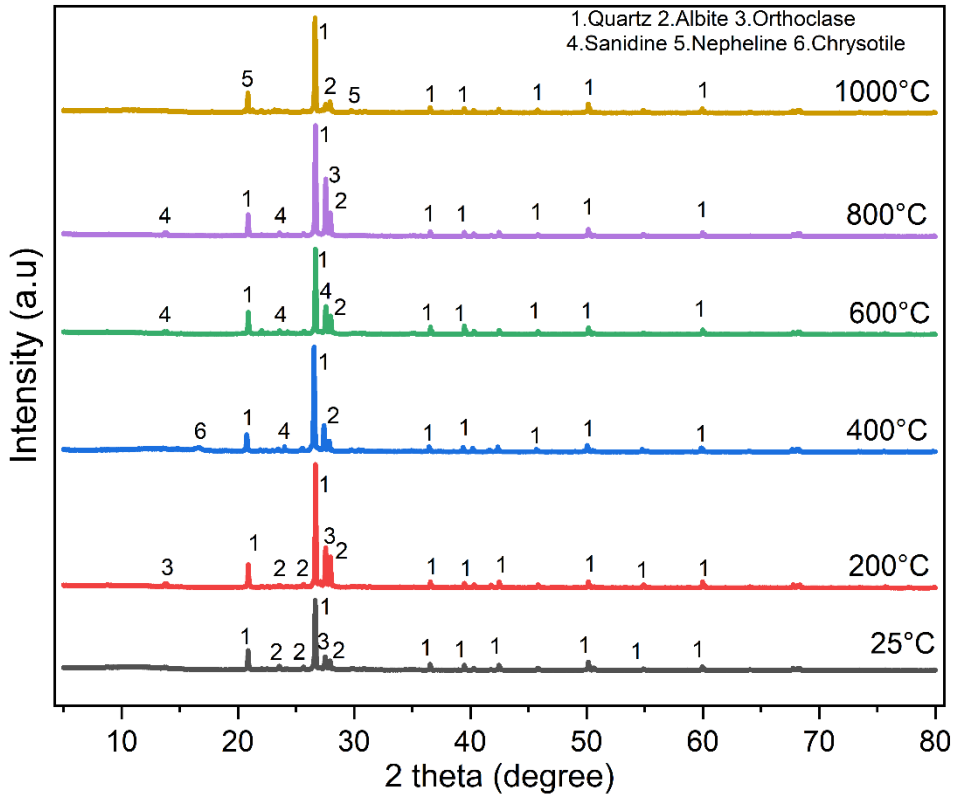

Figure 28: The XRD for heat-exposed and non-exposed geopolymer

4.4 Effect of Rice Husk Ash on Geopolymer Performance

This section reports the effect of rice husk ash (RHA) on the performance of geopolymer materials, highlighting its potential as a supplementary pozzolanic material. The section documents how varying proportions of RHA influence key performance indicators, such as compressive strength and durability, of the metakaolin-based geopolymer.

4.4.1 The influence of rice Husk ash on Compressive Strength

Figure 30 illustrates the compressive strength behavior of the metakaolin-rice husk ash (RHA) geopolymer blend as a function of the RHA replacement level. The data indicate that compressive strength increases progressively with the incorporation of RHA up to a substitution level of 15%, suggesting an enhancement in the material's mechanical properties within this range. However, beyond this threshold, a decline in compressive strength is observed, with the geopolymer blend demonstrating markedly reduced performance. Notably, when the RHA content exceeds 20% replacement of metakaolin, the blend exhibits plastic deformation characteristics accompanied by significantly diminished strength, indicating a loss of structural integrity and mechanical robustness at higher replacement levels (Borges *et al*., 2016; Hamada *et al*., 2025). The plastic behavior and low strength may be due to higher levels

of silica that might have disrupted the optimum balance of the reactive phase for effective geo-polymerization. Additionally, the plastic behavior may have led to an incomplete polymerization reaction, resulting in low strength and higher deformation under compressive loads (Borges *et al*., 2016; Zhu *et al*., 2019).

Conversely, the SEM images in Fig. 29 for the metakaolin-RHA geopolymer blend show the effect of varying rice husk ash (RHA) content from 0% to 30%, providing valuable insights into the microstructural changes that directly impact compressive strength. At 0% RHA, the images reveal a compact and homogenous microstructure, indicating strong inter-particle bonding associated with high compressive strength. As the RHA content increases to 15%, the SEM images reveal a favorable distribution of RHA particles, which enhances the formation of geopolymer gels, thereby improving overall cohesion and mechanical performance. Beyond a 15% replacement level of rice husk ash (RHA), microstructural images reveal a pronounced increase in irregular particle distribution, which is likely due to the lower density and weaker bonding characteristics of the RHA particles within the matrix. This deterioration in structural uniformity is directly associated with a notable decline in compressive strength, as evidenced by the data presented in Fig. 30. The compromised particle arrangement adversely affects the integrity of the geopolymer composite, thereby reducing its mechanical performance at higher RHA substitution levels.

GPR1

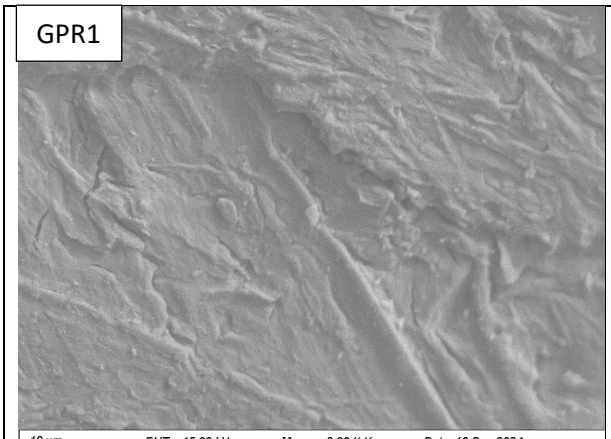

GPR2

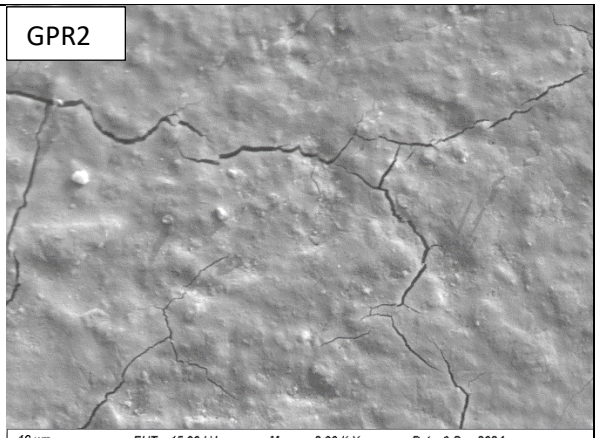

GPR3

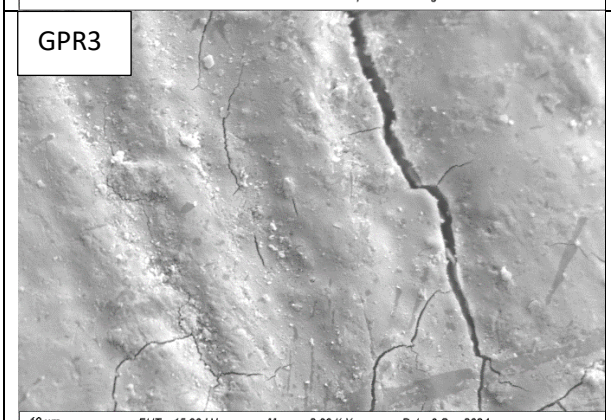

GPR4

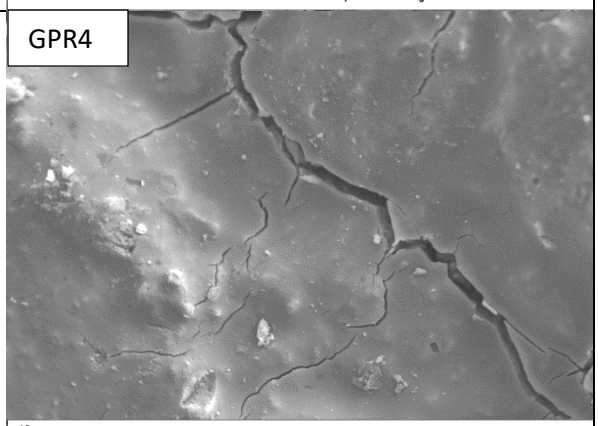

GPR5

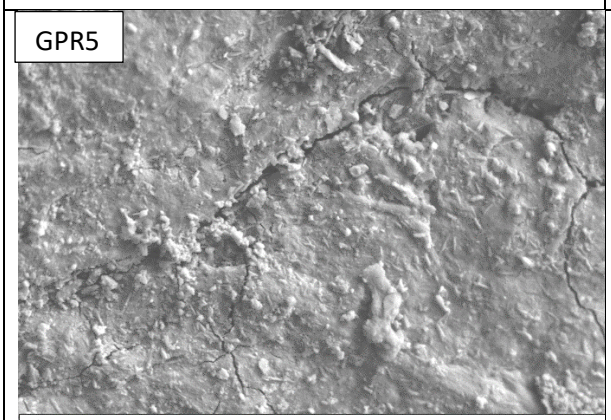

GPR6

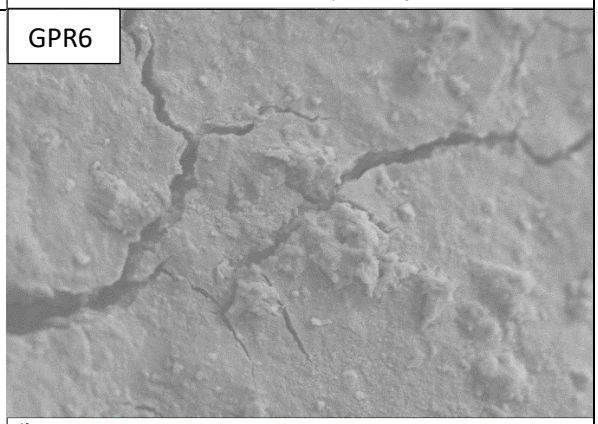

GPR7

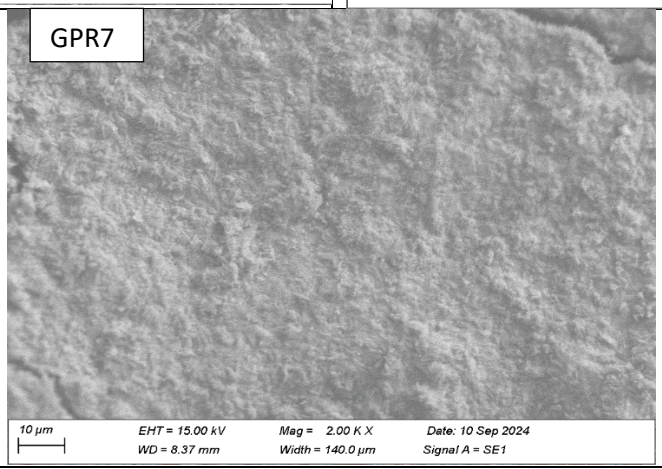

Figure 29: The SEM for the different Metakaolin-RHA blend geopolymer

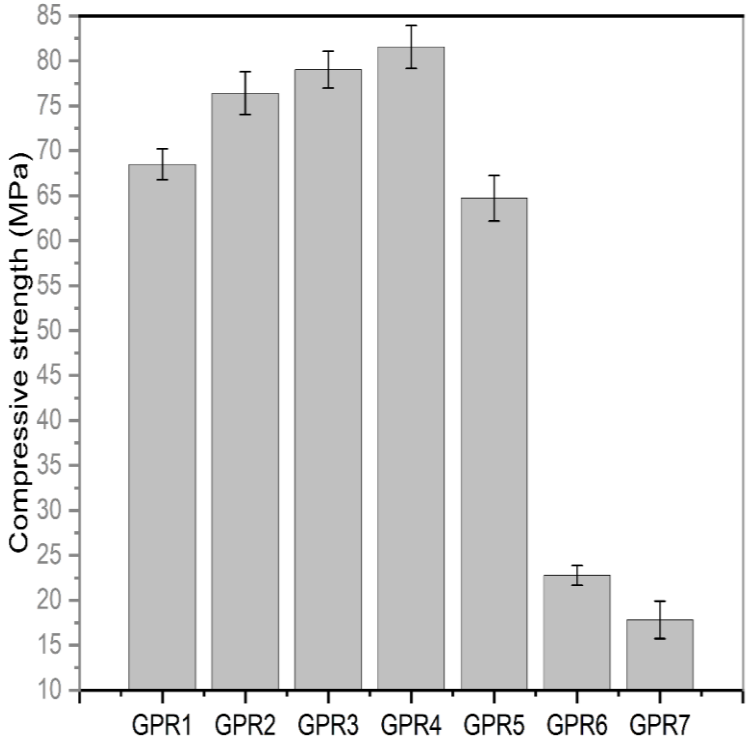

Figure 30: Compressive strength of Metakaolin-RHA blend geopolymer

Table 21: Compressive strength comparison of different metakaolin geopolymer mortars

Source material	28days Compressive Strength (MPa)	Curing Condition	Reference
100MK	68.5	Ambient curing	This study
85MK15RHA	82.7	Ambient curing	This study
40MK40SG20POFA	52.0	80°C for 2 h	Aboshia *et al*. (2017)
20PC80MK	25.0	60°C for 72 h	Wianglor *et al*. (2017)
96FA4NMK	52.8	70°C for 24 h	Kaur *et al*. (2018)
50GBFS50MK	58.9	Ambient curing	Hasnaoui *et al*. (2019)
80MK20RHA	56.2	50°C for 28 d	Zhu *et al*. (2019)
70MK30GBFS	75.9	Ambient curing	Chen *et al*. (2021b)
50MK50SG	52.3	Ambient curing	Khalil *et al*. (2020)
10MK90PC	49.1	3 d wet curing	Dong *et al*. (2022)
100MK	17.8	Ambient curing	dos Reis Ferreira *et al*. (2024)
100MK	40.0	Ambient curing	Taborda-Barraza *et al*. (2024)
100MK	34.8	70 °C for 28 d	Aouan *et al*. (2021)
50MK50RPP	57.5	Ambient curing	Liu *et al*. (2023)
50MK50RCP	50.0	Ambient curing	Liu *et al*. (2023)

MK: Metakaolin, RHA: Rice husk Ash, POFA: Palm Oil fuel Ash, PC: Portland cement, NMK: Nano-Metakaolin, FA: Fly Ash, GBFS: Ground Blast Furnace Slag, RPP: recycled paste powder, RCP: recycled concrete powder

Comparative studies listed in Table 21 show the compressive strength of the metakaolin geopolymer mortar made from metakaolin and other metakaolin replacement materials. The studies indicate that numerous variables, including the alkali activator's concentration level, the precursor's composition, the curing conditions and the additives, affect the compressive strength of geopolymer mortar. Studies demonstrate that optimizing NaOH molarity (8–14 M) and Na_2SiO_3/NaOH ratios (1.5–2.5) enhances geopolymerization, yielding strengths of 40–65 MPa (Chen *et al*., 2021b; Kaur *et al*., 2018; Zhu *et al*., 2019). Blending precursors such as fly ash (FA), metakaolin (MK), and ground granulated blast-furnace slag (GGBS) improves performance, with FA-GGBS mixes achieving compressive strengths of 50–70 MPa (Dong *et al*., 2022) and MK-based mortars exhibiting early strength gains (Hasnaoui *et al*., 2019). Heat curing (60–80 °C for 24–48 h) significantly enhances low-Ca systems, increasing strength by 20–30% compared to ambient curing (Aboshia *et al*., 2017; Khalil *et al*., 2020).

Additives like nano-silica (2–5%) refine pore structures, enhancing strength by 15–25% (dos Reis-Ferreira *et al*., 2024), while fibers (e.g., basalt) improve ductility without compromising strength (Taborda-Barraza *et al*., 2024). Sustainability-driven mixes using industrial by-products (e.g., rice husk ash) achieve 40–60 MPa but require careful dosing to avoid silica-induced brittleness (Wianglor *et al*., 2017). When recycled concrete powder (RCP) and paste powder (RPP) are used as a replacement for metakaolin up to 50%, they significantly enhance the strength of blended geopolymer mortar due to their hydration products, which can participate in new polymerization reactions and contribute to strength development. When the substitution exceeds 50%, a reduction in strength occurs because the RCP and RPP have low reactivity, resulting in unreacted particles in the formulation (Liu *et al*., 2023).

4.4.2 Influence of rice Husk ash on Rapid Chloride permeability Resistance of the Geopolymer

The rapid chloride permeability test is one of the efficient ways to evaluate the covering protection of reinforcement against exposure to marine or de-icing salt environments. The standardized test measures the total electrical charge passed on a specimen over a specified duration. The lower the charge value, the better the resistance of the specimens against exposure to the marine environment or de-icing salt exposure.

As seen fromTable 22, the coulomb value for OPC mortar is higher at 28 days and 56 days of curing compared to geopolymer specimens. The weak OPC against chloride penetration compared to geopolymer mortar was also observed in the study on the durability properties of

geopolymer mortar containing slag (Bingöl *et al*., 2020). The enhanced performance observed in the geopolymer system can be attributed to its inherently denser microstructure and superior chemical stability when compared to ordinary Portland cement (OPC). These characteristics contribute to improved durability and resistance against aggressive agents. Notably, a reduction in the measured charge value is evident as the proportion of rice husk ash (RHA) in the mix increases, which signifies an enhanced resistance to chloride ion penetration. This trend underscores the beneficial role of RHA in mitigating the ingress of deleterious ions that typically compromise concrete durability.

Supporting evidence from prior studies indicates that RHA is rich in amorphous silica, a reactive component that facilitates the generation of additional aluminosilicate gel within the geopolymer matrix. The formation of this gel contributes to the refinement of the pore structure, effectively reducing overall permeability. Consequently, the denser and less permeable microstructure impedes chloride transport, leading to lower coulomb charge values and enhanced durability performance. This mechanism highlights the critical function of RHA in improving the long-term resistance of geopolymer concrete to chloride-induced deterioration (Sadrmomtazi *et al*., 2021; Thirukumaran *et al*., 2023).

Table 22: Rapid Chloride Permeability Results

Sample ID	28-day Chloride Permeability		56-day Chloride Permeability	
	Charge (C)	Remark	Charge (C)	Remark
OPC	5084	H	1570	L
GPR1	1443	L	914	VL
GPR2	924	VL	460	VL
GPR3	863	VL	305	VL
GPR4	669	VL	289	VL

Definitions H: High M: Medium L: Low VL: Very Low

4.4.3 Influence of Rice Husk Ash on Acidic Resistance of the Geopolymer

The influence of rice husk ash on acidic resistance is presented in Fig. 31. A moderate loss in strength was observed at 15-20% RHA for 28 and 56 days of acidic immersion. The increased acidic resistance could result from the geopolymer's reaction with sulphuric acid, which can create protective layers that prevent further deterioration; decreased porosity as RHA fills in the mortar matrix's voids; and the additional silica in RHA, which promotes silicate hydrate (C-S-H) gel formation and increases overall durability against acidic attacks (Das *et al*., 2022; Rihan *et al*., 2025).

A high loss in compressive strength is observed below 15% and above 20% RHA inclusion, primarily due to the insufficient reactive silica available to participate in the pozzolanic reaction with calcium. Excessive RHA often results in unreacted particles within the mixture, contributing to a less dense matrix (Rihan *et al*., 2025). This increase in porosity enables higher permeability, rendering the geopolymer more susceptible to acid ingress and environmental degradation. After 56 days of immersion, the samples with more than 20% RHA lost shape, and their compressive strength couldn't be measured. Other research indicates that after 56 days of immersion, the ability to measure compressive strength becomes severely compromised, particularly in samples with excessive RHA content (Rathee *et al*., 2024). Prolonged acidic exposure leads to significant degradation of the microstructure, characterized by the dealumination of the aluminosilicate gel network; this weakens the bonds between particles, resulting in a less cohesive structure (Bakharev, 2005; Rathee *et al*., 2024).

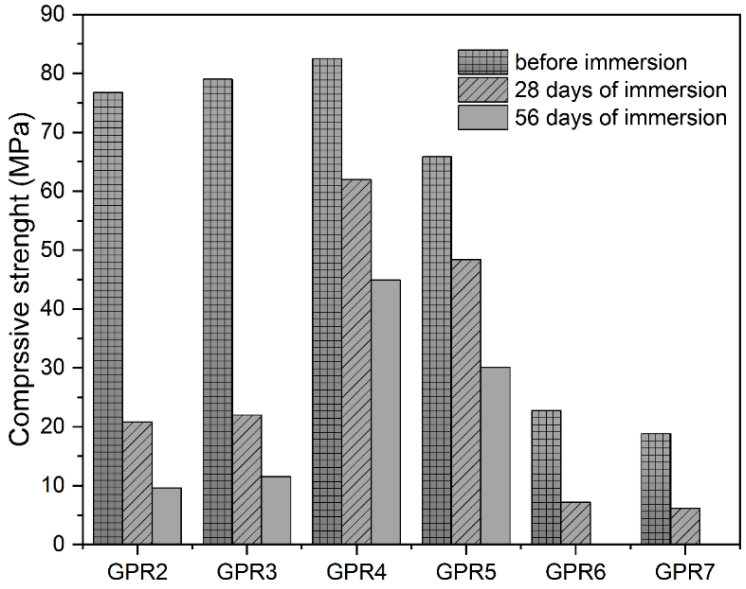

Figure 31: Compressive strength of Metakaolin-RHA blend geopolymer before and after acidic immersion

CHAPTER FIVE

CONCLUSION AND RECOMMENDATIONS

5.1 Conclusion

This study produced highly reactive metakaolin from kaolinite clay and adopted it for synthesizing metakaolin-based geopolymer mortar. The effect of calcination temperature (650-850°C), heating rate (1-19°C/min), and soaking time (1-12 h) in maximizing the pozzolanic reactivity of metakaolin was experimentally studied using surface response methodology. Metakaolin was the primary precursor in producing metakaolin-based geopolymer by optimizing the mixing ingredients. Using Taguchi design, three factors: the concentration of sodium hydroxide solution (NaOH: 8-12M), the ratio of the Na_2SiO_3 to NaOH (SS/SH-1.5-2.5), and the solution to binder ratio (S/B-0,6-1.0) were adopted in optimizing the process to enhance mechanical properties. The optimized specimen was then experimentally studied against heat resistance. Enhancing mechanical and durability was taken as the key aspect of the study, whereby different percentages of RHA (5-30% RHA) were incorporated in the optimized mixture to produce a metakaolin-RHA geopolymer blend, which was tested against compressive strength, rapid chloride permeability resistance, and acidic resistance. The test results and analysis done from this study suggest the following conclusions;

(i) Pozzolanic reactivity increases as the temperature rises from 650°C to 765°C and then declines as the temperature increases further. The temperature of 765°C, at a rate of 10°C/min, and 6.46 h of soaking were the optimum conditions to yield the highly reactive metakaolin. The pozzolanic reactivity at this optimum condition was 1382.15 mg $Ca(OH)_2$/g.

(ii) Compressive strength was observed to increase with higher sodium hydroxide concentration, an elevated sodium silicate to sodium hydroxide (SS/SH) ratio, and a reduced solution-to-binder (S/B) ratio. The optimal compressive strength was achieved at a sodium hydroxide concentration of 12 M, an SS/SH ratio of 2.5 and an S/B ratio of 0.6. However, the mixture corresponding to the 0.6 solution-to-binder ratio exhibited excessive stiffness and poor workability, posing practical challenges during handling and placement. Consequently, to balance mechanical performance with ease of application, the S/B ratio was adjusted to 0.8 while maintaining the other parameters at

their optimized levels. This adjustment ensured a workable mix without significantly compromising the compressive strength.

(iii) Incorporating 15% RHA in metakaolin-based geopolymer improved mechanical properties and enhanced durability against rapid chloride permeability.

(iv) Although the 5% H_2SO_4 immersion showed a tremendous deterioration of compressive strength, especially at long-term (56 days) exposure, it was still much better than metakaolin-based geopolymer alone, except at higher values (beyond 20% RHA), which resulted in volumetric change and destruction of the specimen.

5.2 Recommendations

The study of metakaolin-based geopolymers has gained significant traction due to their potential as sustainable alternatives to traditional cement-based materials. Following the categorical investigation done in this study, the need to advance the mechanical and enhance durability properties is strategically crucial. Hence, the following recommendations are worth sharing:

(i) A systemic method of improving workability at low values of the alkaline solution-to-binder ratio is highly recommended to facilitate easier handling, mixing, and placement, ultimately leading to better overall performance and durability of the metakaolin-based geopolymer.

(ii) A comparative study of rice husk ash (RHA) and nano-silica as additives for enhancing the durability of metakaolin-based geopolymers is warranted. A hybrid approach that combines both additives may also be explored to leverage their complementary benefits. Research should evaluate the optimal mass fraction for improved performance.

(iii) Techno-economic analysis and life cycle assessment: Implementing life cycle assessments for metakaolin-based geopolymers can provide valuable insights into their environmental impacts compared to conventional materials. This evaluation should encompass energy consumption, carbon footprint, and resource utilization throughout the production and application phases.

(iv) Accelerating the application of metakaolin-based geopolymer requires a better understanding of many properties to determine its viability in construction and engineering applications. Exploring the incorporation of fibers (e.g., steel, glass or synthetic fibers) is also recommended to improve metakaolin geopolymers' tensile strength and toughness.

REFERENCES

Abbas, R., Khereby, M. A., Ghorab, H. Y., & Elkhoshkhany, N. (2020). Preparation of geopolymer concrete using Egyptian kaolin clay and the study of its environmental effects and economic cost. *Clean Technologies and Environmental Policy*, 2020, 1-19.

Abiodun, Y. O., Olanrewaju, O. A., Gbenebor, O. P., Ochulor, E. F., Obasa, D. V., & Adeosun, S. O. (2022). Cutting Cement Industry CO_2 Emissions through Metakaolin Use in Construction. *Atmosphere*, *13*(9), 1494. https://doi.org/10.3390/atmos13091494

Aboshia, A. M. A., Rahmat, R. A., Zain, M. F. M., & Ismail, A. (2017). Enhancing mortar strengths by ternary geopolymer binder of metakaolin, slag and palm ash. *International Journal of Building Pathology and Adaptation*, *35*(5), 438-455.

Adewumi, A. A., Ariffin, M. A. M., Yusuf, M. O., Maslehuddin, M., & Ismail, M. (2021). Effect of sodium hydroxide concentration on strength and microstructure of alkali-activated natural pozzolan and limestone powder mortar. *Construction and Building Materials*, *271*, 121530.

Aiken, T. A., Kwasny, J., & Sha, W. (2020). Resistance of fly ash geopolymer binders to organic acids. *Materials and Structures*, *2020, 53*, 1-18.

Akintunde, A. M., Ajala, S. O., & Betiku, E. (2015). Optimization of Bauhinia monandra seed oil extraction via artificial neural network and response surface methodology: A potential biofuel candidate. *Industrial Crops and Products*, *67*, 387-394.

Al Obeidy, N. F., Khalil, W. I., & Ahmed, H. K. (2024). Optimization of local modified metakaolin-based geopolymer concrete by Taguchi method. *Open Engineering*, *14*(1), 20220561.

Alcántara, J., De la Fuente, D., Chico, B., Simancas, J., Díaz, I., & Morcillo, M. (2017). Marine atmospheric corrosion of carbon steel: A review. *Materials*, *10*(4), 406.

Almutairi, A. L., Tayeh, B. A., Adesina, A., Isleem, H. F., & Zeyad, A. M. (2021). Potential applications of geopolymer concrete in construction: A review. *Case Studies in Construction Materials*, *15*, e00733. https://doi.org/10.1016/j.cscm.2021.e00733

Alzeebaree, R., Mawlod, A. O., Amen, D. K., Younis, K. H., & Mohammedameen, A. (2021). *Fire Resistance Performance of Fiber Reinforced Geopolymer Concrete. In E3S Web of Conferences (Vol. 318, p. 03003)*. https://scholar.google.com

Amran, M., Debbarma, S., & Ozbakkaloglu, T. (2021a). Fly ash-based eco-friendly geopolymer concrete: A critical review of the long-term durability properties. *Construction and Building Materials*, *270*, 121857.

Amran, M., Fediuk, R., Murali, G., Vatin, N., Karelina, M., Ozbakkaloglu, T., Krishna, R., Sahoo, A. K., Das, S. K., & Mishra, J. (2021b). Rice husk ash-based concrete composites: A critical review of their properties and applications. *Crystals*, *11*(2), 168.

Aouan, B., Alehyen, S., Fadil, M., Alouani, M. E., Khabbazi, A., Atbir, A., & Taibi, M. H. (2021). Compressive strength optimization of metakaolin-based geopolymer by central composite design. *Chemical Data Collections*, *31*, 100636.

Assi, L. N., Carter, K., Deaver, E., & Ziehl, P. (2020). Review of availability of source materials for geopolymer/sustainable concrete. *Journal of Cleaner Production*, *263*, 121477.

American Society for Testing and Materials. (2008). *ASTM C618–Standard Specification for Coal Fly Ash and Raw or Calcined Natural Pozzolan for Use in Concrete.* https://scholar.google.com

Atiş, C., Görür, E., Karahan, O., Bilim, C., İlkentapar, S., & Luga, E. (2015). Very high strength (120 MPa) class F fly ash geopolymer mortar activated at different NaOH amount, heat curing temperature and heat curing duration. *Construction and Building Materials*, *96*, 673-678.

Aydın, S. (2013). A ternary optimisation of mineral additives of alkali activated cement mortars. *Construction and Building Materials*, *43*, 131-138.

Ayeni, O., Onwualu, A. P., & Boakye, E. (2021). Characterization and mechanical performance of metakaolin-based geopolymer for sustainable building applications. *Construction and Building Materials*, *272*, 121938.

Aziz, I. H., Abdullah, M. M. A. B., Yong, H. C., Ming, L. Y., Hussin, K., Kadir, A. A., & Azimi, E. A. (2016). *Manufacturing of Fire Resistance Geopolymer: A Review. In MATEC Web of Conferences (Vol. 78, P. 01023)*. https://scholar.google.com

Azzahran-Abdullah, S. F., Yun-Ming, L., Al Bakri, M. M., Cheng-Yong, H., Zulkifly, K., & Hussin, K. (2018). Effect of Alkali Concentration on Fly Ash Geopolymers. *Conference Series: Materials Science and Engineering*, *343*, 012013. https://doi.org/10.1088/1757-899x/343/1/012013

Badogiannis, E., Kakali, G., & Tsivilis, S. (2005). Metakaolin as supplementary cementitious material: Optimization of kaolin to metakaolin conversion. *Journal of Thermal Analysis and Calorimetry*, *81*(2), 457-462.

Bajpai, R., Choudhary, K., Srivastava, A., Sangwan, K. S., & Singh, M. (2020). Environmental impact assessment of fly ash and silica fume based geopolymer concrete. *Journal of Cleaner Production*, *254*, 120147.

Bakharev, T. (2005). Resistance of geopolymer materials to acid attack. *Cement and Concrete Research*, *35*(4), 658-670.

Benhelal, E., Shamsaei, E., & Rashid, M. I. (2021). Challenges against CO_2 abatement strategies in cement industry: A review. *Journal of Environmental Sciences*, *104*, 84-101.

Bich, C., Ambroise, J., & Péra, J. (2009). Influence of degree of dehydroxylation on the pozzolanic activity of metakaolin. *Applied Clay Science*, *44*(3-4), 194-200. https://doi.org/10.1016/j.clay.2009.01.014

Bingöl, Ş., Bilim, C., Atiş, C. D., & Durak, U. (2020). Durability properties of geopolymer mortars containing slag. *Iranian Journal of Science and Technology, Transactions of Civil Engineering*, *44*, 561-569.

Bish, D. L. (1993). Rietveld refinement of the kaolinite structure at 1.5 K. *Clays and Clay Minerals*, *41*(6), 738-744.

Borges, P. H., Nunes, V. A., Panzera, T. H., Schileo, G., & Feteira, A. (2016). The influence of rice husk ash addition on the properties of metakaolin-based geopolymers. *The Open Construction and Building Technology Journal*, *10*, 406-417.

C0207, A. (2020). *C0267 Standard Test Methods for Chemical resistance of Mortars, Grouts, and Monolithic Surfacings and Polymer Concretes. In Annual book of ASTM Standards 2020*. https://scholar.google.com

C1202, A. (2012). C1202: *Standard Test Method for Electrical Indication of Concrete's Ability to Resist Chloride ion Penetration, American Society for Testing Materials*. https://scholar.google.com

Cai, R., Wu, T., Fu, C., & Ye, H. (2022). Thermal degradation of potassium-activated ternary slag-fly ash-silica fume binders. *Construction and Building Materials*, *320*, 126304. https://doi.org/10.1016/j.conbuildmat.2021.126304

Catti, M., Ferraris, G., & Ivaldi, G. (1989). Thermal strain analysis in the crystal structure of muscovite at 700 degree C. *European Journal of Mineralogy*, *1*(5), 625-632.

Chao, S., Hargreaves, A., & Taylor, W. (1940). The structure of orthoclase. *Mineralogical Magazine and Journal of the Mineralogical Society*, *25*(168), 498-512.

Chen, K., Wu, D., Xia, L., Cai, Q., & Zhang, Z. (2021a). Geopolymer concrete durability subjected to aggressive environments: A review of influence factors and comparison with ordinary Portland cement. *Construction and Building Materials*, *279*, 122496.

Chen, K., Wu, D., Yi, M., Cai, Q., & Zhang, Z. (2021b). Mechanical and durability properties of metakaolin blended with slag geopolymer mortars used for pavement repair. *Construction and Building Materials*, *281*, 122566.

Dai, S., Wang, H., An, S., & Yuan, L. (2022). Mechanical properties and microstructural characterization of metakaolin geopolymers based on orthogonal tests. *Materials*, *15*(8), 2957.

Das, S. K., Adediran, A., Kaze, C. R., Mustakim, S. M., & Leklou, N. (2022). Production, characteristics, and utilization of rice husk ash in alkali activated materials: An overview of fresh and hardened state properties. *Construction and Building Materials*, *345*, 128341.

Davis, R., & John, P. (2018). *Application of Taguchi-Based Design of Experiments. Statistical Approaches with Emphasis on Design of Experiments Applied to Chemical Processes*, 137. https://scholar.google.com

De Oliveira, L. B., De Azevedo, A. R., Marvila, M. T., Pereira, E. C., Fediuk, R., & Vieira, C. M. F. (2022). Durability of geopolymers with industrial waste. *Case Studies in Construction Materials*, *16*, e00839.

Değirmenci, F. N. (2017). *Effect of Sodium Silicate to Sodium Hydroxide Ratios on Durability of Geopolymer Mortars Containing Natural and Artificial Pozzolans.* https:// scholar. google. com. https://scholar.google.com

Deju, R., Mazilu, C., Stanculescu, I., & Tuca, C. (2020). Fourier transform infrared spectroscopic characterization of thermal treated kaolin. *Romanian Reports in Physics*, *72*, 1-11.

Devarajan, P., Sivalinga-vijayan, D., Sanjay-Kumar, R., & Arun-Frait-King, J. (2023). A short review on Substantial role of Geopolymer in the sustainable construction industry. *Conference Series: Earth and Environmental Science*, *1130*(1), 012002.

Dong, Y., Pei, L., Fu, J., Yang, Y., Liu, T., Liang, H., & Yang, H. (2022). Investigating the mechanical properties and durability of metakaolin-incorporated mortar by different curing methods. *Materials*, *15*(6), 2035.

Dos Reis Ferreira, R., Gratão, L., & De Castro Motta, L. (2024). Evaluation and optimization of the replacement of fine aggregate by waste tire rubber in geopolymer Mortar with metakaolin. *Mechanics of Composite Materials*, *59*(6), 1223-1238.

El-Sayed, A. M., Faheim, A. A., Salman, A. A., & Saleh, H. M. (2021). *Introductory Chapter: Cement Industry. In Cement Industry-Optimization, Characterization and Sustainable Application.* https://scholar.google.com

Eldin, H. S., Abdullah, N. A., Ismail, M. F., & Hashem, A. I. (2022). Preparation of meta phase of kaolinite as a precursor for geopolymer adsorbent fabrication. *Epitoanyag: Journal of Silicate Based and Composite Materials*, *74*(3), 82-87.

Elimbi, A., Tchakoute, H. K., & Njopwouo, D. (2011). Effects of calcination temperature of kaolinite clays on the properties of geopolymer cements. *Construction and Building Materials*, *25*(6), 2805-2812. https://doi.org/10.1016/j.conbuildmat.2010.12.055

EN, B. (2011). *Methods of Testing Cement–Part 5: Pozzolanicity Test for Pozzolanic Cement*. British Standards Institution, London, UK, 196-195.

Endale, S. A., Taffese, W. Z., Vo, D. H., & Yehualaw, M. D. (2022). Rice husk ash in concrete. *Sustainability*, *15*(1), 137.

Erasmus, E. (2016). The influence of thermal treatment on properties of kaolin. *Hemijska Industrija*, *70*(5), 595-601. https://doi.org/10.2298/hemind150720066e

Esparham, A., & Moradikhou, A. B. (2021). A novel type of alkaline activator for geopolymer concrete based on class C fly ash. *Advance Researches in Civil Engineering*, *3*(1), 1-13.

Fabbri, B., Gualtieri, S., & Leonardi, C. (2013). Modifications induced by the thermal treatment of kaolin and determination of reactivity of metakaolin. *Applied Clay Science*, *73*, 2-10.

Ferone, C., Colangelo, F., Roviello, G., Asprone, D., Menna, C., Balsamo, A., Prota, A., Cioffi, R., & Manfredi, G. (2013). Application-Oriented Chemical Optimization of a Metakaolin Based Geopolymer. *Materials (Basel)*, *6*(5), 1920-1939.

Görhan, G., & Kürklü, G. (2014). The influence of the NaOH solution on the properties of the fly ash-based geopolymer mortar cured at different temperatures. *Composites Part b: Engineering*, *58*, 371-377.

Gualtieri, A. F. (2000). Accuracy of XRPD QPA using the combined Rietveld–RIR method. *Journal of Applied Crystallography*, *33*(2), 267-278.

Guggenheim, S., Chang, Y. H., & Koster van Groos, A. F. (1987). Muscovite dehydroxylation: High-temperature studies. *American Mineralogist*, *72*(5-6), 537-550.

Güneyisi, E., Gesoğlu, M., Özturan, T., & Mermerdaş, K. (2012). Microstructural properties and pozzolanic activity of calcined kaolins as supplementary cementing materials. *Canadian Journal of Civil Engineering*, *39*(12), 1274-1284.

GÜVEN, N., & Burnham, C. W. (1967). The crystal structure of 3T muscovite. *Zeitschrift für Kristallographie-Crystalline Materials*, *125*(1-6), 163-183.

Hamada, H. M., Al-Attar, A., Beddu, S., Askar, M. K., Yousif, S. T., & Majdi, A. (2025). Impact of rice husk ash on geopolymer concrete: A literature review and future directions. *Case Studies in Construction Materials*, 2025, e04476.

Hamzaçebi, C., Li, P., Pereira, P., & Navas, H. (2020). *Taguchi Method as a Robust Design Tool. Quality Control-Intelligent Manufacturing, Robust Design and Charts*. https://scholar.google.com

Hasnaoui, A., Ghorbel, E., & Wardeh, G. (2019). Optimization approach of granulated blast furnace slag and metakaolin based geopolymer mortars. *Construction and Building Materials*, *198*, 10-26.

Hazen, R., Finger, L., Hemley, R., & Mao, H. (1989). High-pressure crystal chemistry and amorphization of α-quartz. *Solid State Communications*, *72*(5), 507-511.

Hossain, S. S., Roy, P., & Bae, C. J. (2021). Utilization of waste rice husk ash for sustainable geopolymer: A review. *Construction and Building Materials*, *310*, 125218.

Huseien, G. F., Mirza, J., Ismail, M., Ghoshal, S. K., & Ariffin, M. A. M. (2018). Effect of metakaolin replaced granulated blast furnace slag on fresh and early strength properties of geopolymer mortar. *Ain Shams Engineering Journal*, *9*(4), 1557-1566. https://doi.org/10.1016/j.asej.2016.11.011

Ibrahim, M., Wan Ibrahim, W. M., Abdullah, M. M. A. B., Nabialek, M., Putra Jaya, R., Setkit, M., Ahmad, R., & Jeż, B. (2023). Synthesis of Metakaolin Based Alkali Activated Materials as an Adsorbent at Different Na_2SiO_3/NaOH Ratios and Exposing Temperatures for Cu^{2+} Removal. *Materials*, *16*(3), 1221.

Ikuta, D., Kawame, N., Banno, S., Hirajima, T., Ito, K., Rakovan, J. F., Downs, R. T., & Tamada, O. (2007). First in situ X-ray identification of coesite and retrograde quartz on a glass thin section of an ultrahigh-pressure metamorphic rock and their crystal structure details. *American Mineralogist*, *92*(1), 57-63.

Ilic, B., Mitrovic, A., & Milicic, L. (2010). Thermal treatment of kaolin clay to obtain metakaolin. *Hemijska Industrija*, *64*(4), 351-356.

Imtiaz, L., Rehman, S. K. U., Ali Memon, S., Khizar-Khan, M., & Faisal-Javed, M. (2020). A Review of Recent Developments and Advances in Eco-Friendly Geopolymer Concrete. *Applied Sciences*, *10*(21), 7838. https://doi.org/10.3390/app10217838

Irfan-Khan, M., Khan, H. U., Azizli, K., Sufian, S., Man, Z., Siyal, A. A., Muhammad, N., & Faiz ur Rehman, M. (2017). The pyrolysis kinetics of the conversion of Malaysian kaolin to metakaolin. *Applied Clay Science, 146*, 152-161.

Jan, A., Pu, Z., Khan, K. A., Ahmad, I., Shaukat, A. J., Hao, Z., & Khan, I. (2022). A review on the effect of silica to alumina ratio, alkaline solution to binder ratio, calcium oxide+ ferric oxide, molar concentration of sodium hydroxide and sodium silicate to sodium hydroxide ratio on the compressive strength of geopolymer concrete. *Silicon*, 14(7), 3147-3162.

Jindal, B. B. (2019). Investigations on the properties of geopolymer mortar and concrete with mineral admixtures: A review. *Construction and Building Materials*, *227*, 116644.

Jindal, B. B., Alomayri, T., Hasan, A., & Kaze, C. R. (2022). Geopolymer concrete with metakaolin for sustainability: A comprehensive review on raw material's properties, synthesis, performance, and potential application. *Environmental Science and Pollution Research*, 2022, 1-26.

John, S. K., Nadir, Y., & Girija, K. (2021). Effect of source materials, additives on the mechanical properties and durability of fly ash and fly ash-slag geopolymer mortar: A review. *Construction and Building Materials*, *280*, 122443.

Joshi, P., & Chan, C. (2002). Rapid chloride permeability testing. *Concrete Construction*, *47*(12), 37-43.

Juenger, M., Winnefeld, F., Provis, J. L., & Ideker, J. (2011). Advances in alternative cementitious binders. *Cement and Concrete Research*, *41*(12), 1232-1243.

Kakali, G., Perraki, T., Tsivilis, S., & Badogiannis, E. (2001). Thermal treatment of kaolin: The effect of mineralogy on the pozzolanic activity. *Applied Clay Science*, *20*(1-2), 73-80.

Kantarcı, F., Türkmen, İ., & Ekinci, E. (2019). Optimization of production parameters of geopolymer mortar and concrete: A comprehensive experimental study. *Construction and Building Materials*, 228, 116770.

Karna, S. K., & Sahai, R. (2012). An overview on Taguchi method. *International Journal of Engineering and Mathematical Sciences*, *1*(1), 1-7.

Kaur, M., Singh, J., & Kaur, M. (2018). Microstructure and strength development of fly ash-based geopolymer mortar: Role of nano-metakaolin. *Construction and Building Materials*, *190*, 672-679.

Kenne Diffo, B. B., Elimbi, A., Cyr, M., Dika Manga, J., & Tchakoute Kouamo, H. (2018). Effect of the rate of calcination of kaolin on the properties of metakaolin-based geopolymers. *Journal of Asian Ceramic Societies*, *3*(1), 130-138.

Khalil, M. G., Elgabbas, F., El-Feky, M. S., & El-Shafie, H. (2020). Performance of geopolymer mortar cured under ambient temperature. *Construction and Building Materials*, *242*, 118090.

Khan, M. N. N., & Sarker, P. K. (2020). Effect of waste glass fine aggregate on the strength, durability and high temperature resistance of alkali-activated fly ash and GGBFS blended mortar. *Construction and Building Materials*, *263*, 120177.

Khan, M. Z. N., Hao, Y., & Hao, H. (2016). Synthesis of high strength ambient cured geopolymer composite by using low calcium fly ash. *Construction and Building Materials*, *125*, 809-820.

Kihara, K. (1990). An X-ray study of the temperature dependence of the quartz structure. *European Journal of Mineralogy*, *2*(1), 63-77.

Kim, B., Lee, S., Chon, C. M., & Cho, S. (2021). Setting behavior and phase evolution on heat treatment of metakaolin-based geopolymers containing calcium hydroxide. *Materials*, 15(1), 194.

Kim, Y. Y., Lee, B. J., Saraswathy, V., & Kwon, S. J. (2014). Strength and durability performance of alkali-activated rice husk ash geopolymer mortar. *The Scientific World Journal*, *2014*(1), 209584.

Klima, K., Schollbach, K., Brouwers, H., & Yu, Q. (2022). Thermal and fire resistance of Class F fly ash based geopolymers: A review. *Construction and Building Materials*, *323*, 126529.

Kljajević, L., Nenadović, M., Ivanović, M., Bučevac, D., Mirković, M., Mladenović Nikolić, N., & Nenadović, S. (2022). Heat treatment of geopolymer samples obtained by varying concentration of sodium hydroxide as constituent of alkali activator. *Gels*, 8(6), 333.

Komnitsas, K., Zaharaki, D., Vlachou, A., Bartzas, G., & Galetakis, M. (2015). *Effect Of Synthesis Parameters on the Quality of Construction and Demolition Wastes.* https://scholar.google.com

Koushkbaghi, M., Kazemi, M. J., Mosavi, H., & Mohseni, E. (2019). Acid resistance and durability properties of steel fiber-reinforced concrete incorporating rice husk ash and recycled aggregate. *Construction and Building Materials*, *202*, 266-275.

Król, M., & Rożek, P. (2019). *The Effect of Calcination Temperature on Metakaolin Structure.* https://scholar.google.com

Lahalle, H., Benavent, V., Trincal, V., Wattez, T., Bucher, R., & Cyr, M. (2021). Robustness to water and temperature, and activation energies of metakaolin-based geopolymer and alkali-activated slag binders. *Construction and Building Materials*, *300*, 124066.

Lämmlein, T. D., Messina, F., Wyrzykowski, M., Terrasi, G. P., & Lura, P. (2019). Low clinker high performance concretes and their potential in CFRP-prestressed structural elements. *Cement and Concrete Composites*, *100*, 130-138.

Lee, T., Jeong, K., & Choi, H. (2021). Effect of thermal properties of aggregates on the mechanical properties of high strength concrete under loading and high temperature conditions. *Materials*, *14*(20), 6093.

Lezzerini, M., Aquino, A., & Pagnotta, S. (2024). Acid Resistance of Metakaolin-Based Geopolymers and Geopolymeric Mortars Reinforced with Coconut Fibers. *Fibers*, *12*(5), 40.

Li, Z., Lu, D., & Gao, X. (2021). Optimization of mixture proportions by statistical experimental design using response surface method: A review. *Journal of Building Engineering*, *36*, 102101. https://doi.org/10.1016/j.jobe.2020.102101

Lingyu, T., Dongpo, H., Jianing, Z., & Hongguang, W. (2021). Durability of geopolymers and geopolymer concretes: A review. *Reviews on Advanced Materials Science*, *60*(1), 1-14.

Liu, D., Zhang, Y., Zhou, A., Nnachi, E., Huo, S., & Zhang, Q. (2021). The Kaolinite Crystallinity and Influence Factors of Coal-Measure Kaolinite Rock from Datong Coalfield, China. *Minerals*, *12*(1), 54. https://doi.org/10.3390/min12010054

Liu, M., Hu, R., Zhang, Y., Wang, C., & Ma, Z. (2023). Effect of ground concrete waste as green binder on the micro-macro properties of eco-friendly metakaolin-based geopolymer mortar. *Journal of Building Engineering*, *68*, 106191.

Liu, X., Jiang, J., Zhang, H., Li, M., Wu, Y., Guo, L., Wang, W., Duan, P., Zhang, W., & Zhang, Z. (2020). Thermal stability and microstructure of metakaolin-based geopolymer blended with rice husk ash [Article]. *Applied Clay Science*, *196*, 105769. https://doi.org/10.1016/j.clay.2020.105769

Ma, Z., Dan, H., Tan, J., Li, M., & Li, S. (2023). Optimization design of MK-GGBS based geopolymer repairing mortar based on response surface methodology. *Materials*, 16(5), 1889.

Madirisha, M. M., Dada, O. R., & Ikotun, B. D. (2024). Chemical Fundamentals of Geopolymers in Sustainable Construction. *Materials Today Sustainability*, 2024, 100842.

Mathur, S. (2014). *Understanding the Benefits of High Reactivity Metakaolin, Extraordinary Performance in Concrete, Mortar and Grout*. https://scholar.google.com

Mehsas, B., Siline, M., & Zeghichi, L. (2021). Development of supplementary cementitious materials from Algerian kaolin: Elaboration of metakaolin and assessment of pozzolanicity. *Innovative Infrastructure Solutions*, *6*(2), 50.

Mhanna, H. H., Hawileh, R. A., Abdalla, J. A., Ayman, A., Moussa, A., El-Din-Mahdi, B., & Kuwatly, Y. (2023). *Mechanical Properties and Durability of GGBS Based Geopolymer Mortar. Materials Today: Proceedings*. https://scholar.google.com

Miller, S. A., & Moore, F. C. (2020). Climate and health damages from global concrete production. *Nature Climate Change*, *10*(5), 439-443.

Mohamed, O. A., Al-Khattab, R., & Al-Hawat, W. (2022). Effect of relative GGBS/fly contents and alkaline solution concentration on compressive strength development of geopolymer mortars subjected to sulfuric acid. *Scientific Reports*, *12*(1), 5634.

Mohammed, B. S., Khed, V. C., & Nuruddin, M. F. (2018). Rubbercrete mixture optimization using response surface methodology. *Journal of Cleaner Production*, *171*, 1605-1621. https://doi.org/10.1016/j.jclepro.2017.10.102

Monteiro, P. J., Miller, S. A., & Horvath, A. (2017). Towards sustainable concrete. *Nature Materials*, *16*(7), 698-699.

Morsy, M., Alsayed, S., Al-Salloum, Y., & Almusallam, T. (2014). Effect of sodium silicate to sodium hydroxide ratios on strength and microstructure of fly ash geopolymer binder. *Arabian Journal for Science and Engineering*, *39*, 4333-4339.

Myers, R., Montgomery, D., & Anderson-Cook, C. (2009). *Probability and Statistics: Response Surface Methodology.* https://scholar.google.com

Naghizadeh, A., & Ekolu, S. O. (2019). *Effect of Mix Parameters on Strength of Geopolymer Mortars-Experimental Study*. https://scholar.google.com

NFP18-513. (2010). *Metakaolin. Pozzolanic Addition for Concrete. Definitions, Specifications and Conformity Criteria. In: Association Française De Normalisation, La Plaine Saint-Denis (France).* https://scholar.google.com

Noordin, M. Y., Venkatesh, V. C., Sharif, S., Elting, S., & Abdullah, A. (2004). Application of response surface methodology in describing the performance of coated carbide tools when turning AISI 1045 steel. *Journal of Materials Processing Technology*, *145*(1), 46-58. https://doi.org/10.1016/s0924-0136(03)00861-6

Oakes, L., Magee, B., Millar, P., McIlhagger, A., & McCartney, M. (2018). *A Simplified Mix Design Procedure for Geopolymer Cement Mortars Based on Metakaolin and Industrial Waste Products Activated with Potassium Silicate.* https://scholar.google.com

Ofosu-Adarkwa, J., Xie, N., & Javed, S. A. (2020). Forecasting CO_2 emissions of China's cement industry using a hybrid Verhulst-GM (1, N) model and emissions' technical conversion. *Renewable and Sustainable Energy Reviews*, *130*, 109945.

Oleiwi, S. M., Algın, Z., Nassani, D. E., & Mermerdaş, K. (2018). Multi-Objective Optimization of Alkali Activator Agents for FA- and GGBFS-Based Geopolymer Lightweight Mortars. *Arabian Journal for Science and Engineering*, *43*(10), 5333-5347. https://doi.org/10.1007/s13369-018-3170-x

Ouda, A. S., & Gharieb, M. (2021). Behavior of alkali-activated pozzocrete-fly ash paste modified with ceramic tile waste against elevated temperatures and seawater attacks. *Construction and Building Materials*, *285*, 122866.

Oyebisi, S. O., Ede, A. N., & Olutoge, F. A. (2021). Optimization of design parameters of slag-corncob ash-based geopolymer concrete by the central composite design of the response surface methodology. *Iranian Journal of Science and Technology, Transactions of Civil Engineering*, *45*, 27-42.

Pillars, W. W., & Peacor, D. R. (1973). The crystal structure of beta eucryptite as a function of temperature. *American Mineralogist: Journal of Earth and Planetary Materials*, *58*(7-8), 681-690.

Prince, E., Donnay, G., & Martin, R. (1973). Neutron diffraction refinement of an ordered orthoclase structure. *American Mineralogist: Journal of Earth and Planetary Materials*, *58*(5-6), 500-507.

Ramezanianpour, A. A. (2014). *Metakaolin.* https://scholar.google.com

Rashad, A. M. (2013). Metakaolin as cementitious material: History, scours, production and composition: A comprehensive overview. *Construction and Building Materials*, *41*, 303-318. https://doi.org/10.1016/j.conbuildmat.2012.12.001

Rathee, M., & Misra, A. (2024). Performance of alkali-activated aluminosilicate geopolymer mortar under exposure to acid, sulfate and high temperature. *Magazine of Concrete Research*, *77*(3-4), 209-227.

Razak, S. N. A., Shafiq, N., Guillaumat, L., Farhan, S. A., & Lohana, V. K. (2022). Fire-exposed fly-ash-based geopolymer concrete: Effects of burning temperature on mechanical and microstructural properties. *Materials*, *15*(5), 1884.

Redhammer, G. N. J., Beran, A., Schneider, J., Amthauer, G., & Lottermoser, W. (2000). Spectroscopic and structural properties of synthetic micas on the annite-siderophyllite binary: Synthesis, crystal structure refinement, Mossbauer, and infrared spectroscopy. *American Mineralogist*, *85*(3-4), 449-465.

Rihan, M. A. M., Onchiri, R. O., Gathimba, N., & Sabuni, B. (2024). Effect of sugarcane bagasse ash addition and curing temperature on the mechanical properties and microstructure of fly ash-based geopolymer concrete. *Open Ceramics*, 100616.

Rihan, M. A. M., & S. Alahmari, T. (2025). Review of recent development regarding strength, durability, and microstructure properties of geopolymer concrete containing rice husk ash. *Advances in Civil Engineering*, 2025(1), 7211661.

Ro, J. W., Cunningham, P. R., Miller, S. A., Kendall, A., & Harvey, J. (2024). Technical, economic, and environmental feasibility of rice hull ash from electricity generation as a mineral additive to concrete. *Scientific Reports*, *14*(1), 9158.

Sadrmomtazi, A., Khameneh, N. G., Khoshkbijari, R. K., & Amooie, M. (2021). A study on the durability of the slag-based geopolymer concretes containing binary solid mixtures in corrosive environments. *Revista Romana de Materiale*, *51*(2), 195-206.

Salahudeen, N. (2018). Metakaolinization effect on the thermal and physiochemical propperties of kankara kaolin. *Applied Science and Engineering Progress*, *11*(2), 127-135.

Samuel, R., Puppala, A. J., & Radovic, M. (2020). Sustainability benefits assessment of metakaolin-based geopolymer treatment of high plasticity clay. *Sustainability*, *12*(24), 10495.

Sanchez, T., Conciatori, D., & Keserle, G. C. (2022). Influence of the type of the de-icing salt on its diffusion properties in cementitious materials at different temperatures. *Cement and Concrete Composites*, *128*, 104439.

Sata, V., Sathonsaowaphak, A., & Chindaprasirt, P. (2012). Resistance of lignite bottom ash geopolymer mortar to sulfate and sulfuric acid attack. *Cement and Concrete Composites*, *34*(5), 700-708.

Shafiq, N., Nuruddin, M. F., Khan, S. U., & Ayub, T. (2015). Calcined kaolin as cement replacing material and its use in high strength concrete. *Construction and Building Materials*, *81*, 313-323. https://doi.org/10.1016/j.conbuildmat.2015.02.050

Shvarzman, A., Kovler, K., Grader, G., & Shter, G. (2003). The effect of dehydroxylation/amorphization degree on pozzolanic activity of kaolinite. *Cement and Concrete Research*, *33*(3), 405-416.

Shvarzman, A., Kovler, K., Schamban, I., Grader, G., & Shter, G. (2002). Influence of chemical and phase composition of mineral admixtures on their pozzolanic activity. *Advances in Cement Research*, *14*(1), 35-41.

Silva, C., Bernal-Camacho, J., Bandeira, J., Guimarães, A., & Corral Higuera, R. (2019). Study of chloride penetration profiles and surface chloride content of concrete structures exposed to marine environment evaluated at different exposure times. *Revista de la Construcción*, *18*(3), 545-553.

Silva, V. (2018). *Statistical Approaches with Emphasis on Design of Experiments Applied to Chemical Processes*. https://scholar.google.com/

Singh, A., Bhadauria, S. S., Thakare, A. A., Kumar, A., Mudgal, M., & Chaudhary, S. (2024). Durability assessment of mechanochemically activated geopolymer concrete with a low molarity alkali solution. *Case Studies in Construction Materials*, *20*, e02715.

Singh, N. B., & Middendorf, B. (2020). Geopolymers as an alternative to Portland cement: An overview. *Construction and Building Materials*, *237*, 117455.

Siyal, A. A., Azizli, K. A., Man, Z., & Ullah, H. (2016). Effects of Parameters on the Setting Time of Fly Ash Based Geopolymers Using Taguchi Method. *Procedia Engineering*, *148*, 302-307. https://doi.org/10.1016/j.proeng.2016.06.624

Slaný, M., Kuzielová, E., Žemlička, M., Matejdes, M., Struhárová, A., & Palou, M. T. (2023). Metabentonite and metakaolin-based geopolymers/zeolites: Relation between kind of clay, calcination temperature and concentration of alkaline activator. *Journal of Thermal Analysis and Calorimetry*, *148*(20), 10531-10547.

Somna, R., Saowapun, T., Somna, K., & Chindaprasirt, P. (2022). Rice husk ash and fly ash geopolymer hollow block based on NaOH activated. *Case Studies in Construction Materials*, *16*, e01092.

Souri, A., Golestani-Fard, F., Naghizadeh, R., & Veiseh, S. (2015). An investigation on pozzolanic activity of Iranian kaolins obtained by thermal treatment. *Applied Clay Science*, *103*, 34-39. https://doi.org/10.1016/j.clay.2014.11.001

Srinivasa, A. S., Swaminathan, K., & Yaragal, S. C. (2023). Microstructural and optimization studies on novel one-part geopolymer pastes by Box-Behnken response surface design method. *Case Studies in Construction Materials*, *18*, e01946.

Taborda-Barraza, M., Tambara Jr, L. U., Vieira, C. M., de Azevedo, A. R. G., & Gleize, P. J. (2024). Parametrization of Geopolymer Compressive Strength Obtained from Metakaolin Properties. *Minerals*, *14*(10), 974.

Tahwia, A. M., Ellatief, M. A., Bassioni, G., Heniegal, A. M., & Elrahman, M. A. (2023). Influence of high temperature exposure on compressive strength and microstructure of ultra-high performance geopolymer concrete with waste glass and ceramic. *Journal of Materials Research and Technology*, *23*, 5681-5697.

Tennakoon, C., Shayan, A., Sanjayan, J., & Xu, A. (2017). *Chloride Ingress and Steel Corrosion in Slag and Fly Ash Blended Geopolymer Concrete. Austroads Bridge Conference, 10th, 2017, Melbourne, Victoria, Australia*. https://scholar.google.com

Thirukumaran, T., Krishnapriya, S., Priya, V., Sagai Francis, B., Anandhalakshmi, R., Dinesh, S., Poomalai, R., Vivek, S., & Saravanan, S. (2023). Utilizing rice husk ash as a bio-waste material in geopolymer composites with aluminium oxide. *Global NEST Journal*, *25*(6), 119-129.

Thomas, R., Ariyachandra, E., Lezama, D., & Peethamparan, S. (2018). Comparison of chloride permeability methods for Alkali-Activated concrete. *Construction and Building Materials*, *165*, 104-111.

Tironi, A., Trezza, M. A., Irassar, E. F., & Scian, A. N. (2012a). Thermal Treatment of Kaolin: Effect on the Pozzolanic Activity. *Procedia Materials Science*, *1*, 343-350. https://doi.org/10.1016/j.mspro.2012.06.046

Tironi, A., Trezza, M. A., Scian, A. N., & Irassar, E. F. (2012b). Kaolinitic calcined clays: Factors affecting its performance as pozzolans. *Construction and Building Materials*, *28*(1), 276-281.

Turkane, S. D., & Chouksey, S. K. (2022). Application of response surface method for optimization of stabilizer dosages in soil stabilization. *Innovative Infrastructure Solutions*, *7*, 1-12.

Turkey, F. A., Beddu, S. B., Ahmed, A. N., & Al-Hubboubi, S. (2021). *Behaviour of Geopolymer Concrete to High Temperature. Materials Today: Proceedings*. https://scholar.google.com

Tuyan, M., Andiç-Çakir, Ö., & Ramyar, K. (2018). Effect of alkali activator concentration and curing condition on strength and microstructure of waste clay brick powder-based geopolymer. *Composites Part B: Engineering*, *135*, 242-252.

Unis Ahmed, H., Mahmood, L. J., Muhammad, M. A., Faraj, R. H., Qaidi, S. M. A., Hamah Sor, N., Mohammed, A. S., & Mohammed, A. A. (2022). Geopolymer concrete as a cleaner construction material: An overview on materials and structural performances. *Cleaner Materials*, *5*, 100111. https://doi.org/10.1016/j.clema.2022.100111

Usman, J., Sam, A. R. M., & Sumadi, S. R. (2013). *Optimized Calcination Temperatures and Time for Converting Kaolin to Metakaolin*. EACEF-International Conference of Civil *Engineering.* https://scholar.google.com

Vishwakarma, V., & Ramachandran, D. (2018). Green Concrete mix using solid waste and nanoparticles as alternatives: A review. *Construction and Building Materials*, *162*, 96-103.

Wee, T., Suryavanshi, A. K., & Tin, S. (2000). Evaluation of rapid chloride permeability test (RCPT) results for concrete containing mineral admixtures. *Materials Journal*, *97*(2), 221-232.

Wei, P. (1935). Die Bindung im Quarz Zeitschrift fuer Kristallographie. *Kristallgeometrie, Kristallphysik, Kristallchemie*, *92*, 355-362.

Weise, K., Ukrainczyk, N., & Koenders, E. (2021). A mass balance approach for thermogravimetric analysis in pozzolanic reactivity R3 test and effect of drying methods. *Materials*, *14*(19), 5859.

Weise, K., Ukrainczyk, N., & Koenders, E. (2023). Pozzolanic reactions of metakaolin with calcium hydroxide: Review on hydrate phase formations and effect of alkali hydroxides, carbonates and sulfates. *Materials & Design*, *231*, 112062.

Wianglor, K., Sinthupinyo, S., Piyaworapaiboon, M., & Chaipanich, A. (2017). Effect of alkali-activated metakaolin cement on compressive strength of mortars. *Applied Clay Science*, *141*, 272-279.

Wong, L. S. (2022). Durability performance of geopolymer concrete: A review. *Polymers*, *14*(5), 868.

Xie, N., Dang, Y., & Shi, X. (2019). New insights into how $MgCl_2$ deteriorates Portland cement concrete. *Cement and Concrete Research*, *120*, 244-255.

Yang, Y., Chen, C., Zhuang, Y., & Suo, Z. (2024). Reviewing the progress of corrosion fatigue research on marine structures. *Frontiers in Materials*, *11*, 1399292.

Zhang, H., Li, L., Yuan, C., Wang, Q., Sarker, P. K., & Shi, X. (2020a). Deterioration of ambient-cured and heat-cured fly ash geopolymer concrete by high temperature exposure and prediction of its residual compressive strength. *Construction and Building Materials*, *262*, 120924.

Zhang, P., Gao, Z., Wang, J., Guo, J., Hu, S., & Ling, Y. (2020b). Properties of fresh and hardened fly ash/slag based geopolymer concrete: A review. *Journal of Cleaner Production*, *270*, 122389. https://doi.org/10.1016/j.jclepro.2020.122389

Zhu, H., Liang, G., Zhang, Z., Wu, Q., & Du, J. (2019). Partial replacement of metakaolin with thermally treated rice husk ash in metakaolin-based geopolymer. *Construction and Building Materials*, *221*, 527-538.

RESEARCH OUTPUTS

(i) Publications

Hamisi, H., Jande, Y. A. C., & Hilonga, A. (2023). Highly reactive metakaolin: A multi-parameter optimization by response surface methodology. *Engineering Research Express*, *5*(4), 045064.

Hamisi, H., Chambua, S. T., Mansouri, S., Majdoubi, H., Jande, Y. A. C., Tamraoui, Y., & Hilonga, A. (2025). Compressive strength optimization of the ambient-cured metakaolin-based geopolymer mortar using the Taguchi design approach. *Construction and Building Materials*, *475*, 141248.

(ii) Poster presentation